Republic of Iraq
Ministry of Higher Education
and Scientific Research
Babylon University / College of Engineering
Department of Civil Engineering

Improving Punching Shear Behavior of Flat Slabs by Using Ultra High Performance Concrete

A Thesis
Submitted to the College of Engineering at University of Babylon
in Partial Fulfillment of the Requirements for the Degree of
Master in Engineering / Civil Engineering / Structures

By
Hussein Yousif Talib Abbas
B.Sc. Civil Engineering, 2012

Supervised by
Asst. Prof.Dr. Nabeel Hasan Ali Al-Salim

2023 A.D **1444 A.H**

بِسۡمِ ٱللَّهِ ٱلرَّحۡمَٰنِ ٱلرَّحِيمِ

قَالُواْ سُبۡحَٰنَكَ لَا عِلۡمَ لَنَآ إِلَّا مَا عَلَّمۡتَنَآۖ إِنَّكَ أَنتَ ٱلۡعَلِيمُ ٱلۡحَكِيمُ

صدق الله العلي العظيم

سورة البقرة الآية (32)

Dedication

To my parents

To my beloved wife

To my son muntadher

With respect

Certificate

I certify that **Hussen Youisf Talib** accomplished the preparation of this thesis entitled "**Improving Punching Shear Behavior of Flat Slabs by Using Ultra High Performance Concrete**" under our supervision at the University of Babylon in fulfillment of partial requirements for the degree of Master in Civil Engineering (Structural Engineering).

Signature:

Dr. Nabeel Hasan Ali

Acknowledgments

In the name of Allah, the most gracious, the most merciful

All thanks and praise to Allah who enabled me to achieve this research work. As well as thanks to the great Prophet Muhammad and his family, for they are my means to Allah and the door of his mercy.

Firstly, I would like to express my sincerest gratitude to my supervising Dr. Nabeel Hasan Ali, for his invaluable insight, wisdom, and guidance. I want to express my thanks and appreciation to the staff of (Al-Nawafith Company for the production of sand and gravel filters) for their help in supplied me with gravel material, which I have used in my experimental work. I would like to thank the support staff of the Department of Civil Engineering of Babylon University for their assistance with daily matters throughout my graduate academic life. Also, thanks to the technical staff of the structural laboratories for their assistance during the undertaking of my experimental program. I would like to acknowledge the friendly support and assistance of my fellow graduate students who made my overall experience more gratifying among them are Muneer Yousif, Mustafa Hamed, and Zahraa Louay.

Finally, a special thanks and gratitude to my family for their care, and patience, in particular: my parents, and my wife, who have been by my side throughout this entire endeavor. Without their love, encouragement, and support I would not have been able to complete this academic achievement.

Hussein Yousif Talib

2023

ABSTRACT

Punching shear failures are the most critical and the ruling in the design of flat slabs, so this study was done to strengthen the flat slab against the punching shear failure by using hybrid concrete and reinforced concrete (ultra high performance concrete). The experimental part of present research included fifteen specimens; square flat slabs with dimension (90*90 cm) and thickness (8 cm), all specimens contains reinforcing flexure steel at bottom.

Two specimens of normal concrete, one of which is the reference model for the first study case, and the other is normal concrete as well, but it contains punching shear reinforcing steel, which is the reference model for the second study case.

The first study case, is contains three cast groups of hybrid concrete (normal concrete and UHPC) for half the thickness of the slab in the face of compression. Each group consists of three models, the first group has a square shape in the center of the slab along the rib (1d+c) where (d) the effective depth (c) column section, and (2d+c) for the second (3d+c) for the third.

The second group the same as the specimens of the first group, but the strengthen area (UHPC) is tilted at an angle 45. In the third group, we used the circular form of strengthen with an area equivalent to the models of the first and second groups. The model's resistance to shear improved by a large percentage for the models of hybrid concrete compared to the reference model of ordinary concrete, and it reached double.

1. In addition to the improvement in the resistance of the slab to the failure of the punching shear as the strengthen area increases (UHPC), it also helped ultrahigh performance concrete in increasing other mechanical properties such

as energy absorption, ductility and stiffness,these properties have improved due to present of steel fibers. Show practical results rotating the stiffening shape at an angle of 45 is an optimal use for the square shape of the same amount (UHPC), if the results increase to double limits.

As for the case of the second study, it consists of four specimens of hybrid concrete in addition to the reference specimen that contains punching shear reinforcement. This study dealt with on replacing the punching shear reinforcement with (UHPC) with half or all of the thickness of the slab, and then we rotated the reinforcement area by an angle 45 to give great results with a ratio of 70% to for the reference specimen.

In the second part of this study, a three-dimensional finite element (FE) model using the concrete damaged plasticity model and material properties obtained from laboratory tests was conducted to simulate the reinforced concrete flat slabs with or without strengthen within a commercial finite element software package ABAQUS/standard 2017.

The numerical results have shown that the predictions of the finite element model were in good agreement with the experimental data in terms of cracking load, ultimate load and ultimate deflection with average differences about (%5), (%1.5), and (%7) respectively. Parametric study of many variables that not considered in the experimental program was conducted using the validated FE model such as; effect of the concrete compressive strength, effect of the column dimensions.

List of Contents

List of Tables

List of Figures

List of Plates

List of Tables

Notation

Unless otherwise noted in this thesis, all units are metric: dimensions are in millimetres, stresses are in MPa, moduli are in MPa, forces are in kN, and moments are in kN.m.

A_s	longitudinal steel area in tension at bottom of member
A_v	cross-sectional area of transverse steel reinforcement
c	depth of neutral axis measured from extreme compressive fiber
d	depth of longitudinal tension steel
d_b	diameter of steel bar
d_c	concrete compression damage parameter
d_t	concrete tension damage parameter
E_c	concrete initial tangent modulus
E_s	elastic modulus of steel
f_{cu}	concrete cubic strength
f_c'	concrete cylinder strength
f_{st}	concrete tensile strength
fy	yield stress of steel reinforcement
fc	stress of concrete
fs	stress of steel in tension
Gf	fracture energy of concrete
h	height of beam
M_n	total nominal moment
V_n	total nominal shear strength
V_c	shear resistance attributed to concrete
V_s	shear resistance attributed to steel shear reinforcement
β_1	concrete stress-block factor controlling the block height
δ_u	deflection of member at ultimate load
δ_s	deflection of member at service load
ε_c	compressive strain in concrete
ε_{co}	concrete strain corresponding to peak stress
ε_s	strain of steel in tension
ρ	steel reinforcement ratio
ρ_{max}	maximum steel reinforcement ratio
σ_c	axial stress in concrete
ℓd	reinforcement development length

Abbreviations

ACI	American Concrete Institute
ASTM	American Society for Testing and Material
BS	British Standards
C3D8R	8-Node Linear Brick Element, with Reduced Integration
CDP	Concrete Damaged Plasticity
CFRP	Carbon Fiber Reinforced Polymer
Eq.	Equation
et al.	And others
Exp.	Experimental
FE	Finite Element
FEA	Finite Element Analysis
FEM	Finite Element Method
FRP	Fiber Reinforced Polymer
HSC	High strength concrete
IQ.S	Iraqi Specification
N.A	Neutral Axis
NSC	Normal Strength Concrete
RC	Reinforced Concrete
Rebar	Reinforcing Bar
RPC	Reactive Powder Concrete
STM	Strut and Tie Model
T3D2	2-Node, 3D Truss Element
w/c	Water to Cement ratio
3D	Three-Dimensional

CHAPTER ONE

INTRODUCTION

1-1 Introduction

The slab can be called a two-way slab when its length is less than twice its width and its four sides carry it as the slab deflects in two directions and the loads move to all four supports. In such a type of slab, the bending moments are less than those with one-way slabs, and therefore the same slab can carry a higher load when supported on its four sides.

It should be noted that in reinforced concrete structures frames in which slabs are directly supported by columns i.e. without beams or girders, it is defined as slab-column framed system plate or flat plate (Figure 1-1). The flat plate as a system is desirable from an architectural and economic point of view for traditional beam-slab construction. The flat plate system has several advantages, including **[1]:-**

1-1-1 Advantages and dis advantages flat slab.

1- Maintaining the height of the building, lowering the height of the floors will minimize the weight of the building due to the lower partitions, maintain the approximate 10% in the vertical members, and decrease the foundation load.
2- Faster construction, which reduces the construction time.
3- Ease of establishing services, as all services could be connected directly to the bottom of the slab as an alternative to bending it to avoid beams and penetration through beams.
4- Significant reducing in frameworks.

5- Reducing finishing substances.

6- Flexibility in arranging the sections.

Plate (1-1): Slab-column framed system or flat plate **[2]**.

Nevertheless, the lack of beams in flat slab structures generates several troubles (flat slab defects) **[3]**:-

1- It causes a punching-shear failure as a result of generating high shear stresses at the slab-column connections.
2- It has an excess in the vertical deflection.
3- Under lateral loading, it has relatively little stiffness.

The use of shear walls, lifting columns or external support can avoid low lateral stiffness. The deflection can also be controlled by using prestressing. However, the punching shear resistance represent the major trouble with flat slab

structures. Where shear failure occurs suddenly without prior warning. Moreover, improper shear design of the slabs can cause a gradual collapse if the lower floors fail to withstand the shocks that have emerged from the collapsed floors above. In the past, beams were used to support reinforced concrete slabs **[4].** But, at the beginning of the 20^{th} century, specifically in the year 1914, flat slabs were used. And Turner and Eddy confirmed the challenge in designing these slabs, which raised concerns about how to calculate stresses. Since flat plates were designed depended on experimental data as a result of the lack of design guidelines at that time.

1-1-2 Background design punching shear reinforcement

Somewhat divergent approaches to flat plate design, which can best be illustrated by the various schemes used for flexural reinforcement. For instance, in the USA, a four-way flat plate system is utilized by Turner, as presented in Figure (1-1a), while the two-way system is employed by Condron, as displayed in Figure (1-1b) **[5] [6]**. For instance, too, A circumferential flat plate system was developed by Smulski **[7]**, consisting of reinforcements arranged transversely and radially as illustrated in Figure (1-1c). In the same period, a comparable system was presented in Europe by Maillart **[8]**. Also in this period, other new systems for flat plates were proposed, which may be considered relatively special.

Despite the various designs of flexural reinforcement, in all former procedures, an enlarged column was employed. Although the shape is slightly different in each procedure, the prime objective of reaming is to permit the transfer of force from the plate to the column to prevent failure in punching shear. Moreover, the enlargement contributes to increasing the flexural capacity of the slab as a result of reducing the distance between the columns. Over time, a steelhead inside the slab was used as a substitute for column enlargement.

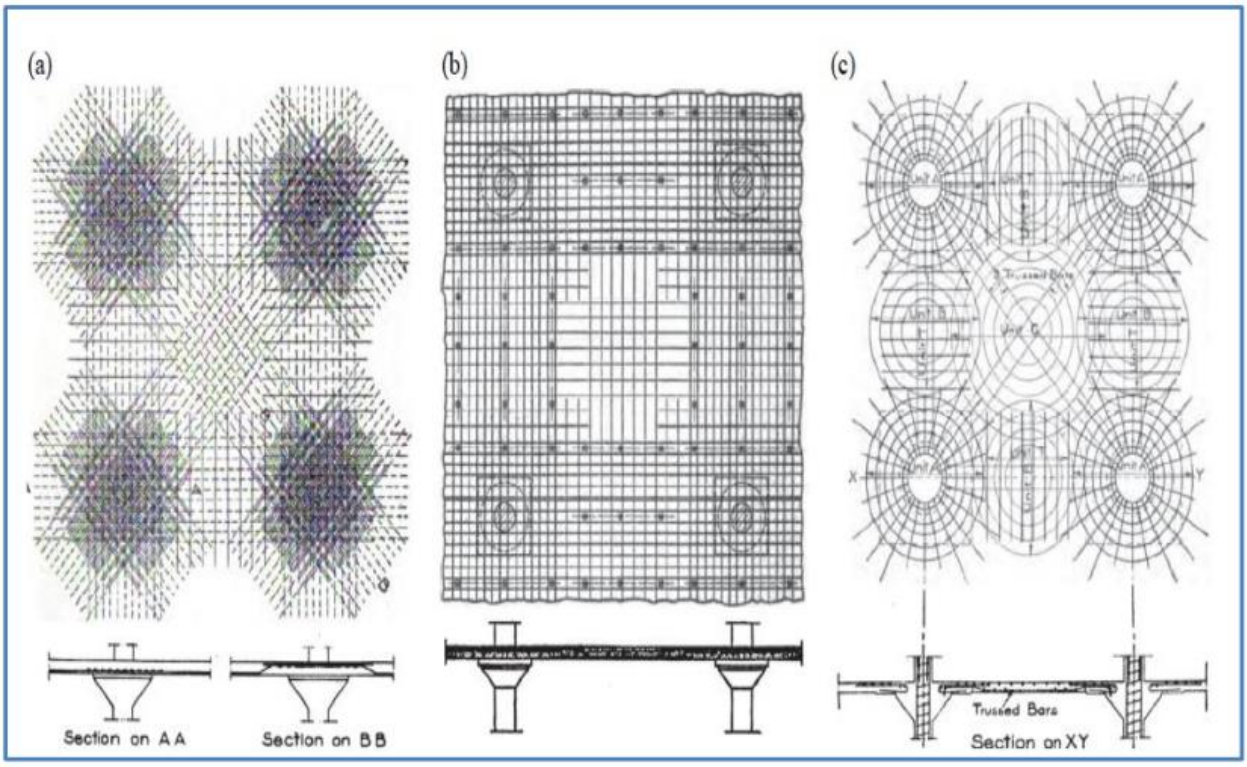

Figure (1-1): Reinforcement layouts in early developed flat plate systems: (a) four-way flat plate system, (b) two-way flat plate system, and(c) circumferential flat plate system **[9]**.

The increase in the number of studies on punching behavior has driven a better perception and assessment of punching shear force. Therefore, flat plates can be designed without the need for special punching shear reinforcement. However, brittle shear failure (which can occur suddenly) remains one of the major problems with this method. To avoid these accidents, safety reinforcement is usually added in order to excess the residual resistance of the flat plate beyond the happening of punching shear failure. The reinforcement can be distributed in different ways, but it must be put in the place where it works best. The deformation capacity and strength capacity should be considered when designing in order to determine the effectiveness of the flat plate.

Considering the deformation capacity, it is easily drawn to the conclusion that flat plate slabs without shear strengthening generally cannot supply sufficient deformation capacity. This is assured by abundant structure collapses. Therefore, the question worth asking does not include whether there is a need to place perforation shear reinforcement or not, but rather what is the amount of perforation shear reinforcement to be used and what is the appropriate place that provides sufficient deformation capacity? A logical answer to these questions requires an experimental search of the load-deformation response of flat plate slabs. Therefore, among the objectives of this study is to investigate the punching strength as well as the overall response of the flat slabs.

1-2 Punching Shear Failure in Flat Plate Slab

Two types of shear failure may have occurred in flat plate systems. The first one is the beam-type (wide beam) shear failure (unidirectional shear) which is similar to beam failure in terms of shear strength calculations and failure criteria, as shown in Figure (1-2a). This type of shear failure is often critical to the footing, but is not critical and scarcely a concern in flat plate design **[10]**.

The second is the failure of the punching shear (bidirectional shear) in which the failure may occur near the supported column or the concentrated load by forming a truncated cone **[11]**, as shown in Figure (1-2b). Typically, the shear stresses caused by punching shear are much higher than the shear stresses of the beam type. Punching shear failure may be caused by gravitational (vertical) load actions besides unbalanced torque, which is caused by unequal spans around the column or by lateral loading (such as earthquakes, wind, etc.). The failure of punching in a flat slab depends on its ability to resist shear stresses, which are caused by the transmission of unbalanced shear forces and moments to the columns.

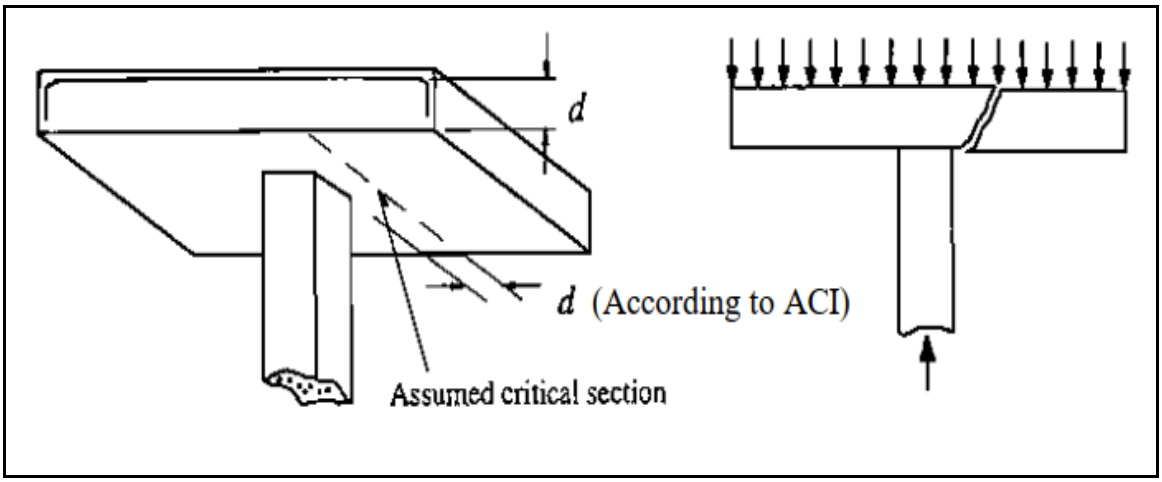

a. Wide beam-type shear failure

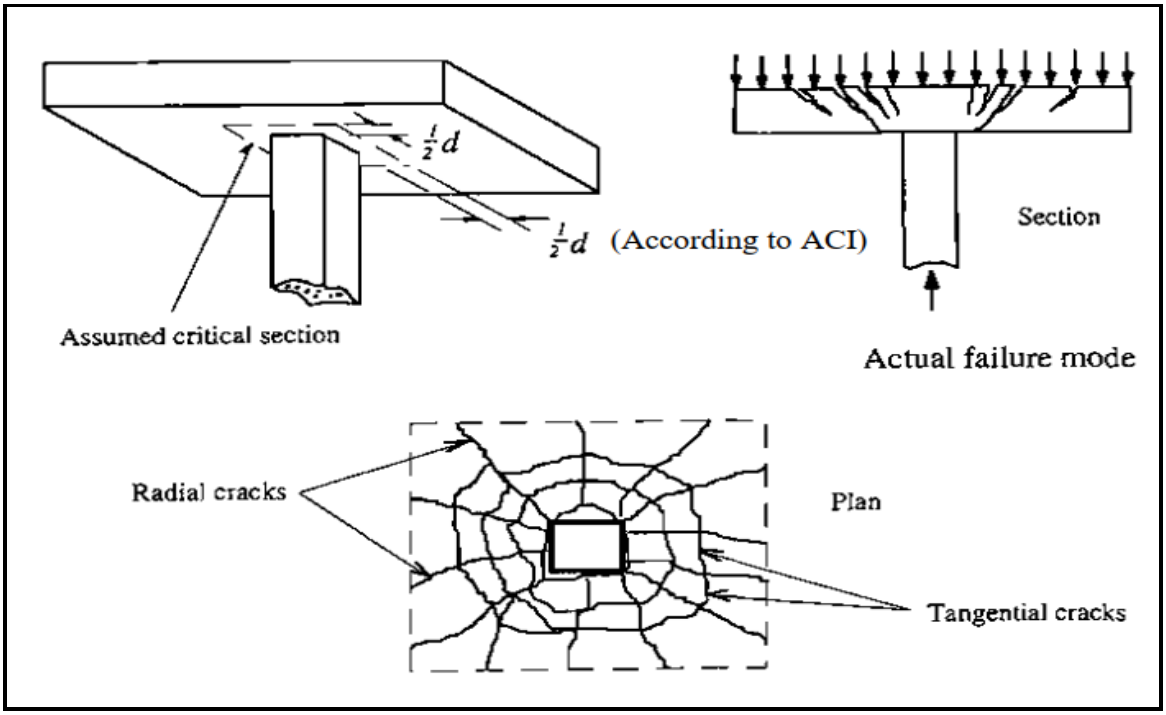

b. Punching shear failure

Figure (1-2): Types of shear failure in flat slab.

The failure of punching shear starts with radial cracks expanding from the column, which are caused by a negative bending moment in the transverse direction and then followed by transverse cracks around the circumference of the column (as a result of the negative bending moment in the radial direction). These radial tension cracks tend to form next to the middle of the slab depth, which are more like web shear cracks than bending shear cracks **[12]**. Therefore, the stiffness of the slab surrounding the cracked zone tends to maintain shear transfer to the column by shear transfer mechanisms, which will be discussed in the following sections. The slab begins to fail with column penetration once the applied load is high enough to conquer the stiffness of the slab. Generally, punching shear failure is sudden and brittle in reinforced flat plates.

1-2-1 Factors Influence Punching Shear Resistance

The punching shear resistance can be improved using several methods, some of which will be discussed as follows:

- **Increasing the slab thickness**

The simplest way to solve this problem is to increase slab thickness. This approach is usually used where there are no other successful or most appropriate methods available. The major disadvantage of this approach was that it raises the structure's cost and the dead load.

- **Increasing the compressive strength of concrete**

It has been noted that the shear stresses at the connections of slab columns in flat slab systems vary according to the compressive strength of the concrete. It was previously reported that shear stress increases with the growth of compressive strength of concrete **[13]**, whereby 40% more shear stress is gained for M50 concrete (compressive strength equal to 50 MPa in 28 days) than for M20 concrete.

• **Shear reinforcement**

The reinforcement of punching shear is an effective way to arise the deformation capacity and strength of slab column connections. The excess in the deformation capacity is important since, in the event of the local failure, the load is distributed to the other supports, which prevents the occurrence of complete failure of the structure. Thus, it presents a satisfying deformation capacity. There are various kinds of systems of punching shear reinforcement (see Figure 1-3) **[14]**:-

a. Closed stirrups
b. Bent-up bars.
c. Shear heads.
d. Stirrup and link with hooks at the tension face.
e. Continuous stirrups or cages of shear links.
f. Corrugated double-headed shear studs.
g. Stirrups or shear links.
h. Smooth double-headed shear studs.
i. Headed stirrups.
j. Steel offcuts.
k. Stirrups with a lap at the vertical branch.

.

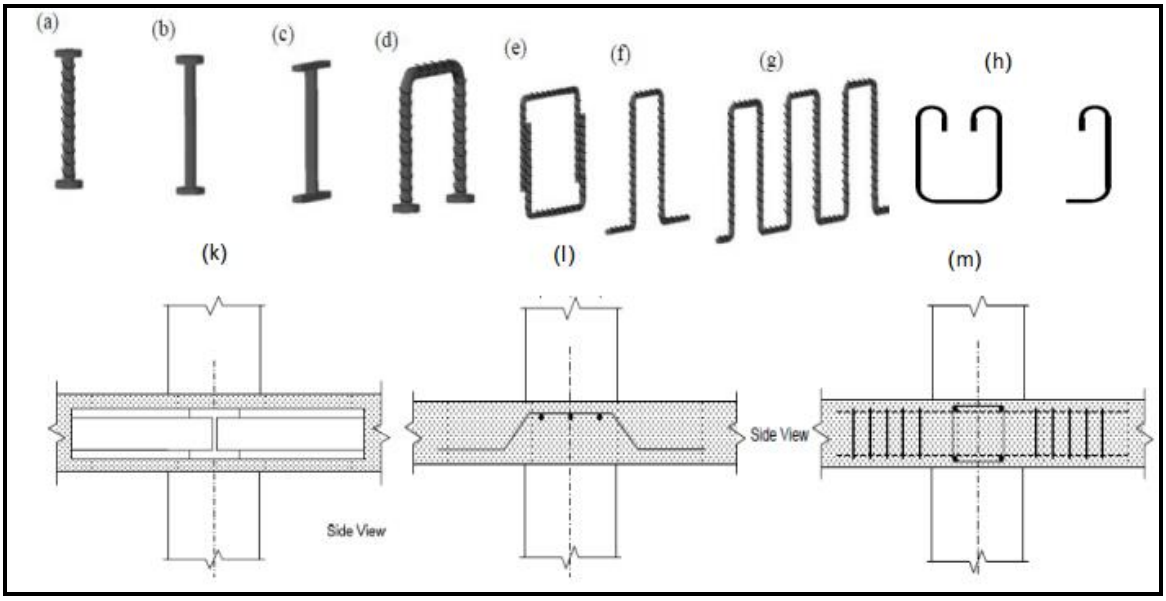

Figure (1-3): Systems of punching shear reinforcement **[15].**

1-3 Ultra-high-performance concrete (UHPC)

Ultra-High-Performance Concrete (UHPC) is a modern building mix that has been produced and improved recently in the world. UHPC is an extremely high-strength, durable and impermeable composite material which has driven its use in a diversity of exciting implementations **[16]**. Accordingly, it is extensively utilized in tall structures [16]. Therefore, the research on this concrete is worthwhile to investigate more new applications and uses.

In general, the election of substances and optimal proportions of components are very firm procedures for UHPC production [17]. Steel fibers are included in the UHPC mixture to improve the mechanical characteristics of the concrete members, especially their ductility. This type of concrete can be satisfied by reducing the water content and using superplasticizers (high-range water reducers) [18].

The structural behavior of post-peak flat slabs can be improved by adding high-strength steel fibers. This has an impact on the lower part of the stress-strain

curve, while the upper part is not affected. The following parameters can have an important influence on the lower part of the curve:

- The content and orientation of the fiber.
- Stiffness of fibers, especially in different fiber combinations.
- The fiber-matrix bond (surface properties, profiling, etc.)
- Fiber diameter and length (geometry), also when compared to the maximum particle size.

1-4 Objectives and Scope of the Study

This study aims mainly to investigate the influence of the below variables on the punching shear behavior of flat slab-column connections and ways to its improvement:

1. Studying the punching shear behavior in terms of load-carrying capacity, deflection, ductility, energy absorption, and failure modes of flat plate slabs.
2. Improving punching shear phenomena using UHPC in different places as a square or circle shape around the column with a dimension of (effective depth d, twice effective depth 2d & three-time effective depth 3d) in compression face to get the perfect region.
3. Studying the effect of replacing punching shear reinforcement by UHPC.
4. Developing a numerical finite element (FE) model for simulating the behavior of a hybrid flat slab by using normal strength concrete and UHPC.
5. Providing recommendations for researchers regarding the design of flat slabs with an optimized method to increase punching shear strength using UHPC.
6. Modeling all examined slab-column connections and comparing the experimental findings with the corresponding numerical ones to assure that the elements, substance characteristics, real constants and closeness criteria are satisfactory.

CHAPTER TWO

LITERATURE REVIEW

2-1 Introduction

This chapter deals with the most important analytical and experimental studies that investigated the structural behavior of the reinforced concrete slab. Previous studies related to the research topic were briefly reviewed. The various repair and strengthening techniques that contribute to the development of flat plates are among the most important topics addressed in this chapter.

Moreover, this chapter contains topics related to punching and shear failure of reinforced concrete flat slab in the presence or absence of the shear reinforcement. Also, the literature on shear failure in most types of flat plates was reviewed. Finally, former research on the repair and strengthening of reinforced concrete flat slab against punching shear failure were also presented.

2-2 Flat Slabs

2-2-1 Flat Slabs Supported on Shear Wall Corners

In 2020, Setiawan et al. [19] supported buildings with a shear wall around stairs and elevators, and by the transfer of loads from the slab to the walls, a punching shear (two-way shear) stress is formed in the slab connection area with the wall in addition to one-way shear as shown in Figure (2-1). Thus, punching shear design should be taken into consideration. The codes and studies did not focus on the failure of punching formed on the ends and corners of walls except for

a few of them, which made this topic subject to the diligence of engineers. That study included the problem of punching shear stress in flat slabs based on shear walls, by suggesting a method for design calculation for use in overlaps with the Critical Shear Crack Theory. The process is verified against test results for slabs booster on elongated columns as well as numerical emulation. The researchers carried out that numerical simulation using the nonlinear finite element theory, and the failure of the punching shear to be designed later.

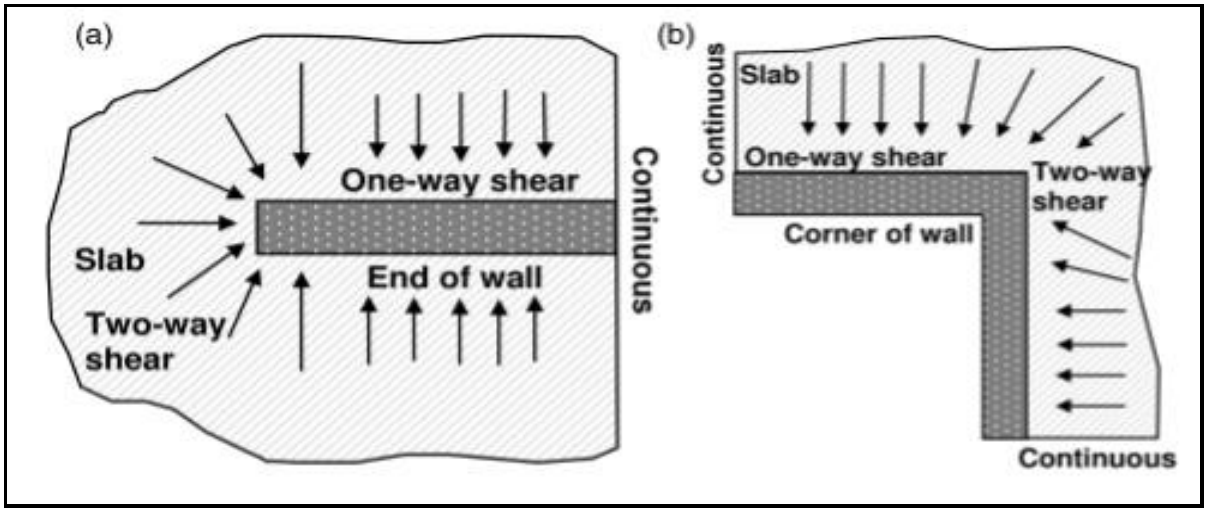

Figure(2-1): One and two-way shear forces transferred from the slab to the support at (a) end of the wall; (b) corner of the wall **[19]**.

2-2-2 Corner Flat Slab

In 1994, Neil and Amin [20] tested five models of flat slabs with corner columns to transfer the shear load. The parameters: the procedure of loading and the amount of shear steel reinforcement. It was found through their research that the American ACI 318-89 code and Standard CAN3-A23.3-M84 equations are conservative and can be improved by adding a part to the equation that includes the moments generated from eccentric shear stress as well as the distance needed for

the shear reinforcement steel. Furthermore, it has been found that the design method described in ACI 352.1R-89 [Clause 4.2.1.2(b)] may result in column-slab connection corner designs not being sufficiently secure.

2-2-3 Flat Slab with Openings

In 2014, Nazar and Thaar [21] prepared a study to find out the effect of openings on shear punching in flat slabs. The researcher used six flat slab models, one of the models does not contain openings, and the other one contained holes with different locations and sizes from the column. The holes were three sizes (100 * 100), (150 * 150) & (225 * 225) mm. The results proved that the resistance decreased, the greater the size of the opening and its distance from the column. The closer the opening is to the column, the less the slab can resist punching shear, also the opening next to the column was more negative on the resistance than the same opening next to the corner of the column. In addition to the effect of the openings on the stiffness, it decreases as the area of the opening. Figure (2-2) shows the crack pattern.

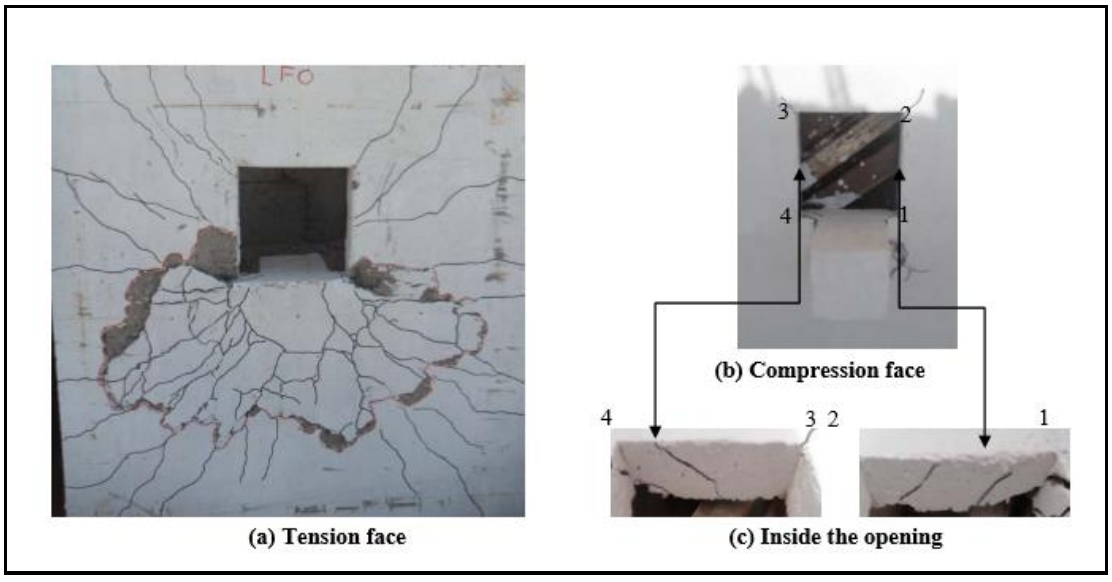

Figure(2-2): Cracks Pattern for Specimen (225×225 mm opening Size) after failure **[21]**.

In 2014, Nazar and Thaar [22] studied the effect of openings on the capacity of punching shear in flat slabs and strengthening them with (CFRP) sheets. Sixteen specimens were used, and all of them contain openings with different arrangements except for the reference model. The researcher used two methods of strengthening with carbon fibers. In the first method, one layer of fibers around the column and the opening was used, while in the second one two layers of fibers were used for half the distance of the opening. The first method was better, and in general, the strengthening of the carbon fibers restored the resistance in good proportions, ranging between 5.1% to 60.6%. addition to other engineering properties such as stiffness. Figure (2-3) shows the pattern of the cracks strengthened with CFRP sheets.

Figure(2-3): Cracks pattern and strengthened with CFRP sheets **[22]**.

2-3 Strengthening Techniques against Punching Shear

In 2014, Yan and Wang [23] used a new method to strengthen the punching shear, by using a steel tubular instead of the column that ends with the shear head which is made in more than one way, as shown in Figure (2-4). This method has good advantages, including ease of manufacture and speed of installation. In this study, the researchers used a circular and square tube, and the analysis was done using the finite element package (ABAQUS) and the results showed the success of

the strengthening idea. This type of strengthening is suitable for thinner slab thickness, this is because thin slab has little strength due to their small thickness.

In 2015, Meisami et al. [24] cast four flat plate specimens, designed according to ACI code 318-08, one without strengthening and the others with FRP strengthening placed after casting in the form of a three-arm fan. The lengths of the three propeller arms of the second, third and fourth specimens were 80 mm, 160 mm, and 240 mm, respectively. The results showed that the adopted reinforcement method can improve both the deformation capacity and ultimate bearing capacity in addition to avoiding the occurrence of brittle failure. It was also able to change the type of plate failure from shear to shear-flexural.

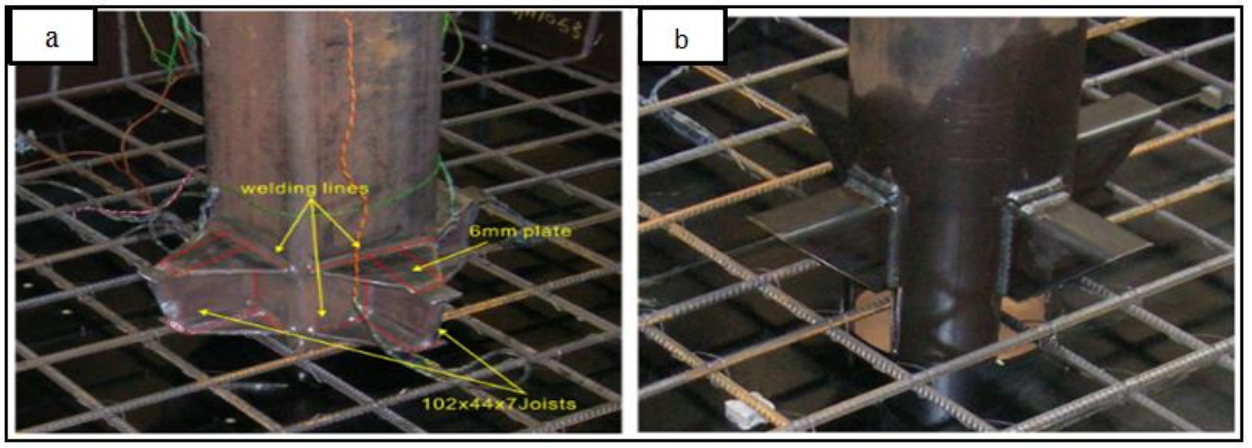

Figure(2-4): Two shear head arrangements (a) Shear head welded on the outside of the tube (b) Shearhead through tube **[24]**.

In 2018, Lapi et al. [25] there are many reasons of failure of the flat slab with a high punching shear as a result of design or implementation errors or non-compliance with the specification of the codes. Therefore, the researcher used several techniques for strengthening, including the use of shear steel reinforcement

and external reinforcement with polymers or layered concrete and a pre-tensioned system. It is also included in his study methods of strengthening from previous literature:

1. Anchored bolts with plate, washer, nut **[26]** and headed bolts **[26]**, Figure(2-5).
2. Bonded bolts **[27] [28],** Figure (2-6).
3. FRP (grids **[29]** or fans **[23]**), Figure (2-7).
4. FRP stirrups **[30],** Figure (2-8).

The researcher tries to find the keys to the problem by offering the possible strengthening methods to give the designer all possible options to choose the best. It was found that using post-installed reinforcement increases the resistance of the slab to shear punching and improves ductility, as applying FRP it can improve the strength a little.

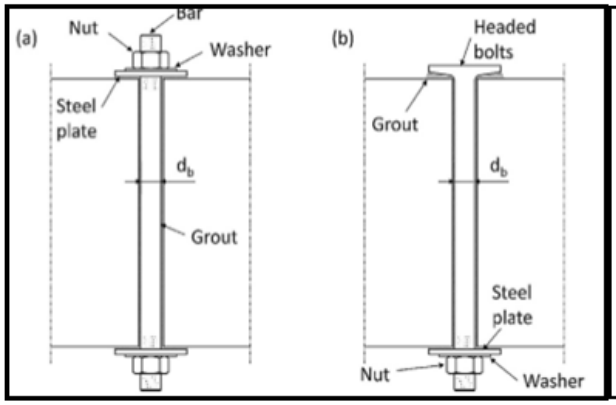

Figure(2-5): (a) Anchored bolts with nut **[26]**.
(b)head bolts **[26]**.

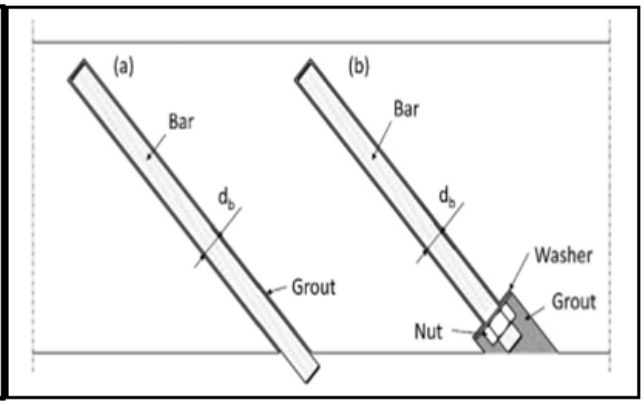

Figure(2-6): (a) Bonded bolts without anchorages**[27]**.
(b) Bonded bolts anchored at the bottom**[28]**.

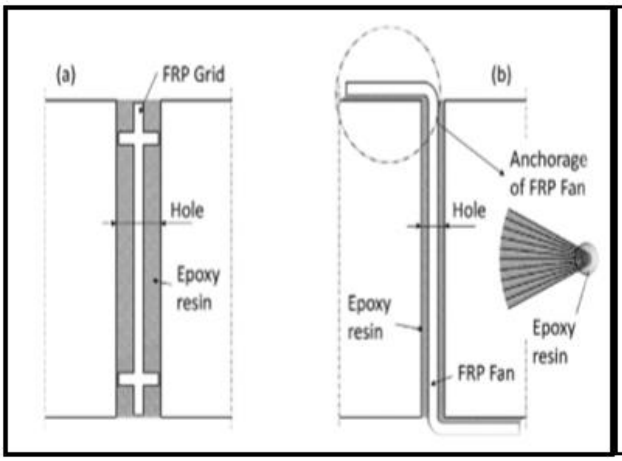

Figure(2-7): (a) FRP grids**[29]**. (b) FRP fans **[23]**.

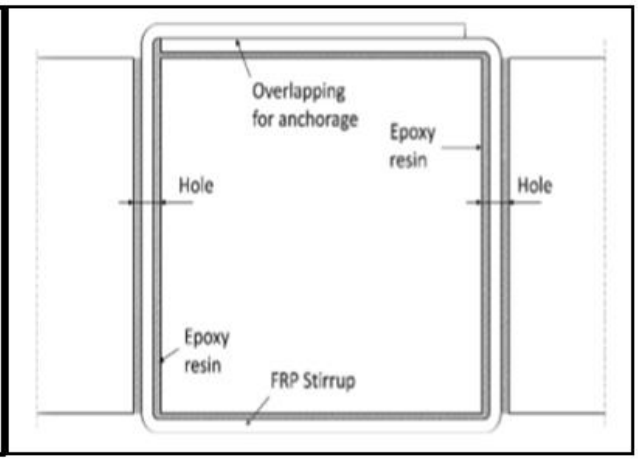

Figure(2-8): FRP stirrups**[30]**.

In 2021, Taresh et al.[31] Used a steel angle plate to strengthen the slab against the failure of punching. The plate was of column width and unequal in length relative to its two arms. It was placed so that the greater length was in the longitudinal direction of the column, in the same way, the plate was placed on top of the slab and they were connected by bolts as Figure (2-9a). The models were checked for failure limit Figure (2-9b), and it was found increases in the stiffness, energy absorption, and deformation capacity, as well as changing the failure type and pattern from punching shear failure to flexural failure and shear formed by flexural outside the reinforced area.

In 2021, Attaa and Haider [32] cast and tested six specimens to study the effect of column capital on shear resistance at the column edge not been practically studied, and this encourages researchers to study the subject. Six models were used, two of them as reference models. Of the four models, two of them contain a column capital with dimensions (300*400mm) and the other two with dimensions (500*800mm). Half of the models have an axial load and the other half have an eccentric load (and the eccentricity of the load may come from wind loads or earthquakes, etc.).

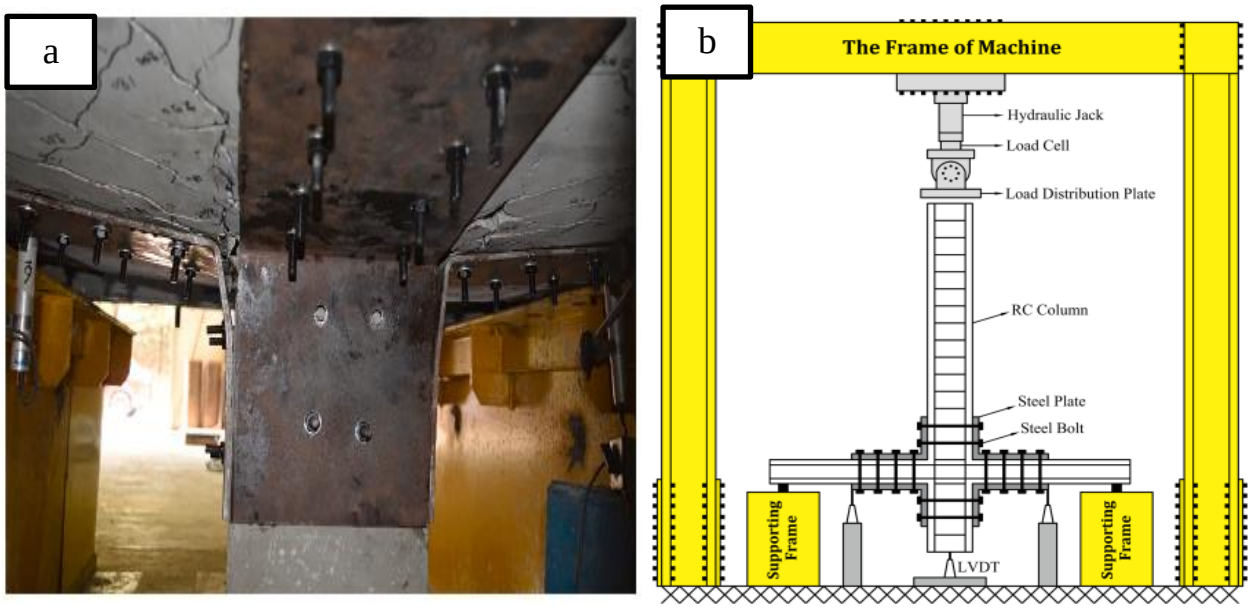

Figure (2-9): (a) specimen after testing and (b) Schematic of typical test set-up **[31]**.

The tests produced an increase in punching shear strength in the two specimens with axial load (17-27.66%) for the reference specimen and two specimens with eccentric load (18-25%) for the reference specimen as shown in Figure (2-10). The shape of the column capital is also effective, if this shape is rectangular, it gives a failure perimeter greater than the failure perimeter formed by the head of a square column of the same area.

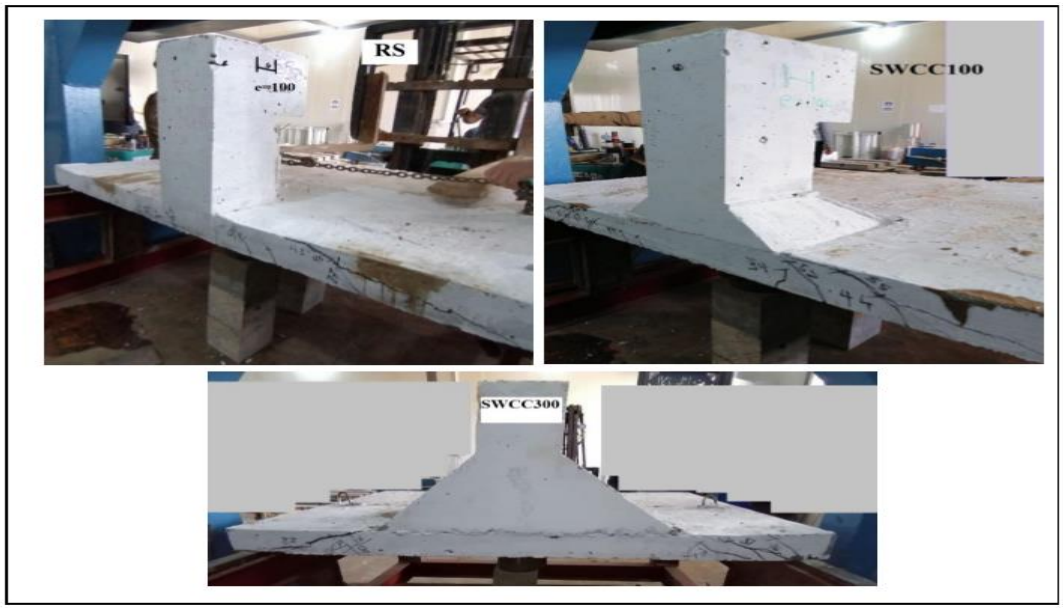

Figure (2-10): Flat slab-edge column **[32]**.

In 2021, Zainab and Munaf [33] studied column head flat slab strengthening against punching shear failure. Six plate samples were executed, two of which were tested as a reference (having no shaft head), one with axial loading and the other with eccentric loading, (biaxial loading). Four samples had a column head in two sizes (600 x 600 and 800 x 800 mm), the slap dimensions were (1600 x 1600 x 100 mm), the column dimensions were (200 x 200 mm), and the eccentricity of the biaxially loaded slab was 150 mm in both directions, Figure (2-11).

The results indicated that (for models strengthened with column capital) the increase in shear strength using column capital ranged from (13 to 25%) for (200 x 200 mm) dimensions with eccentric bi-axially loaded, as well as the deflection increased by about 30% for dimensions with column capital (800*800 mm) compared with the reference models. As well as the shape of the failure shifted from the expected circular shape to the rectangular shape.

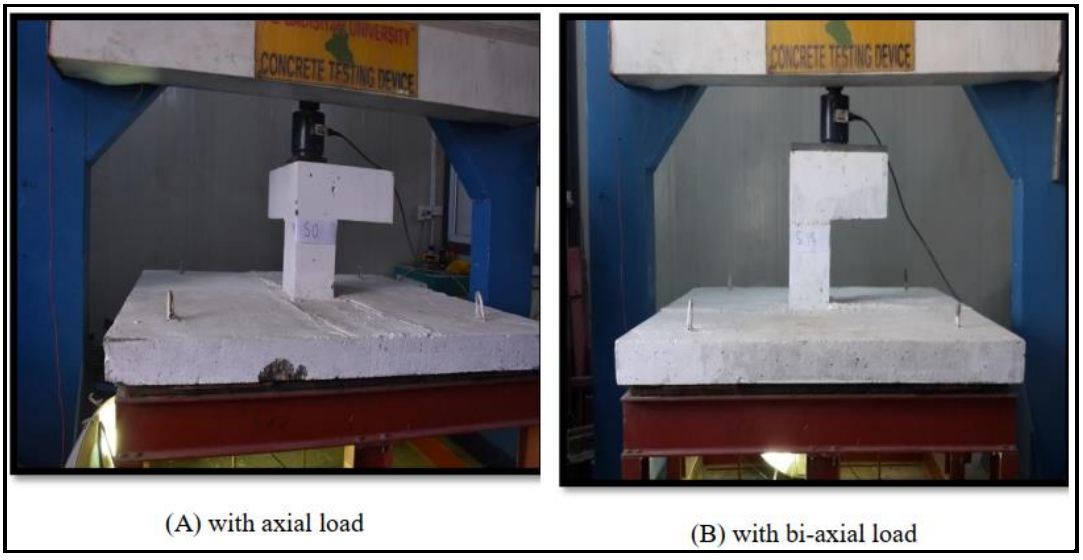

Figure(2-11): References sample test setup **[33]**.

2-4 Shear Reinforcement Strengthening Punching Shear

To bypass adding column heads, beams or drop panels, it is possible to increase the shear capacity of the slab by using shear reinforcement. Several types of shear reinforcement are available such as shear heads stud, open-legged stirrups, closed stirrups, bent-up bars, etc. as illustrated in Figure (2-12). In this study will be on closed stirrups that will be used in this research. Figure (2-13) shows the (ACI Committee 318 2014) limitation and the way of arranging the stirrups.

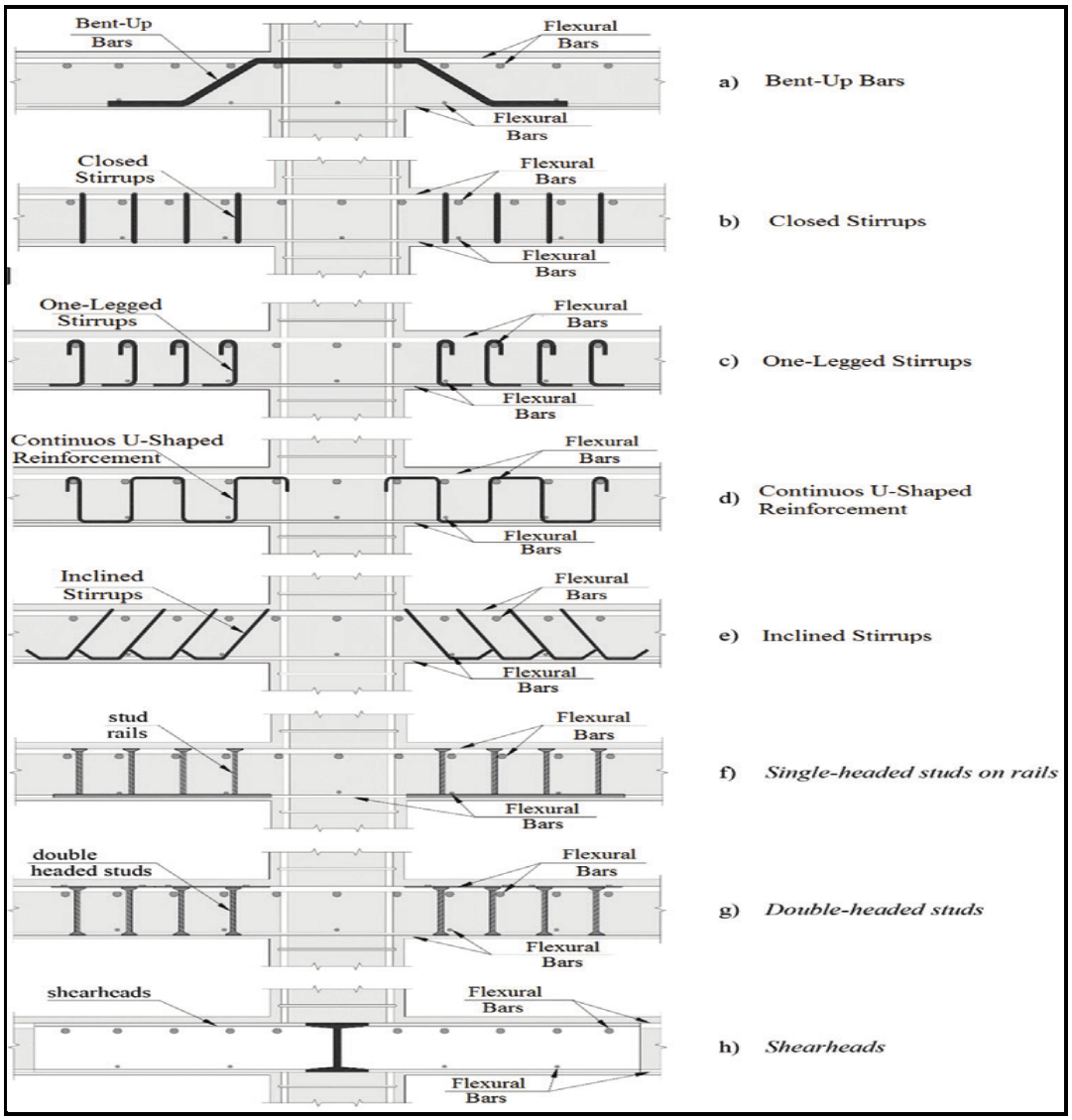

Figure (2-12): Types of shear reinforcement used in slab-column connections **[34]**.

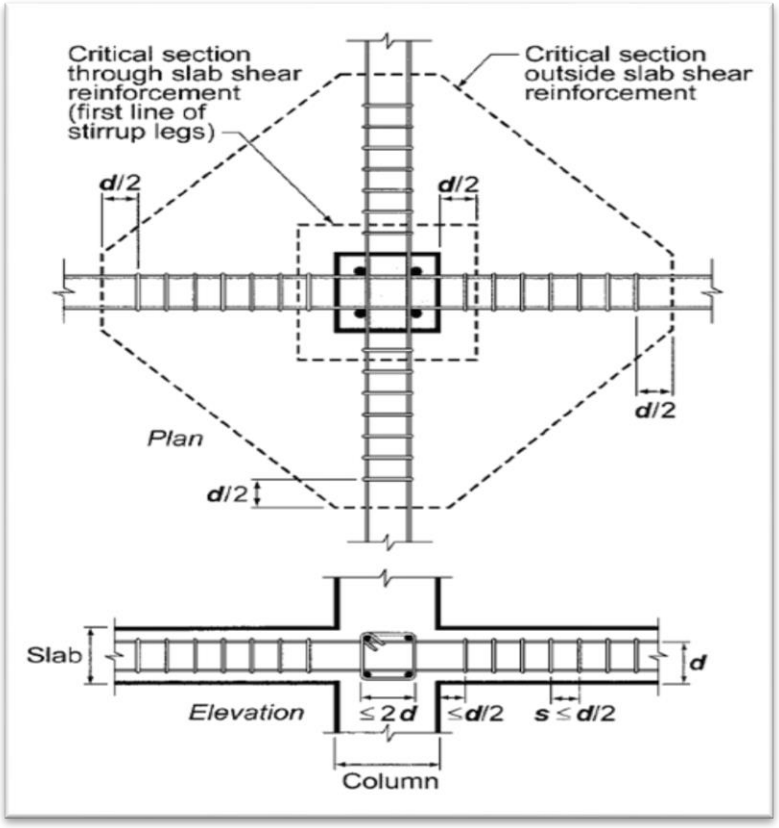

Figure (2-13): Closed stirrups in the flat slab (ACI 318-19) **[35]**.

In 2019, the behavior of flat slabs containing different types of punching shear reinforcement with an average compressive strength of 35 MPa was studied by **Sulaiman Nayef et al. [36].** These types included bent bars, open stirrups and closed stirrups, which were subjected to a concentric compressive load. Twelve slabs of similar dimensions (1100 x 1100 x 120 mm) were cast, containing a square column in the middle (150 x 150 x 400 mm). To ensure that punching failure occurs before bending failure, a bending strengthening ratio of 2.22% is adopted. The cracking pattern, steel strain, deformation and maximum capacity were monitored and recorded during the test. The following was concluded from the test results:

1. The greater the number of closed stirrup branches, the greater the punching capacity for the same diameter. A profit of 10% is achieved in punching capacity for the equal number of branches (4) compared to the reference sample.
2. The addition of vertical shear reinforcement in the form of closed stirrups (8 mm diameter with two branches) led to an increase of (6.67%) in the final punching capacity compared to the control sample, and therefore its effect is considered small on the punching shear capacity of the flat slabs.
3. Increasing the diameter of the closed stirrup leads to improved strength. The increase in punching shear resistance as a result of using diameter stirrups (12 mm with two branches) was about (13.8%) compared to the reference sample.
4. Use of vertical shear reinforcement as an open leg (8 mm diameter with 2 and 4 branches) results in a small boost in punching capacity. The growth in punching force capacity was (5.3%) in comparison to the control sample.
5. Raising the diameter and branches of the open leg increase the punching force of the slab by about (24.7%) more than the reference sample.
6. The addition of shear reinforcement in the form of bars bent at an angle of 45 degrees results in higher punching force. The resistance of the slabs excessed by about (51.1%).
7. In terms of ductility (defined simply as the ability of a material to change shape without losing its strength or breaking) afforded by the various types of punching shear reinforcement, closed stirrups impart the greatest ductility. The percentage of increase in ductility was about (131.6%) compared to the control sample.

2-5 Improving Punching Shear Flat Slab by Hybrid Concrete

2-5-1 Hybrid High-Strength Concrete

In 2018, Suha and Haitham [37] studied the punching shear behavior in flat reinforced concrete slabs cast using hybrid concrete. In that study, it was concluded that in the samples made using high-strength hybrid concrete, the final strength of the samples was increased by about (20%-50%) compared to the normal concrete (NSC). Whereas for the samples poured with high-strength concrete only, the maximum load capacity of the tested slabs increased by about (14% - 40%) compared to the normal-strength concrete only. Also, it was found that the amount of rebar has no significant effect on the value of the first cracking load, but it does have an effect on the value of the final load. Depending on the final shape of the collapsed perimeter, samples cast with high-strength and hybrid concrete increased significantly compared to only normal-strength concrete.

2-5-2 Using Reactive Powder Concrete

In 2021, Mohammed M. Kadhum et al. [38] investigated ten specimens of reactive powder concrete (RPC) and two of normal concrete(NSC) simply supported flat slab, with the parameters of the study, the thickness of the slab and the presence or absence of flexural reinforcement, the researchers divided the specimens into three groups according to the proportion of steel fiber in the mixture, which were (1, 1.5& 2%).

The results showed an increase in the resistance of the slab to shear punching by increasing the proportion of steel fiber (RPC), the thickness of the slab, and the presence of steel reinforcement. The results led to an important conclusion, which is that it is possible to produce a slab (RPC) without steel

reinforcement of flexural and with good resistance to punching shear, and this is useful for the designer who requires him to reduce the reinforcement in this area in addition to the benefit of reducing weight and cost.

The slab (RPC) is more ductile to failure than its counterpart from (NSC) and the addition of steel fiber shows a reduction in the width of the cracks.

2-5-3 Using Mortar Infiltrated Fiber Concrete with Different Fibers

In 2017 Azoom and Rama [39] tested ten slabs with mortar-infiltrated fiber concrete cast with varying types of fiber (steel, polypropylene, and hybrid fibers) in different ranges of volume fraction. The specimens with dimensions of (600 * 600 mm) and thickness of 50 mm are adopted for punching shear studies as shown in Figure (2-14). The mix contained cement, ground-granulated blast-furnace slag (GGBS) and sand are taken in the ratio (1:1:2). Water to binder ratio(*w/b*) adopted is (0.45) and the superplasticizer dosage is found to be (1%). From this study, the following points concluded: -

1. The punching shear of the mortar-infiltrated fiber concrete slabs is much higher than that of NSC and was up to 9 times with steel fibers. While 2 times with polypropylene fibers and 3 times with hybrid fibers.
2. Punching strength increased with an increase in fiber volume varied from 2 to 12 times in the case of polypropylene fibers and from zero to 27 times in the case of specimens with steel fibers.
3. Mortar-infiltrated fiber concrete slabs with a higher volume of fiber possessed a higher deflection zone (dispersion angle).
4. Impact resistance was also found much higher for mortar-infiltrated fiber concrete specimens up to 10 times with steel fibers and 7 times with polypropylene fibers compared to NSC.

Figure (2-14): Experimental setup **[38]**.

In 2020, A. S. I. Shwalia e. al. [40] studied a process for the strengthening of punching shear by hybrid concrete (mortar infiltrated fiber concrete(MIFC) and normal concrete (NSC)) for eight samples of flat slabs with identical dimensions and reinforcement and the method of loading except one that contains punching shear reinforcement two of the samples from (NSC) as control samples and the coefficients were thickness (MIFC) either all thicknesses or half in the pressure or tensile area and the other variable is the area (MIFC) (0.5d, 1d, 1.5d) where d the effective depth from the face of the column. The two types of concrete were poured together as in Figure (2-15). After the examination, the results showed an improvement in the punching shear resistance of the excitable hybrid plates in the control sample, especially in the sample (1.5d) for half the thickness in the compression area directly under the column, reaching (MIFC) in addition to placing (1.5d) under the column that acts as a pillow to distribute the load. And

also, the use of (MIFC) made the failure not sudden. The study proved the use of hybrid fibers leads to an ideal distribution of the fibers.

Figure (2-15): A: Spread the fiber by multi-layers technique and B: Pour the mortar after completing the layer of fiber **[40]**.

2-6 Ultra-High-Performance Concrete

Primary attempts were in the 1980s by Hans Hendrik Bache on compacted reinforcement concrete, which contributed with French contractors Bouygues, were cooperated with Lafarge to develop a new mix of reactive powder concrete RPC **[41]**. The RPC is known as commercialized of the UHPC **[42]**.

2-6-1 Ultra High-Performance Concrete (Materials)

In 1995, Richard and Cheyrezy [43] worked on developing an ultra-strong ductile concrete called RPC (Reactive Powder Concrete). There were two types of concrete: RPC200 and RPC800. Four groups of the mixture were performed in the presence and absence of fibers. Each group of mixtures is changed from the other by post-treatment with heat as well as by adding crushed quartz. The optimum fraction of silica fume content was 25% of the cement content. The envelope

numbers for optimal compressive strength values obtained for different relative density values of RPC concrete, with or without fibers, for both ambient and heat-treated (9 °C) samples are presented in Figure (2-16). The results also revealed that the compressive strength is highly dependent on the relative density compressed upon demolding. The addition of small-size steel fibers (0 = 0.15 mm L = 13 mm) in the ratio of 2-2.5% for each size gave ductile behavior to RPC.

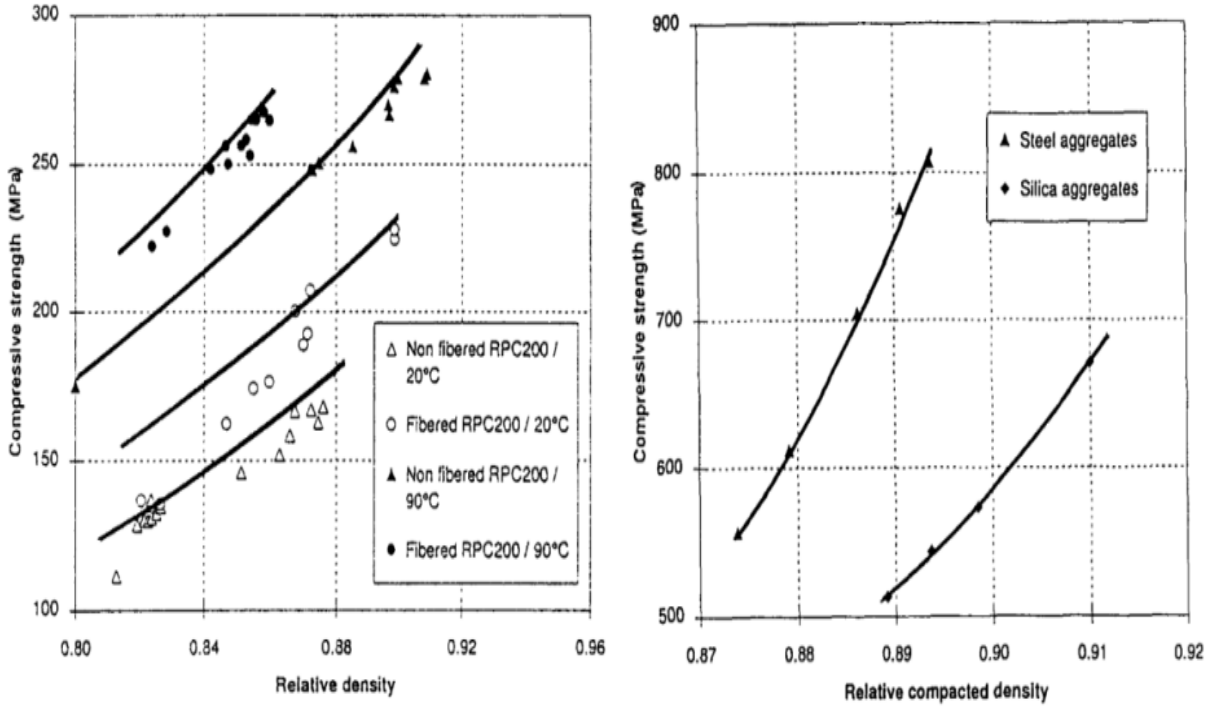

Figure (2-16): Variation in strength with relative density **[43]**.

I**n 2006, Yazici et al. [44]** investigated the effect of aspect ratio (length to the diameter of steel fiber). Also, the fraction volume of the steel fiber reinforced concrete, SFRC, on the mechanical properties of the concrete. Three different types of hooked ends with aspect ratios of 45, 65, and 80 were used. In addition to three fraction volume contents of 0.5%, 1.0%, and 1.5% of steel fiber, were adopted. The experimental program consisted of ten mixtures, one as a control while the other nine were varied. The aggregate is classified into three sizes; 30% for size (0-3) mm, 30% for size (3-5) mm, and 40% for size (5-15) mm. The results obtained that

the increment content of steel fiber reduced the workability of the mixture. The steel fiber possesses a higher aspect ratio with a high fraction content that will be enhanced the mechanical properties of the concrete, as listed in Table (2-1).

Table (2-1): Steel fiber content, aspect ratio, and test results **[44]**.

Mix type	l/d, aspect ratio	Fiber content %by volume	Compressive strength MPa	Split tensile strength MPa	Flexural strength MPa
CC	0	0	49.1	4.06	5.94
SFRC1	45	0.5	50.8	4.5	6.14
SFRC2	45	1.5	53.7	4.69	6.32
SFRC3	45	0.5	57.7	5.69	7.75
SFRC4	65	0.5	53.5	4.51	6.24
SFRC5	65	1.0	58.3	4.77	8.08
SFRC6	65	1.5	56.4	6.25	9.33
SFRC7	80	0.5	56.0	5.58	6.42
SFRC8	80	1.0	58.3	5.18	9.74
SFRC9	80	1.5	52.1	5.9	10.76

In 2011, Allena and Newtson [45] developed the UHPC mixture, which is dependent on local and affordable materials. Type (I/II) Portland cement, silica fume, and fine local sand (75-600 µm) from Las Cruces, New Mexico, and a poly-carboxylate-based HRWRA (Glenium 3030 NS from BASF chemicals), were used. Seven mixes were conducted. Also, cubic specimens of 50mm and cylindrical

specimens with a height of 200 and a diameter of 100mm were used, and three groups of curing were conducted. The first group was cured by ambient temperature until the age of the test. The second regime was achieved by immersion of specimens in the heat bath water of 50C^{O} until the day of the test. The third regime was the same second but removed the samples from heated water and exposed them to dry heat of 200 ºC for the latest two days before the test day. The study showed that prolonging the mixing period increased the workability of the mixtures. Also, the curing by oven drying attained greater strength than the specimens, which were cured by moisture in a 50ºC water bath.

In 2012, Wasan, [46] investigated the properties of the UHPC, namely compressive strength, splitting tensile strength, modulus of rupture, impact strength, and static modulus of elasticity. Three types of HRWR (superplasticizer) were also conducted by three proportions of the best one to find the optimum dosage. The results revealed the effect of the water reducer on the compressive strength. Two types of silica fume were considered the first one as a replacement of cement percentage while the other as an added percent of cement. Generally, the mixture with 15% of silica fume replacement of cement and added 5% of silica fume have the best compressive strength. All specimens were cured by immersion in hot water after 48 hours for a different period with a rate of heating of 20C^{O} per hour until it reached a constant temperature of 60 ºC. The results indicate that the compressive strength of concrete is increased by about 9% for 1% crimped steel fibers, as shown in Figure (2-17).

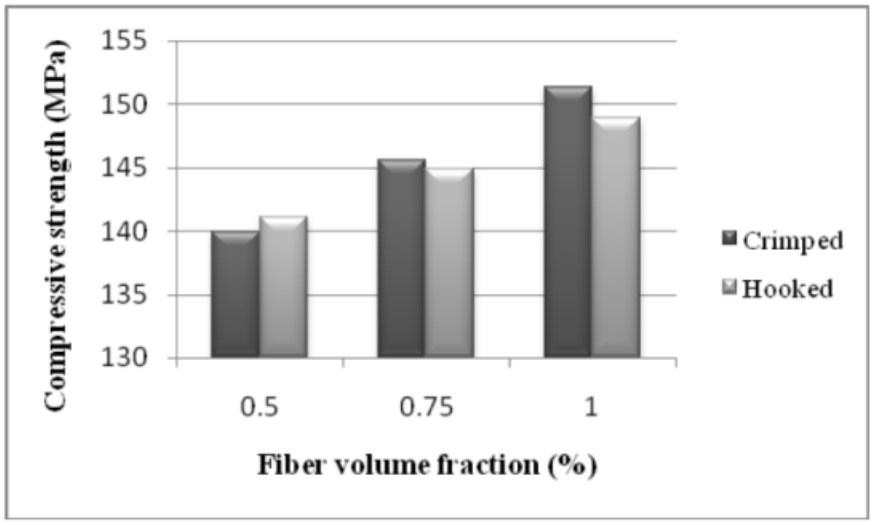

Figure (2-17): Effect of fraction and type of steel **[46]**.

In 2016, Hoang et al. [47] introduced a novel approach to the mix design of UHPC. That program was based on the progressive improvement of particle packing density and strength by discovering conformable affordable substances such as; cement silica fume, superplasticizer and quartz powder. The impact of using four-grain size of fine aggregate: 1 mm, 2.5 mm, 4 mm, and 8 mm without any special treatment on the compressive strength was investigated. Fine aggregates are classified according to their small particle size, so the aggregates are mixed with the other types of fine aggregates to obtain the optimal packing density. An experimental mix was performed to find the optimal cement-water ratio which was found to be equal to 25%.

In 2018, Pourbaba et al [48] investigated the effect of age and steel fiber dosage on the compressive strength of the UHPC matrix. About 112 specimens were tested in periods varied from 2 to 42 days, and the dosage of fiber-reinforced varied from 0 to 6%. This study also examined the modulus of elasticity of cylinder specimens. Seven specimen groups were conducted. For each group, the content of steel fiber varied, while the age of the test was different in one group. The study

revealed that the compressive strength increased when the content of steel fiber increased and the age increased, as demonstrated in Figure (2-18).

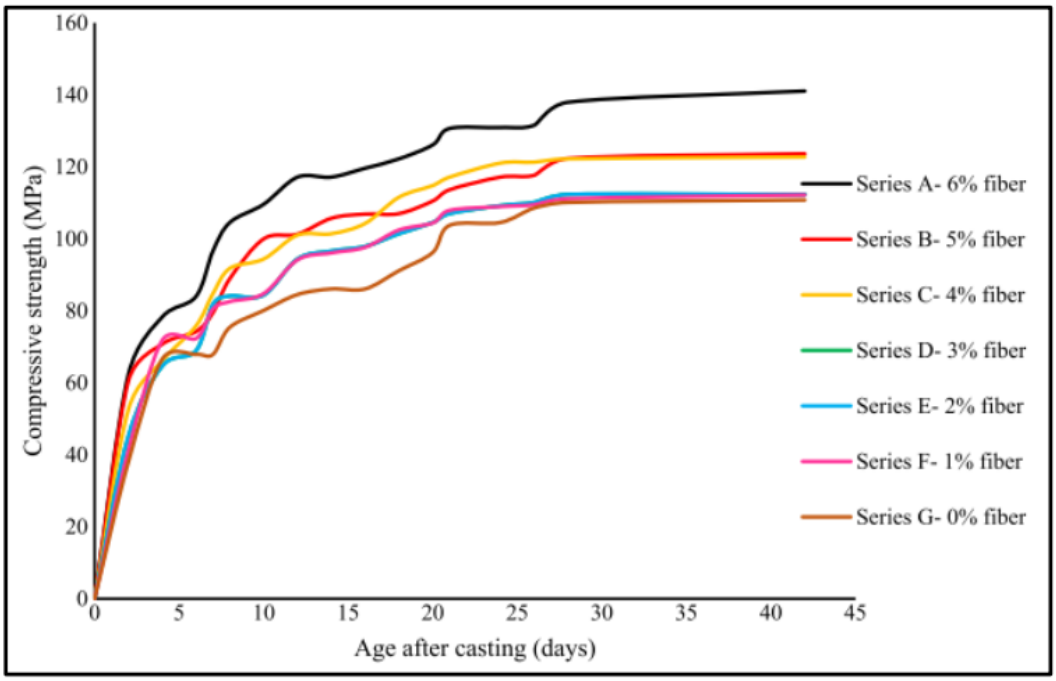

Figure (2-18): Compressive strength of tested UHPC specimens in terms of concrete age **[48]**.

In 2020, Dhafer & Haitham [49] produced Ultra-High-Performance Concrete (UHPC) from some of the available materials in order to reach the optimum percentage of its components (UHPC), see Table (2-2). The researchers experimented with four steel fiber ratios (0, 1.5, 3 and 4%) to study the mechanical properties of UHPC. The mixing process started with the addition of dry materials (cement, fine sand, and silica fume) to the mixer, then potable water and plasticizer were added, and finally, the required volume of steel fibers was added, according to ACI 544R.

Accelerated curing by hot bath water was applied. The results indicated an improvement in the compressive strength, (which was influenced by the size and shape of the mold), the indirect tensile strength (which was measured in terms of

the splitting test and flexure rupture method) and modulus of elasticity (which was arrived at 90000 MPa at 4.5% steel fiber) with the higher the of percentage steel fiber.

Table (2-2): Proportions of components per one cubic meter.

Cement, kg/m^3	Fine sand, kg/m^3	Replacement Silica Fume, kg/m^3	Added Silica Fume, kg/m^3	w/cm ratio	HRWR L/m^3	Steel Fiber, kg/m^3
900	1050	100	100	0.2	45	117.75 235.5&353.25

2-6-2 Ultra High-Performance Concrete in Flat Slab

In 2019, Wu et al. [50] proposed a flat plate slab specimens of hybrid concrete (UHPC-NSC) overlay, using a proposed model for analysis in addition to the analysis with the finite element theory using a program (ABAQUS), and the study parameters of the concrete tensile strength (NCS and UHPC) and thickness (NSC and UHPC) in addition to the effect of longitudinal reinforcement steel. The models were different in terms of reinforcement and thickness.

They concluded the application of UHPC overlay leads to largely load-carrying capacity and deformation capacity, and thus can be a consideration for modern existing RC flat plates, Longitudinal reinforcement steel has little effect on punching shear strength Figure (2-19) shows different steel reinforcement ratios

between specimens, and thickness of the layer (UHPC) has a positive effect on improving the shear ability of the punching, but to a certain area, then its effect becomes small. Usually, a thin layer (UHPC) is acceptable due to weight and cost considerations.

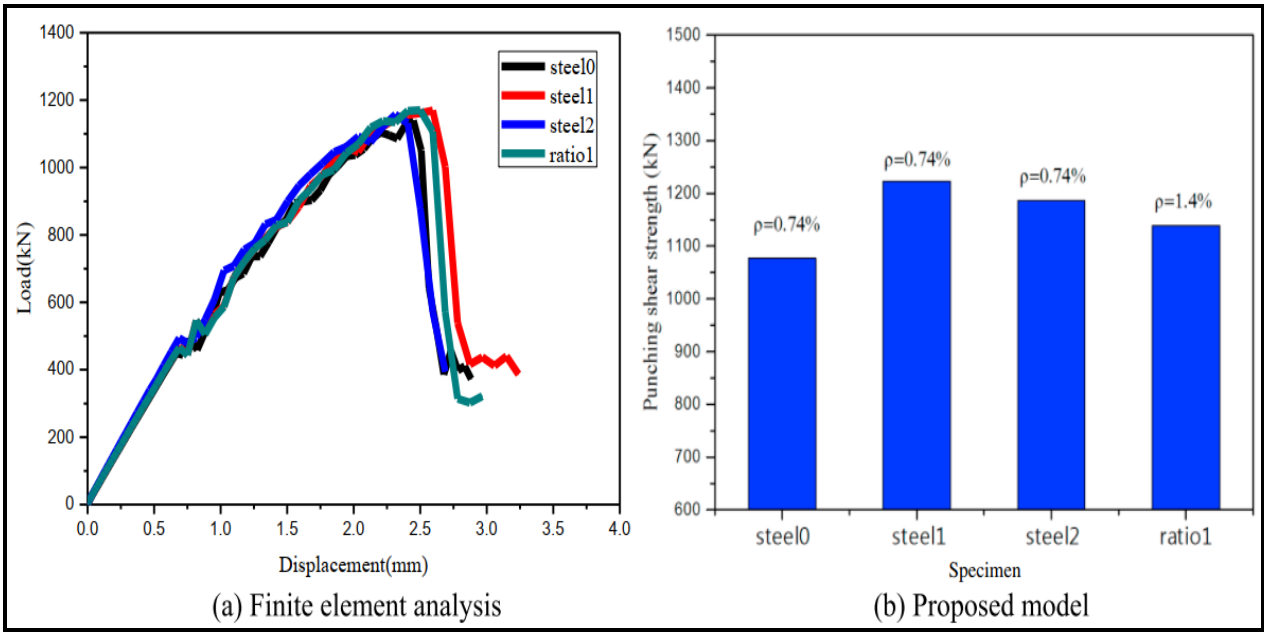

Figure (2-19): Punching strength affected by longitudinal bars **[50]**.

In 2019, Andreas et al. [51] studied flat plates with dimensions (600*600 mm) and four different thicknesses (12, 22, 32 & 42mm) of high-performance concrete (UHPC) with a ratio of steel fiber (3%) were poured and tested experimentally to calculate the shear strength of punching and bending and used **Moreillon [52]** models, to calculate punching shear and to compare with experimental results. It shows that the slab of small thickness (12 & 22 mm) fails to the punching shear, and the slab (32 & 42 mm) fails to the flexure, figure (2-20). Suggested equations for calculating inappropriate punching shear, the thickness of the billet is effective in cutting punching, but it needs a model to calculate it accurately.

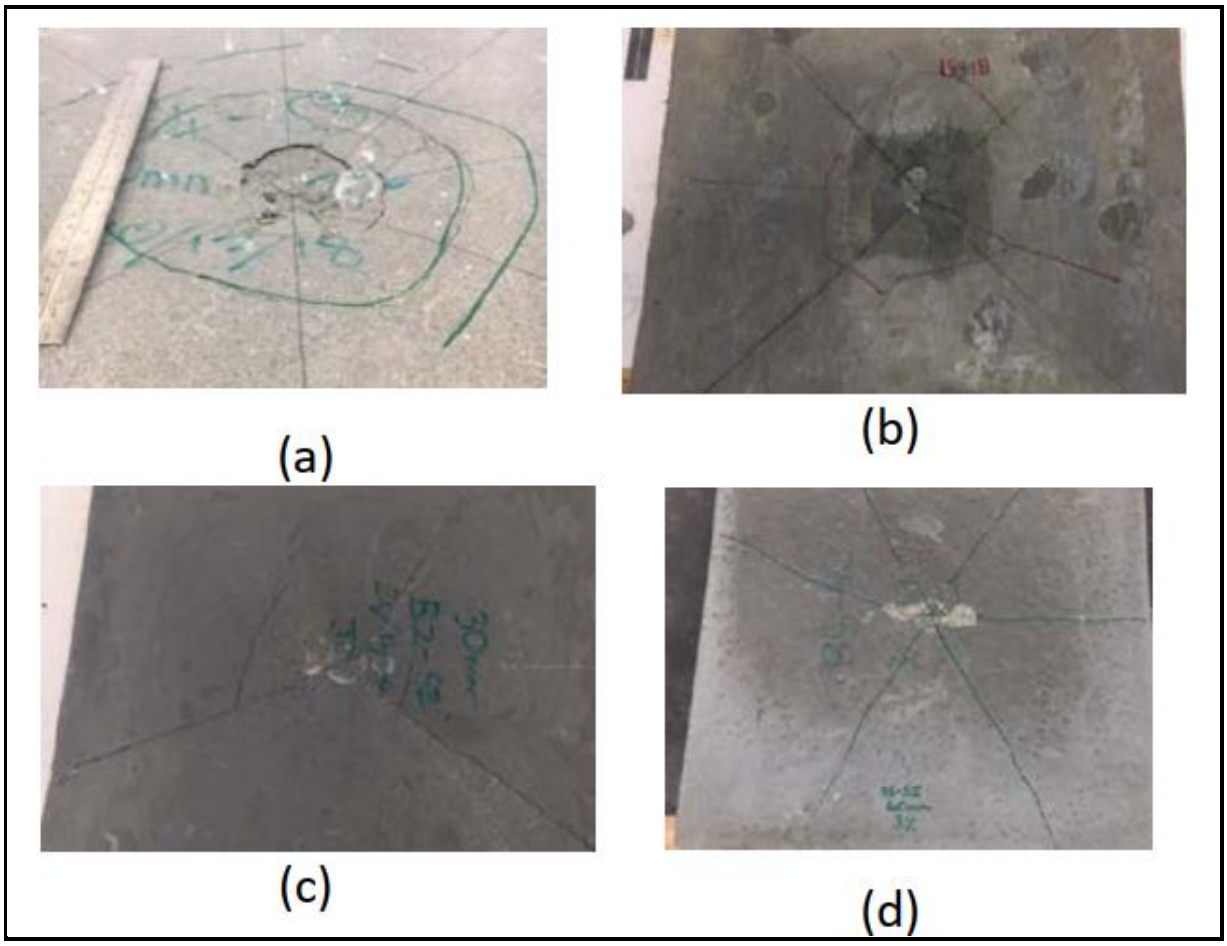

Figure (2-20): (a) & (b) Punching shear failure. (c) & (d) flexural failure **[51]**.

In 2021, Kadhim et al. [53] made a theoretical study using a non-linear finite element (FE) model by ABAQUS, depending on practical research conducted by **Zohrevand et al. [54]** (Experimental background), see Figure (2-22). Then the validated model was used to explore the influence of UHPC compressive strength, UHPC area, column size and slab thickness. The results indicated that code models including ACI 318-14, Eurocode2, and the model in Code 2010 cannot accurately estimate punching shear capacity for reinforced UHPC slabs and hybrid NC/UHPC slabs. Accordingly, the researchers have proposed to modify the existing ACI equation, so they suggested their study model shown below which showed improved accuracy:

bo =max[4(*c*+*d*) or 4L]

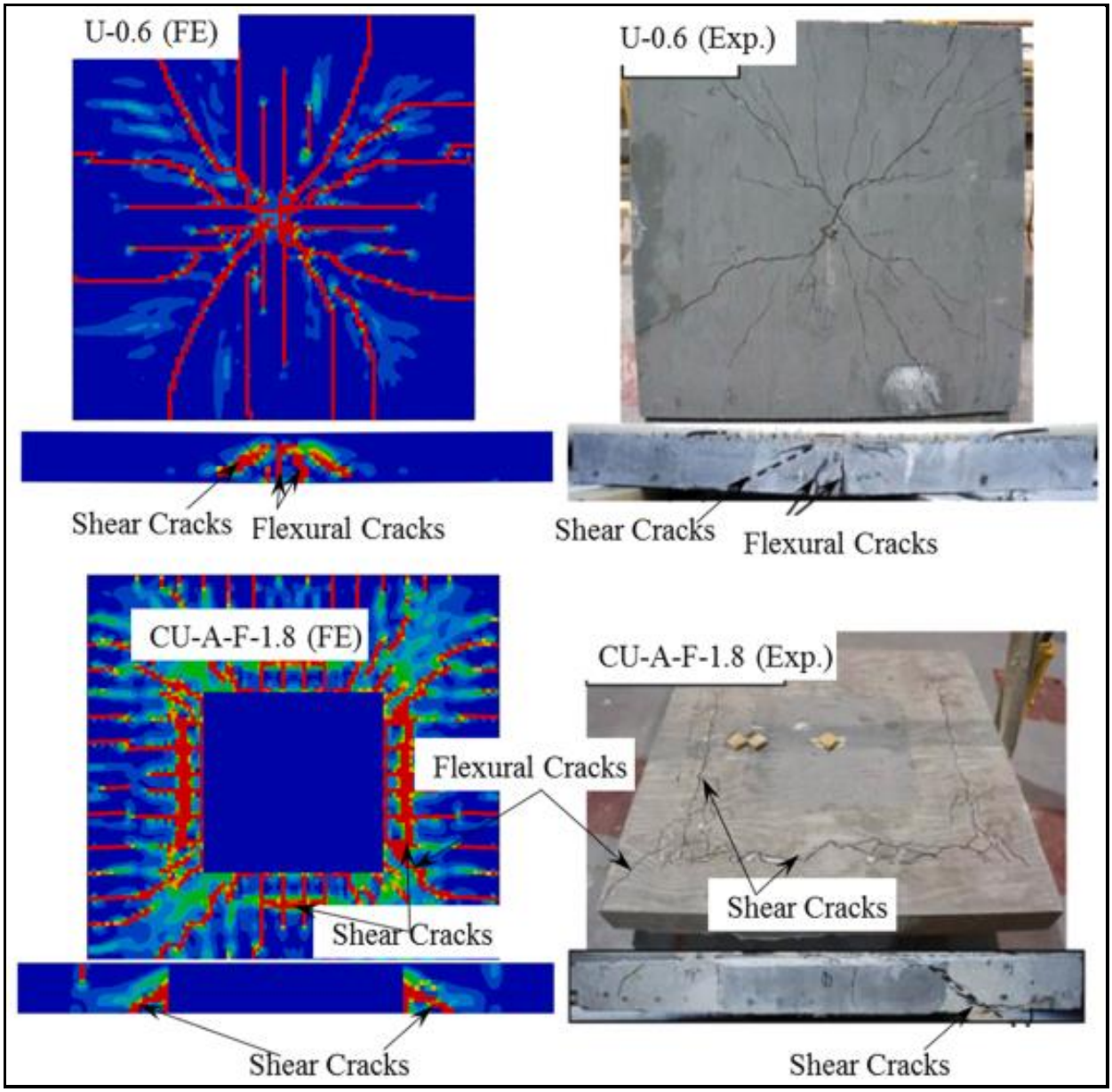

Figure(2-21): Validation study comparison of numerical **[53]** and experimental **[54]** crack patterns.

2-7 Summary and Concluding Remarks

From the previous studies on the behavior of reinforced concrete flat slabs with and without column capital, strengthened or no strengthened, many remarks can be summarized, as follows:

1. There are two stages to improve the punching shear behavior of column slab connections. The first relates to newly established connections and the other to strengthening existing ones.
2. There are two types of studies of shear strengthening studies for punching in flat slabs, one is a direct improvement of the capacity in shear, and the other is an indirect improvement of the capacity in flexural.
3. Many researchers have come up with ways to eliminate brittle punching failure and transform failure mode into flexural-shear failure or flexural failure.
4. Slab thickness and longitudinal rebar are factors affecting the shear capacity and researchers used them to improve the capacity and are variables for their study. However, the compressive strength of concrete is an important factor and it can be developed using special types of concrete.
5. Most of the studies that used hybrid concrete were (NSC) the main material in which their results are compared with codes, but other types of concrete do not have a code to compare the results, only equations are used that were concluded by previous researchers.
6. When using special types of concrete in the literature, the focus was on those whose compressive strength did not exceed (100 MPa). While high-performance concrete was used only by some researchers who used it for the whole slab (which is not economical) or to treat it as an external strengthening.

7. Most of the studies that dealt with UHPC focused on it as a construction material, for example, the type and proportions of its components, its mechanical properties and the proportions of steel fibers.
8. Replacing the reinforcement bar for the punching shear as per the code, with a special type of concrete gives an important solution to the designers because of the density of the reinforcement in this area.

CHAPTER THREE
EXPERIMENTAL WORK

3-1 INTRODUCTION

Details of the experimental program implemented in the current study are provided in this chapter. It was conducted to evaluate the structural behavior of simply supported flat slabs with or without strengthening against punching shear failure, and to better understanding of their effects. The experimental investigation was carried out by testing fifteen specimens of reinforced concrete flat slabs to obtain the most reliable data of load-deflection response, cracking pattern and to evaluate the ultimate load and the failure modes. A series of tests were also conducted on small samples such as cubes, prisms and cylinders for the various mixtures under study to determine the mechanical properties of the produced concrete and compare its results with the control mixture.

In the design and planning phase for the current study, the experimental program includes strengthening slab using hybrid concrete, Ordinary Concrete and Ultra High Performance Concrete (UHPC). The variables that we focus on mainly area, shape and depth (UHPC), also their optimum use. The experimental program involves slab specifications, preparation and test of the materials, test setup, and general instrumentation. This chapter explains the research method only while **Chapter Four** will provide and discuss the results obtained from the tests mentioned. The flowchart presented in **Figure (3-1)** indicates the total experimental investigation.

3-2 DETAILS OF THE TESTED SPECIMENS

The slab specimen is identified by symbols as seen in **Figure (3-2)** to facilitate the comparison between a large number of investigated slabs in this research. **Figure (3-3)** shows an example of specimen identification.

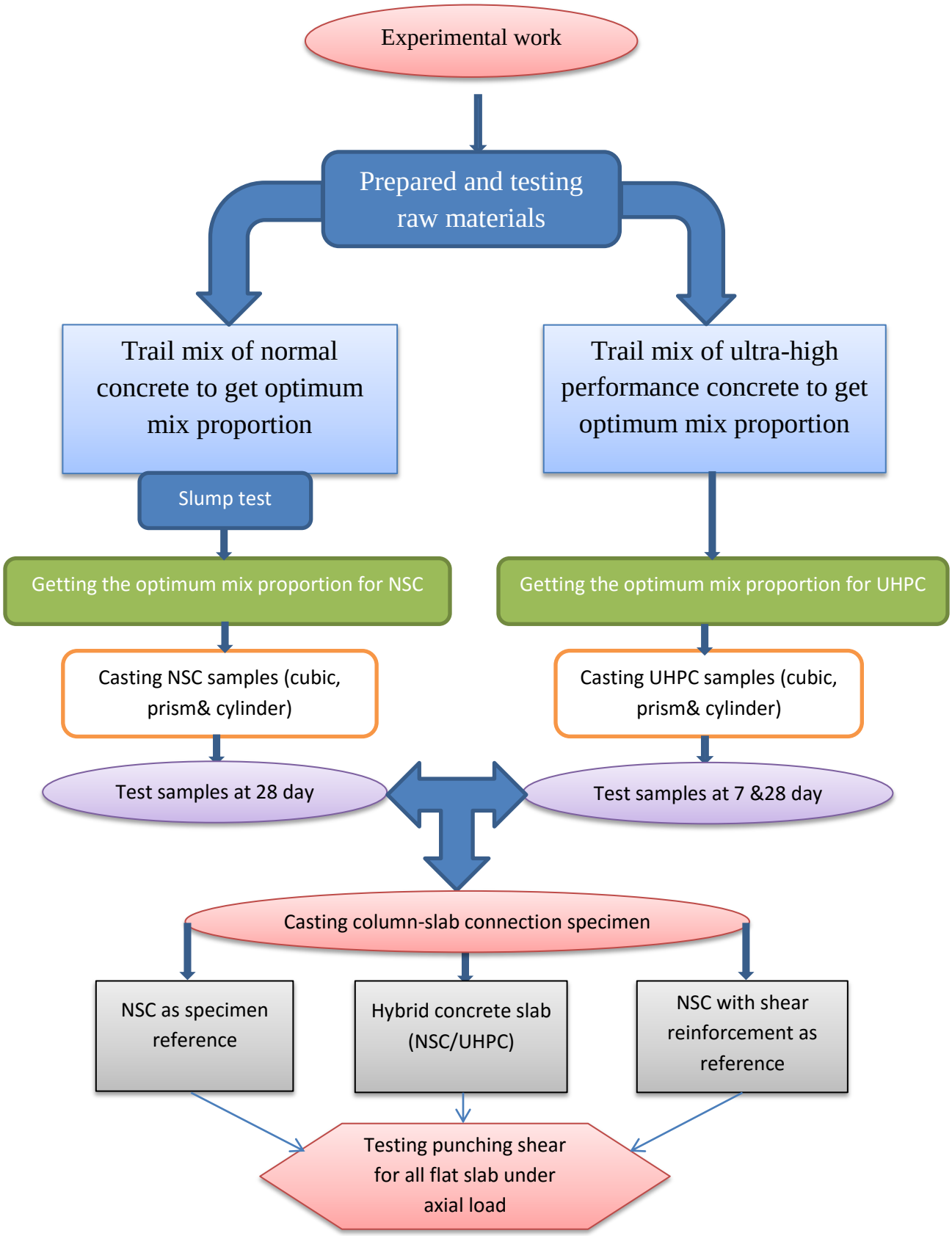

Figure (3-1): Flow chart of the experimental program.

Table (3-1): Details of the tested flat slabs specimens.

Case study	Group No.	Specimen Name	Shape UHPC	volume Cast of UHPC	details
	Reference Specimen	NSC			Normal concrete
I	G1	1d-SC	Square shape	210*210*40	Strengthening by UHPC in compression zone half depth **s**quare shape (constant) and variable area, as shown in Figure (3-4 b, c &d)
		2d-SC		320*320*40	
		3d-SC		430*430*40	
	G2	1d-SI C	Rhombic shape	210*210*40	Same details G1 but rotated area of UHPC by angle 45°, Figure (3-4 e, f &g)
		2d-SI C		320*320*40	
		3d-SI C		430*430*40	
	G3	120-RC	Circular shape	$\pi *120^2*40$	Same amount UHPC in G1 and G2 but use UHPC circular shape, as shown in Figure (3-4 h, I &j)
		180-RC		$\pi*180^2*40$	
		243-RC		$\pi *243^2*40$	
	Reference Specimen	Sh.RN			Normal concrete
II	G4	187-PF	Cross shape (+. Shape)	[187*100*4 +100^2]*80 = [400*100*4 +100^2]*40	Replacing punching shear reinforcement by UHPC, Figure (3-4 k, l, m&n)
		400-PC			
		187-XF	Cross shape rotated 45° (X. shape)		
		400-XC			

The experimental program consists of (15) square flat slab sample addition to one pilot slab as listed in **Table (3-1)** and **Figure (3-4)** with a dimensions (900*900*80 mm). Twelve specimens flat slab with square column cross section (100*100 mm) at

center of the slab, and three specimens flat slab with circular column of diameter 113 mm with a cross section area equal to that area of a square column. All slabs were designed to failure in shear, as shown in **Appendix (A).** The specimens are divided into two case studies as **Table (3-1)** the first without shear reinforcement while the second the punching shear reinforcement has been added.

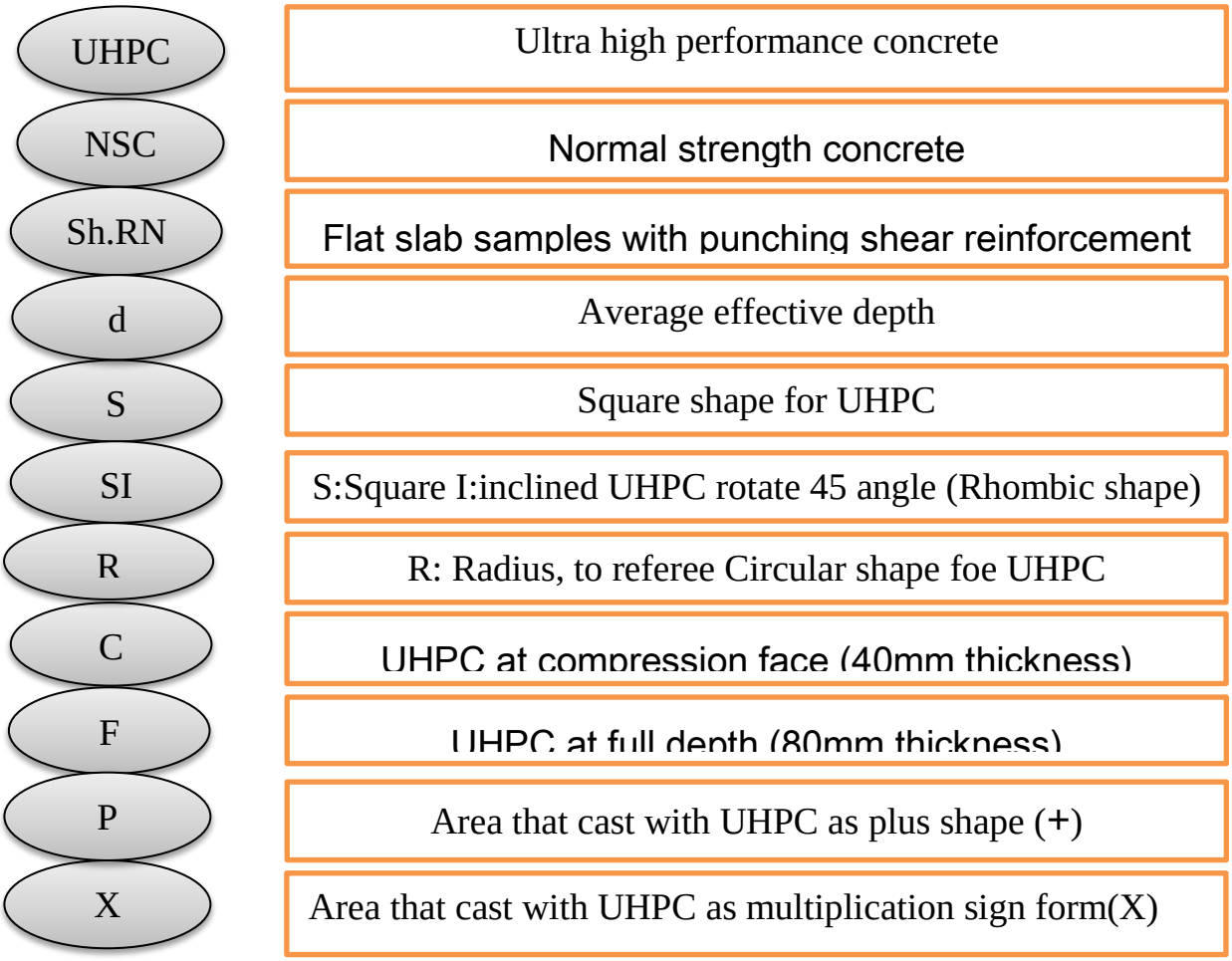

Figure (3-2): Slab specimen's identification.

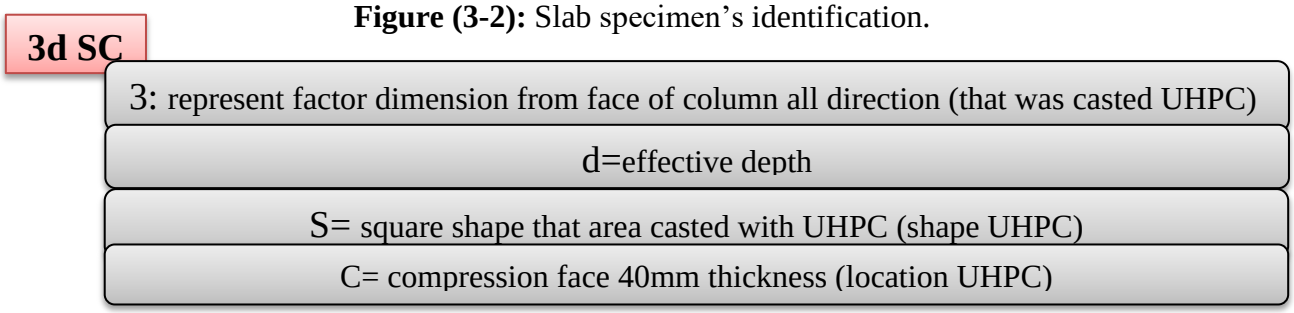

Figure (3-3): Example for Specimen Identification.

All the specimens have the same flexural reinforcement steel and are tested under (concentric) loading. The first case study **(I**) consisted of three groups in addition to two slabs that were cast with normal strength concrete (NSC) as a reference, all specimen hybrid concrete (NSC with UHPC) where the UHPC cast for half thickness at compression face under column, UHPC was not laid in the tension face because it does not provide significant results as mentioned in **[55].** The first group (G1) consisted of three specimens, a hybrid concrete (NSC with UHPC) where the UHPC cast as a square shape at the center of the slab with a dimension of (1d, 2d & 3d) from the face of the column in all directions for the three samples, respectively. The second group (G2) consisted of three specimens, UHPC cast as a rhombic shape at the center of the slab, area UHPC in this group is the same as area UHPC in the first group and the same shape, but rounded by an angle 45 (rhombic shape). The three group (G3) consisted of three specimens also, UHPC cast as a circular shape at the center of the slab, area UHPC in this group is the same as UHPC area in (G1 & G2), UHPC was casted in circular shapes, the radius of the circle for the first sample (120 mm) with an area equivalent to the square of UHPC for the first sample in the first and second groups, and the second sample with a radius (180 mm) and it is equivalent in area (UHPC) to the second sample in the first and second groups, and the third one with a radius (243 mm) and it is equivalent in UHPC area to the third sample in the first and second groups. Circular columns in (G3) with a diameter (113mm) were used with an area equivalent to that of the square columns (100*100) mm.

The second case study (**II**), has only one Group (G4) consisted of four slabs, in addition one slab that casted of a NSC with punching shear reinforcement as a reference for this group, while in the remaining four slabs the punching shear reinforcement was replaced by UHPC. The shear reinforcing steel was replaced by UHPC with the same steel dimensions specified by (ACI 318-19) and with full depth slab and second specimen, the same UHPC in first specimen, but rotated at an angle (45). The other two

samples are similar to the previous one in shape and quantity UHPC except that they are half the depth of the slab, as **Table (3-1)** for to get optimum use of ultrahigh performance concrete.

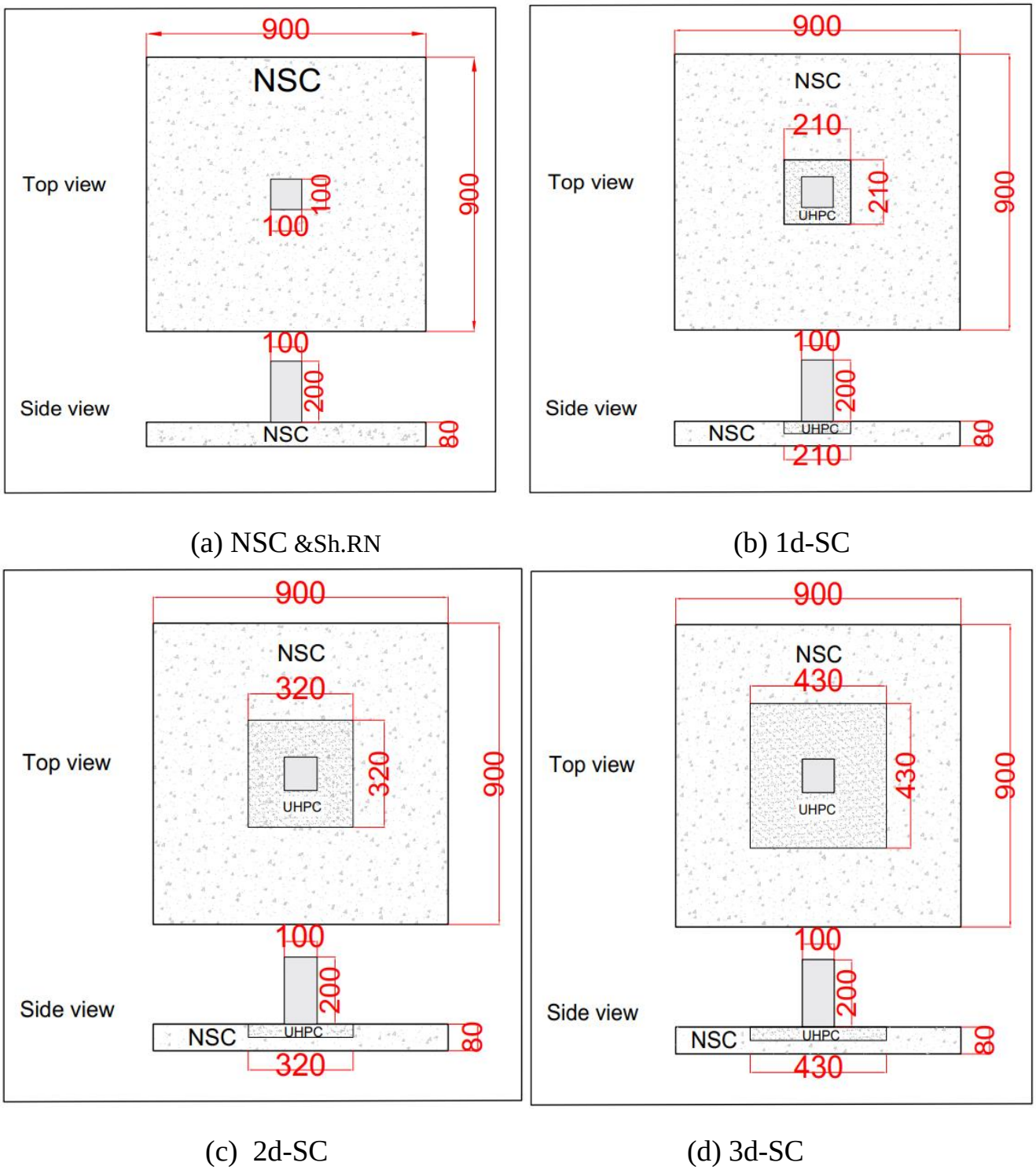

(a) NSC &Sh.RN (b) 1d-SC

(c) 2d-SC (d) 3d-SC

Figure (3-4): Geometric details and UHPC locations of RC specimens (all dimensions are in mm).

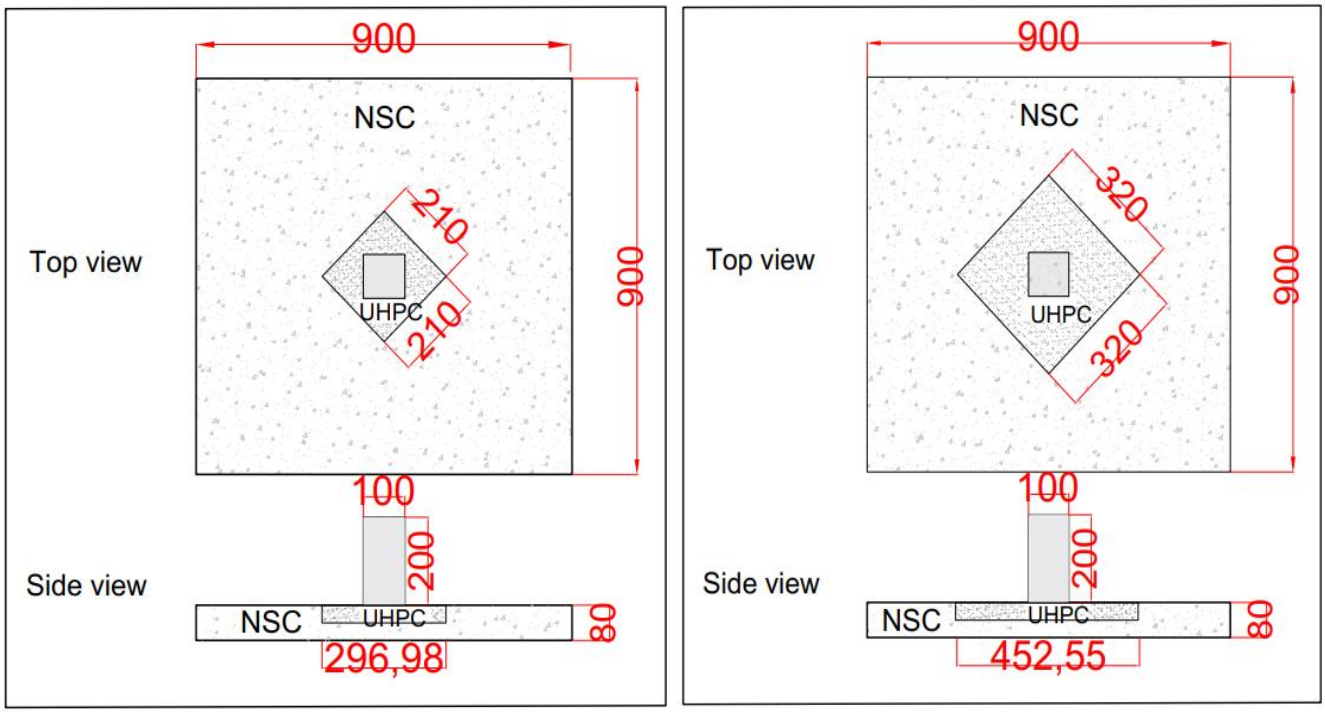

(e) 1d-SI C (f) 2d-SI C

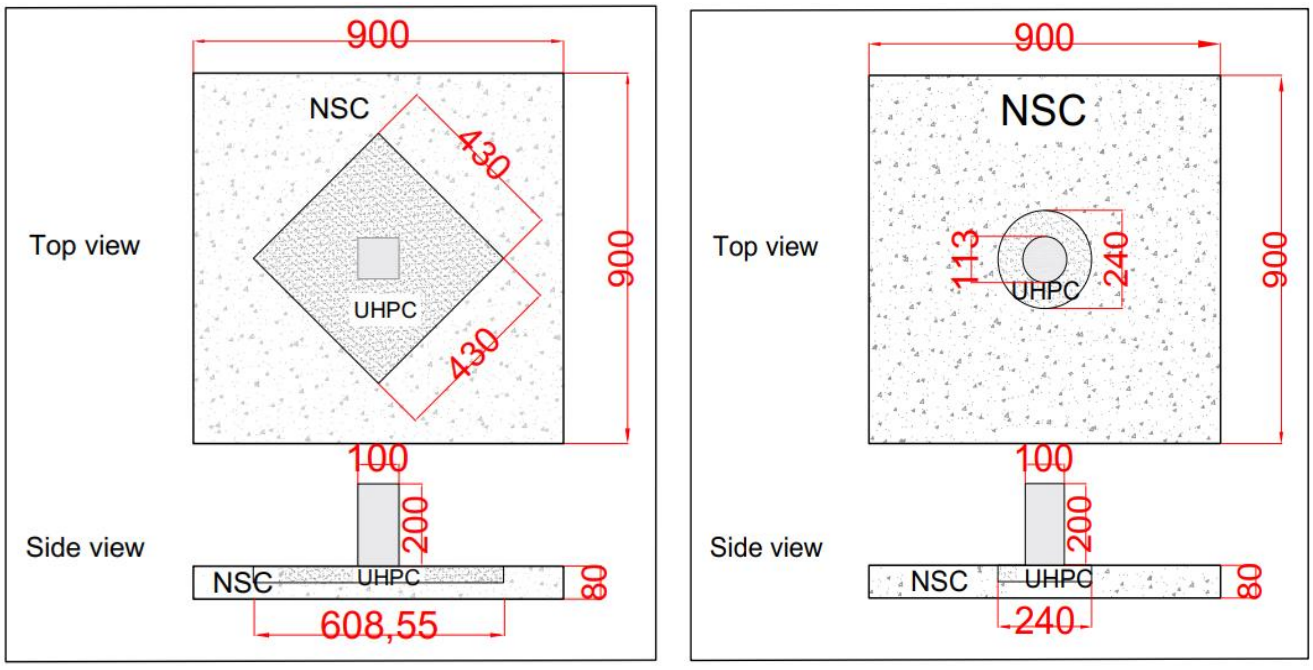

(g) 3d-SI C (h) 120-RC

Figure (3-4): Geometric details and UHPC locations of RC specimens (all dimensions are in mm) (Continued)

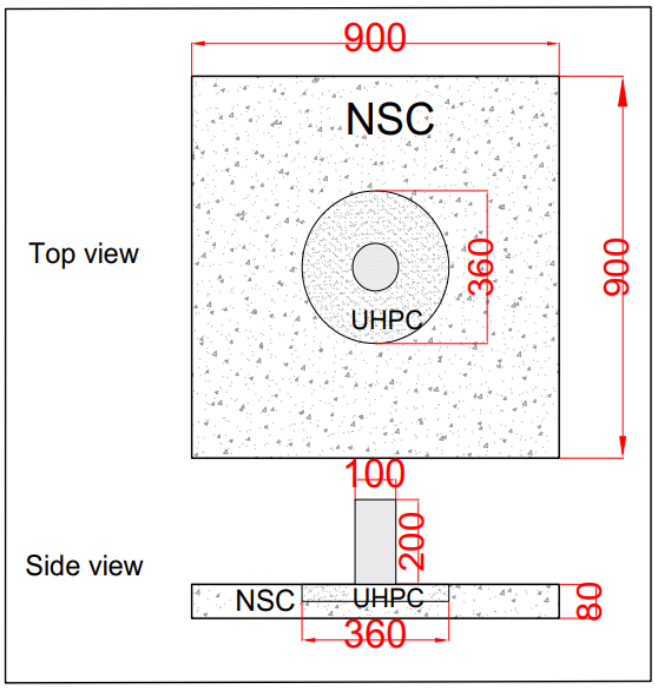

(i) 180-RC

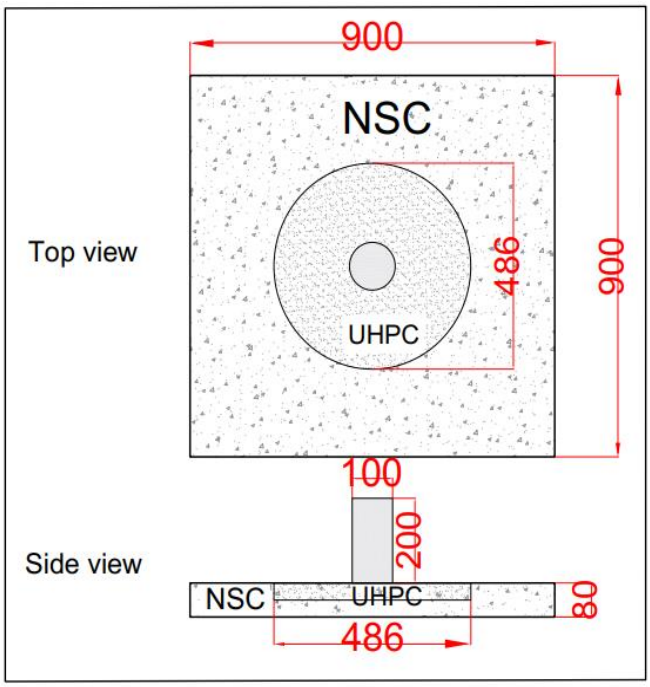

(j) 243-RC

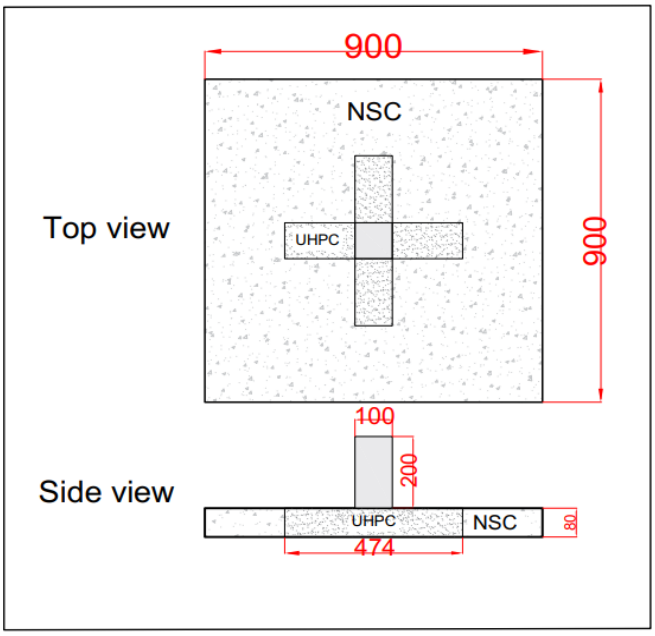

(k) 187-PF

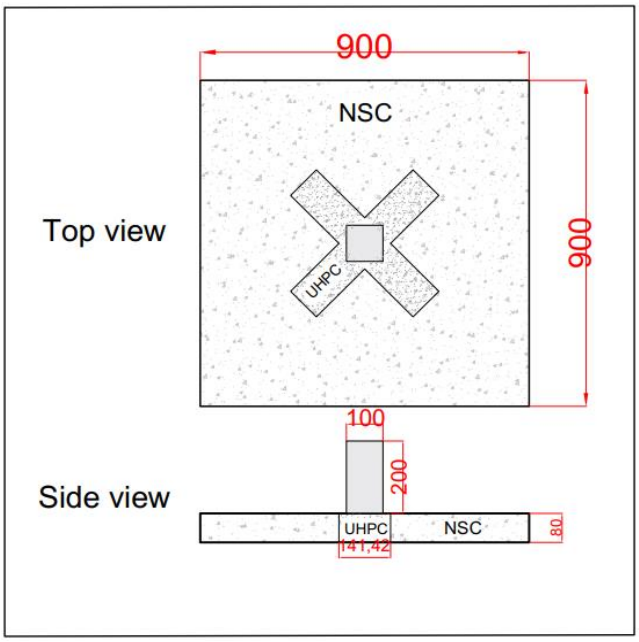

(l) 187-XF

Figure (3-4): Geometric details and UHPC locations of RC specimens (all dimensions are in mm) (Continued)

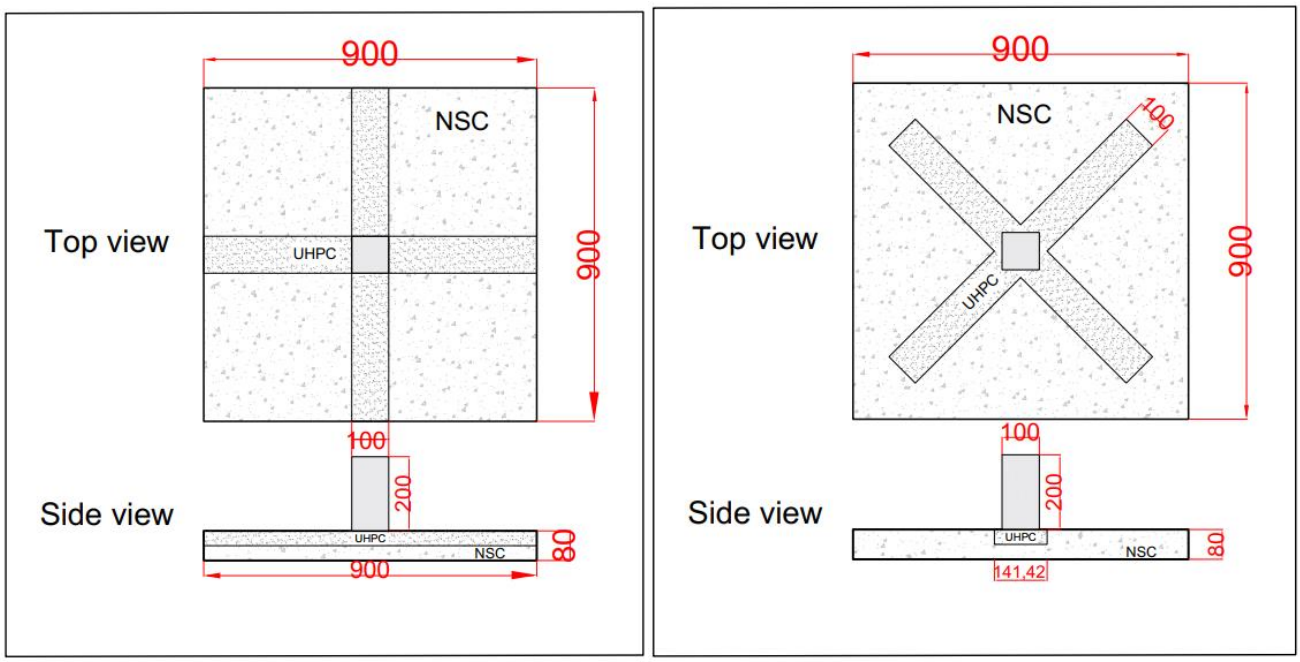

(m) 400-PC (n) 400-XC

Figure (3-4): Geometric details and UHPC locations of RC specimens (all dimensions are in mm) (Continued)

3-3 Materials Properties

Knowing the characteristics of the materials from which concrete is composed is essential for their effect on the properties of concrete as a whole. Concrete is a composite material consisting mainly of cement, fine and coarse aggregates (usually natural sand and gravel), water and additives. In order to obtain high-quality concrete, strict procedures were adopted in this experimental study in selecting the type and proportions of materials. Detailed material descriptions and their physical and chemical properties are given in subsequent sections.

3-3-1 Concrete

Locally available substances were utilized in the production of both types of concrete implemented in this study (NSC and UHPC), which include cement, silica fume, sand, gravel, superplasticizer, steel fibers and water.

3-3-1-1 Cement

Locally made ordinary Portland cement (Type I), commercially named Karasta, was utilized during this investigation for casting all samples (NSC and UHPC). The chemical composition and physical properties provided by the manufacturer are shown in Table (3-2) and Table (3-3) respectively, which are in accordance with Iraqi Specifications **(IQS No. 5/1984) [56]**.

Table (3-2): Chemical analysis and main compounds of the used cement.

Chemical composition	Item	Test Result %	I.Q.S No.5/1984 limits
Silicon oxide	SiO_2	20.58	-
Calcium oxide	CaO	62.79	-
Ferric oxide	Fe_2O_3	3.28	-
Aluminum oxide	Al_2O_3	5.6	-
Sulphur trioxide	SO_3	2.35	≤ 2.8%
Magnesium oxide	MgO	2.79	≤ 5.0%
Insoluble residue	I.R	1	≤ 1.5%
Loss of ignition	L.O.I	1.94	≤ 4.0%
Lime saturation factor	L.S.F	0.9	0.66-1.02
Main compound composition			
Di-calcium silicate	C_2S	21.26	-
Tri-calcium silicate	C_3S	50.12	-
Tetra-calcium aluminate ferrite	C_4AF	9.98	-
Tri-calcium aluminate	C_3A	9.29	-

Table (3-3): The physical characteristic of the cement.

Item	Test Result	Iraqi specification No. 5/1984 limits
Blaine fineness (m^2/kg)	314	≥ 230
Compressive Strength (MPa) 3 days 7 days	 20.7 28.0	 ≥ 20 ≥ 23
Time of setting (Vicat) Initial (hours: minutes) Final (hours: minutes)	 2:05 4:20	 ≥ 00:45 ≤ 10:00 hrs

3-3-1-2 Fine Aggregate (Sand)

Natural sand with a maximum size of 4.75 mm was used in this research for NSC. The sand has been washed and cleaned with water several times before use, and then dried in air to get rid of excess moisture that may affect the mixing water content significantly. Table (3-4) shows the classification and characteristics of fine aggregates that comply with Iraqi specifications **(I.Q.S No.45/1984) [57].** Fine aggregate has been examined in the Construction Material and Environmental Laboratories of the Civil Engineering Department at the University of Babylon.

Table (3-4): Fine aggregate grading and properties.

Sieve's opening size (mm)	**Passing %**	
	Fine aggregate	**Iraqi specification (No. 45/1984)** limits
10	100	100
4.75	93	90 - 100
2.36	82	75 - 100
1.18	72	55 - 90
0.6	51	35 - 59
0.3	22	8 - 30
0.15	6	0 - 10
Physical and chemical properties of fine aggregate		
Property	**Test Results**	**Limits of IQS No. 45/1984**
Specific gravity	2.60	-
Fineness modulus	1.45	-
Sulfate content SO_3 (%)	0.38%	≤(0.5)

3-3-1-3 Fine Aggregate (Extra Fine)

Natural fine aggregate brought from the region of (Al-Najef) was utilized as a natural sand in UHPC. This natural sand was too coarse to be used successfully in making mortar. Thus, the fine sand that was sifted by a 600-micron sieve to separate the coarse particles is used in preparing the mortar, and the use of this size of sand has proved successful for all mortar mixtures during the experimental work. Table (3-5) shows the grading and sieve analysis and physical and chemical characteristics of fine aggregate. It conforms to the **(IQ.S No.45/1984) [57]** limitation zone (4). The fine aggregate has been examined in the Construction Material and Environmental Laboratories of the Civil Engineering Department at the University of Babylon.

Table (3-5): Fine aggregate (extra fine) grading and properties.

Sieve's opening size	**passing %**	
	Fine aggregate	**Iraqi specification No. 45/1984 limits**
10	100	100
4.75	100	95 - 100
2.36	100	95 - 100
1.18	100	90 - 100
0.6	100	80 - 100
0.3	45	15 - 50
0.15	10	0 - 15
Physical and chemical properties of fine aggregate		
Property	**Test Results**	**Limits of IQS No. 45/1984**
Specific gravity	2.60	-
Fineness modulus	1.45	-
Sulfate content SO3(%)	0.38%	≤(0.5)

3-3-1-4 Coarse Aggregate (Gravel)

Local gravel from Al-Nabai region with a maximum size of 14 mm was used as a coarse aggregate in the current study. The gravel has been washed and cleaned with water several times and allowed to be dried in air before being employed. Table (3-6) shows the classification and characteristics of coarse aggregates that obey with Iraqi specifications **No.45/1984 [57].** Coarse aggregate has been examined in the Construction Material and Environmental Laboratories of the Civil Engineering Department at the University of Babylon.

Table (3-6): Coarse aggregate grading and sulfate content.

Sieve's opening size	**Passing %**	
	Fine aggregate	**Iraqi specification No. 45/1984** limits
14	100	90 - 100
10	83	50 - 85
5	3	0 - 10
2.36	0.6	-------
SO_3 content= 0.07% (specification requirements up to 0.1%)		

3-3-1-5 Silica Fume

Silica fume is a fine granule with a particle size hundreds of times less than cement. It is usually used as a partial substitute for cement in relatively small proportions to improve its properties as a result of the ability of this material to interact with calcium hydroxide (resulting from cement hydration) and form a gel similar to cement gel and thus contribute to improving the different properties of concrete. MEYCO MS610 condensed silica gray fume from Master Builders Solutions was used for UHPC. Table (3-7) shows the physical and chemical properties of silica fume, which comply with the standard **ASTM C1240-04 [58].**

Table (3-7): Silica fume properties as provided by the manufacturer (Master Builders Solutions Company).

Oxide / Property	Content %	Limits of ASTM C 1240
SiO_2	95.14	>85
Specific surface (m^2/g)	20.75	>15
Loss on Ignition	1.42	<6.0
Absorption (%)	0.73	-

3-3-1-6 Steel Fibers

A commercially available micro steel fiber (type WSF0213) was used in this study to produce UHPC, as shown in Plate (3-1). This kind of fiber is manufactured by a company in Jiangxi Province, China. The aspect ratio (Lf/Df) of the fibers is equal to 65. A volume fraction (Vf) of 1.5% was adopted for this study. The properties of steel fibers are presented in Table (3-8).

Table (3-8). Properties of steel fibers as provided by the manufacturer.

Property	Value
Type	WSF0213
Diameter	0.2 mm
Length	13 mm
Aspect Ratio	65
Density	7860 kg/m3
Tensile Strength	Minimum 2300 MPa
Modulus of Elasticity	203 GPa
Melting Point	1500°C
Surface	Brass coated
Shape	Straight

Plate (3-1): Steel Fibers Material Used in UHPC (by Author).

3-3-1-7 Admixtures (Super plasticizer)

A superplasticizer commercially called Sika ViscoCrete 5930- L produced by Sika company (Switzerland) was utilized in this study. The properties of this superplasticizer, which is conformed to **ASTM C494 [59]** Type F and G, are illustrated in Table (3-9).

Table (3-9) Technical description of Sika ViscoCrete-5930-L Superplasticizer as provided by the manufacturer

Properties	Sika ViscoCrete 5930-L
Density	1.1 kg/It
Color	Light yellow
Appearance	Turbid liquid
Chloride content	None
PH	6-8

3-3-1-8 Mixing Water

Tap water was used for casting and curing the slab samples. additionally, it was used for washing fine and coarse aggregates.

3-3-2 Reinforcing Steel Bars

Deformed reinforcing steel bars with diameters (ø6mm and ø10mm) were used in this work. Reinforcement steel (ø10mm) was used for the flexural strengthening of all slabs in both directions. The main steel of the columns for all samples was reinforced with (4 ø10 mm) steel bars and closed stirrups (3 ø 6 mm) to prevent initial failure. The reinforcing bars used with different diameters were subjected to a tensile test in the laboratory of the College of Materials Engineering - at the University of Babylon as shown in Plate (3-2). Table (3-10) shows tensile test results for bars with diameters (ø6 & ø10). Figure (3-5) shows the typical reinforcement of the tested samples. There is only one sample that differs from the others by adding additional steel bars of 4 ø 6 mm and stirrups with a diameter of 6 mm as a punching shear reinforcement as shown in Figure (3-6).

a **b** **c**

Plate (3-2): (a) ø6 stenosis (b) ø10 stenosis (c) ø10 cutting.

Table (3-10): Test results of steel reinforcement bars.

Nominal diameter (mm)	Measured diameter (mm)	Yield stress (MPa)	Tensile strength (MPa)	Elongation %*
10	9.95	448	545	10
6	5.95	420	740	6.5

* Min. value for diameter ø10, is (9) according to **ASTMA615/A615M-05a[60]**

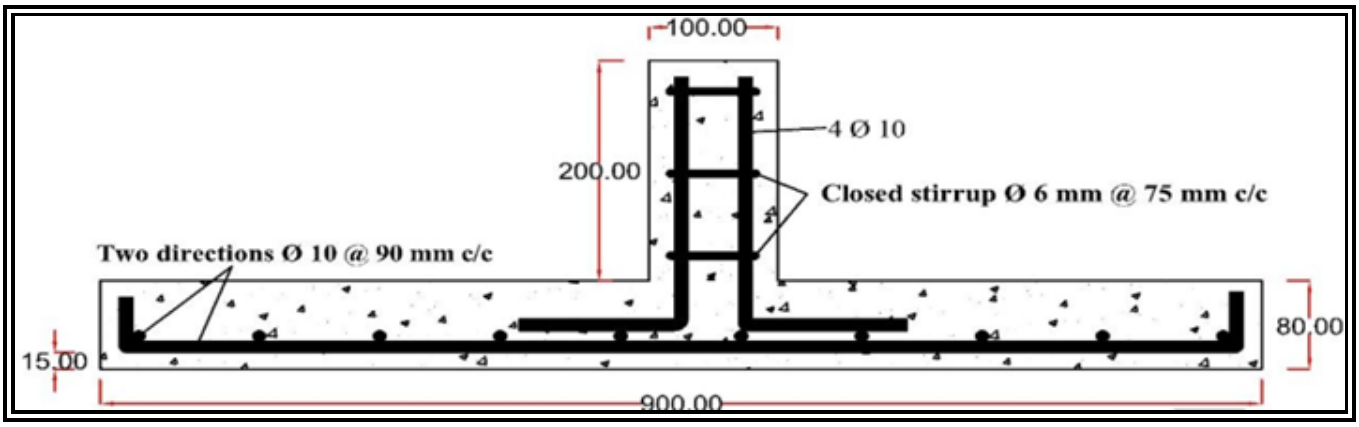

Figure (3-5): Typical Reinforcement For Specimens.

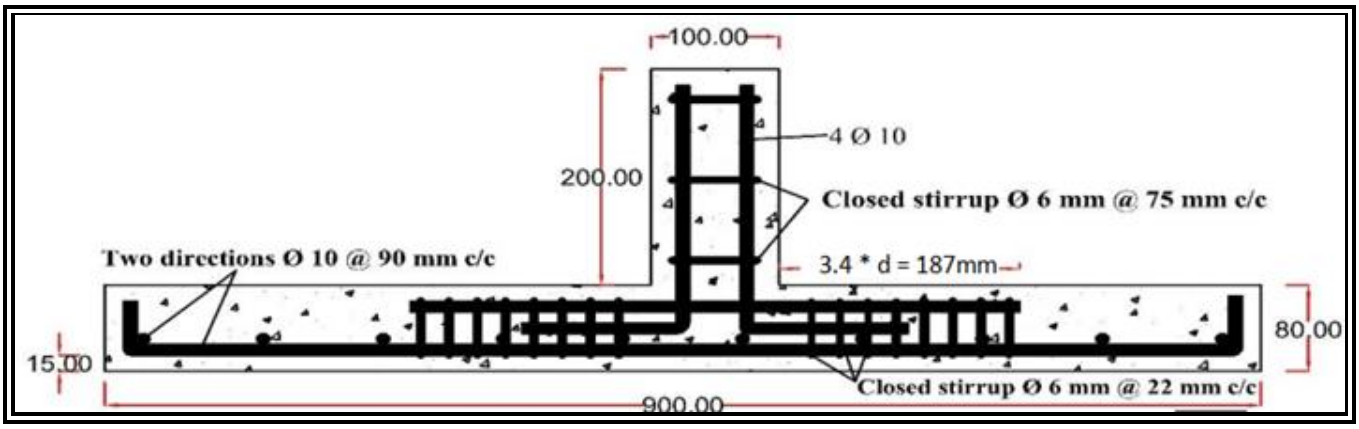

Figure (3-6): Specimen With Additional Punching Shear Reinforcement (Sh.RN).

3-4 Concrete Mix Design

3-4-1 Normal Strength Concrete (NSC)

3-4-1-1 Mix Proportion of Normal Strength Concrete

Normal-strength concrete was used to pour different areas of the samples. It was designed according to **ACI-211.1 [61]**. The target strength of concrete (f'c) for all slabs was (23 MPa) at (28 days) of age. Experimental trail mixes were performed to adjust the proportion of the mixed design to reach the required compressive strength. Table (3-11) shows the optimal mixtures used (in a weight ratio per cubic meter).

Table (3-11): Details of normal strengthmix proportions (in kg/m^3).

Material	Cement	Fine Aggregates	Coarse Aggregate	Water
Weight (kg)	368	850	900	213

3-4-1-2 Mixing Procedure of Normal Strength Concrete

The normal concrete ingredients were mixed according to **ASTM C192-07 [62]**. It was mixed in the structural materials laboratory at the Department of Civil Engineering, University of Babylon, with an electric mixer with a capacity of (0.02 m^3). Coarse aggregate was added to the mixer with about 20% of the mixing water. After several revolutions, the fine aggregate was added along with about 20% of the mixing water. After that, the mixer was turned on for a few seconds. Then, cement and the remaining water were added. The concrete was mixed for three minutes then at three-minute rest, and thereafter at two minutes as a final mixing.

3-4-2 Ultra-High-Performance Concrete (UHPC)

3-4-2-1 Mix Proportion of Ultra-High Performance Concrete

Ultra-high-performance concrete (with a 2% steel fiber by volume) was used to reinforce the flat slabs. During the early stage of the current study, several experimental mixes were made and tested at the age of 28 days, as shown in Table (3-12). The selected mixture ratios were sufficient to give a compressive strength of about (126) MPa and suitable workability.

Table (3-12): Trail mixes proportion of UHPC.

No. of Mix	1	2	3 (Selected)
Cement (kg/m^3)	975	1000	1000
Micro silica fume (kg/m^3)	230	245	255
Fine sand (kg/m^3)	1050	1050	1050
Steel fiber % by volume	2	2	2
Superplasticizer % by weight of cementitious material	4.25	4.5	5
water/(cement +silica fume)	0.19	0.17	0.155
fc' (28 days) MPa	85.63	105	126

3-4-2-2 Mixing Procedure of Ultra-High-Performance Concrete

For ultra-high-performance concrete, cement and fine sand were mixed in a dry state for approximately two minutes to disperse fine sand particles among the cement particles. Then, silica fume was added and the mixture was mixed for two minutes. The solution of water and superplasticizer (pre-mixed) was gradually added during the mixing process, and then the mixture was thoroughly mixed for 5 minutes. The steel fibers were uniformly distributed in the mixture for 3 minutes. In total, mixing one batch

involves approximately 14 minutes. An electric handled mixer was used to mix the UHPC as described in Plate (3–3).

Plate (3-3): Drilling Mixer.

3-5 Specimens Preparation for Testing.

This part describes the preparation of reinforcement cages and mold, mixing procedure, casting and curing of the tested specimens**.**

All specimens in this study were cast in plywood molds with net dimensions (900 * 900 * 80 mm). Five plywood molds were superimposed to accommodate the reinforcing cages inside. The mold consists of ten separate parts that can be assembled in an easy way with special screws (for wood use) and metal pieces to fix the corners. The mold can be used more than once. It was designed to be easy to assemble or disassemble without any effect on the molded sample, as shown in panels (3–5a).

A steel mold of different shapes and dimensions is used to separate and isolate the area to be cast using UHPC and for columns of circular cross-section, as in slab (3-5b).

Before casting, the mold was oiled and placed in horizontal planes, then the main rebar was placed in the mold followed by placing the steel mold in the center of the slab to separate the NSC from the UHPC. The two types of concrete were poured simultaneously and the mold was filled to the required level. Moreover, the vibration was applied to both types of concrete at the same time to achieve complete bonding. The steel mold was removed by steady pulling. The following stages describe the casting process:

1. Before casting, the plywood and steel molds were prepared by cleaning them and lubricating the inner surface with oil to prevent sticking to the hardened concrete and placed on leveled ground.
2. After the formwork was prepared, the previously prepared rebar was placed and centered with a 15 mm cover in all directions and then the rebar was connected to the column in the middle of the slab as shown in Plate (3-5).
3. The specimens were cast on three separate dates. One batch of concrete is used to pour all five slabs. The concrete was mixed in an electric mixer with a horizontal rotating drum with a capacity of (0.09 m^3). Concrete mixing was performed in accordance with **ASTM C192-07 [62]**. Before mixing, all quantities were weighed and filled into a clean container. In all mixtures, first, coarse and fine aggregates were put into the mixer and mixed in two-thirds of the water required for one minute. Then cement and remaining water were added and mixed for three minutes. On each casting day, five slabs (shown in Plate (3-6)), samples from three cylinders with a diameter of 150 mm and a height of 300 mm, and six cubes (150 x 150 x 150) mm for the NSC and (50 x 50 x) 50), (70 x 70 x 70) and (100 x 100 x 100) mm for UHPC were cast to determine the mechanical properties of concrete, as shown in Plate (3-7). The high-performance concrete was mixed as per (3.4.2.2).
4. After mixing, the concrete was poured into a lightly oiled mold in two layers and compacted well by a mechanical plunger vibrator (3500 rpm), for 5 seconds per entry.

While UHPC is compacted using a staple stick. The surface of the concrete was leveled and finished using a steel trowel, taking due care not to move the rebar of the post. NSC and UHPC were cast together. Thereafter, the spacers (steel mold) were carefully removed in a stepwise manner and the other concrete type (UHPC) was poured directly (at the same time) as shown in Plate (3–8).

Plate (3-4): Preparing the wooden and steel mold.

Plate (3-5): Preparing of the mold wood and upload reinforcement steel with plastic spacers.

5. After (24) hours, the plywood mold was removed and the column was cast using a square plywood mold with dimensions (100 * 100 * 200 mm in height) and a steel round mold (113 mm in diameter and 200 mm in height) as shown in Plate (3-10), column cast with NSC. Then, burlap was placed over the slabs and kept wet until 28 days as shown in Plate (3-10). Cylinders, cubes and prisms were placed in the curing water tank and kept hydrated according to standard specifications.
6. After (28) days, the specimens were removed from the curing basin and then tested. On the other hand, the concrete surfaces of the slab samples were painted white, then their symbols were written and they were prepared for testing as shown in Plate (3-11).

Plate (3-6): The casting process of the five slabs (per one day).

Plate (3-7): The casting of the control samples.

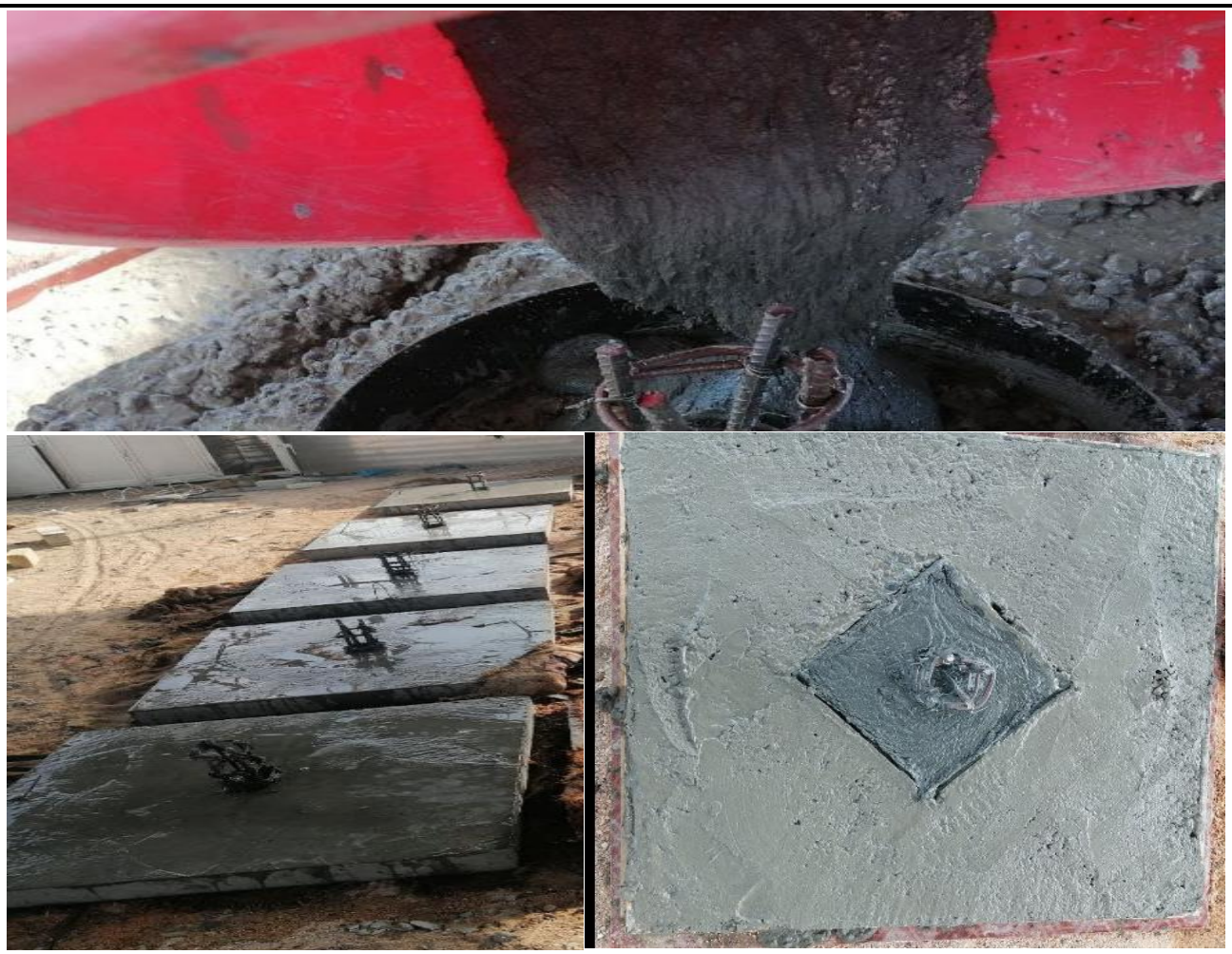

Plate(3-8): The pouring of NSC and UHPC together with surface leveling.

Plate (3-9): Casting the columns with NSC.

Plate (3-10): Curing all Specimens.

Plate (3-11): The coating of slab samples with white color (after curing) and preparing them for testing.

3-6 Mechanical Properties of Concrete.

3-6-1 Fresh Properties of Concrete.

The slump test of NSC was executed according to **ASTM C 143/C 143M-05a** as an indicator of the workability of fresh concrete as presented in Plate (3-13).

Plate (3-12): Slump Test.

3-6-2 Mechanical Properties of Hardened Concrete

All samples (cubes and cylinders) were left in the molds for 24 hours. After that, they were removed from the molds and placed in a basin filled with clean water. After 28 days, they were taken out from the container and tested with each corresponding flat slab sample at the same time according to **BS1881-116-89 [63]** and **ASTM-C496-11 [64]** to obtain the compressive and splitting tensile strength respectively, using 2000 kN-capacity universal testing machine.

3-6-2-1 Compressive Strength (fcu)

The concrete cube compressive strength of the control samples (f_{cu}) was obtained according to British Standard **BS1881-part 116:1989 [63]**. The tests were conducted in the Structural Laboratory of the University of Babylon. All cubes (150 × 150 × 150) for NSC mm and (50 × 50 × 50) (70 × 70 × 70) mm for UHPC were tested at 28 days as shown in Plate (3–13).

3-6-2-2 Tensile Strength (f_{st})

The splitting tensile strength test was performed as per **ASTM C496-11 [64]**. A total of 6 cylinders were tested with (150 x 300) mm for NSC and (100 x 200) mm for UHPC. Two loaded strips of 3.0 mm thick plywood, 300 mm long, were placed above and below the sample to provide uniform pressure on the surface of the test cylinder, as shown in Plate (3–14). The load was applied continuously without shock until the failure using a 2000 kN testing machine. The splitting tensile strength was calculated from the following equation:

$$\mathbf{fst} = \frac{2P}{\pi LD} \qquad \textbf{…… (3-1).}$$

Where D and L are the cylinder diameter and length (mm), respectively. P is the applied load (N) while fst is the splitting tensile strength (MPa).

Plate (3-13): Compressive strength test setup for NSC and UHPC.

3-6-2-3 Modulus of Elasticity (Ec)

The modulus of elasticity of concrete is one of the fundamental factors influencing the behavior of reinforced concrete slabs because it is directly related to its stiffness. An automatic universal cylinder compression tester with a capacity of 2000 kN equipment was utilized to carry out this test. Each of the tested samples was equipped with a pressure gauge. The test was performed according to **ASTM C 469-2010 [65]**. The method includes loading the cylinder with three loading cycles up to 40% of its

compressive strength value, whereby using the average of the last two cycles, the modulus of elasticity is calculated from the following equation:

$$Ec = \frac{S2-S1}{\epsilon 2-0.00005} \qquad \text{..... (3.2)}$$

Where S**1** is stress corresponding to a longitudinal strain (ε_1) of 50 millionths, S_2 is stress corresponding to 40% of the ultimate load, Ec is modulus of elasticity in MPa, and ε_2 is longitudinal strain produced by stress S_2.

Plate (3-14): The splitting tensile test setup.

3-7 Test Procedure and Instrumentations

3-7-1 Testing Machine

A hydraulic testing machine (600 kN of capacity), which is available in the Civil Engineering Laboratory, Department of the College of Engineering, University of Babylon, was used to observe the response of the flat slab samples.

3-7-2 Testing Instruments, Supporting and Loading Conditions

All slabs tested were simply supported along the perimeter of the slab and centrally loaded by the square or circular column. The structural behavior (load, deflection, and cracking pattern) of the flat slabs at each stage of loading was detected using several tools. Through each step, the load deflection and crack width were recorded. The tests continued until the final load, and the crack width at the first crack, the final load at the end, and up to complete failure (collapse) were recorded. The instruments used in the tests, as shown in **Plate (3-15)**, are listed below:

1. A new testing system (load cell) was connected and after calibration, this system was approved for testing.
2. The test started with a small pre-load cycle of about 5 kN to settle the slab and maintain the position before the start of the test.
3. The crack width of all slab samples was measured using an optical micrometer with a resolution of 0.02 mm.

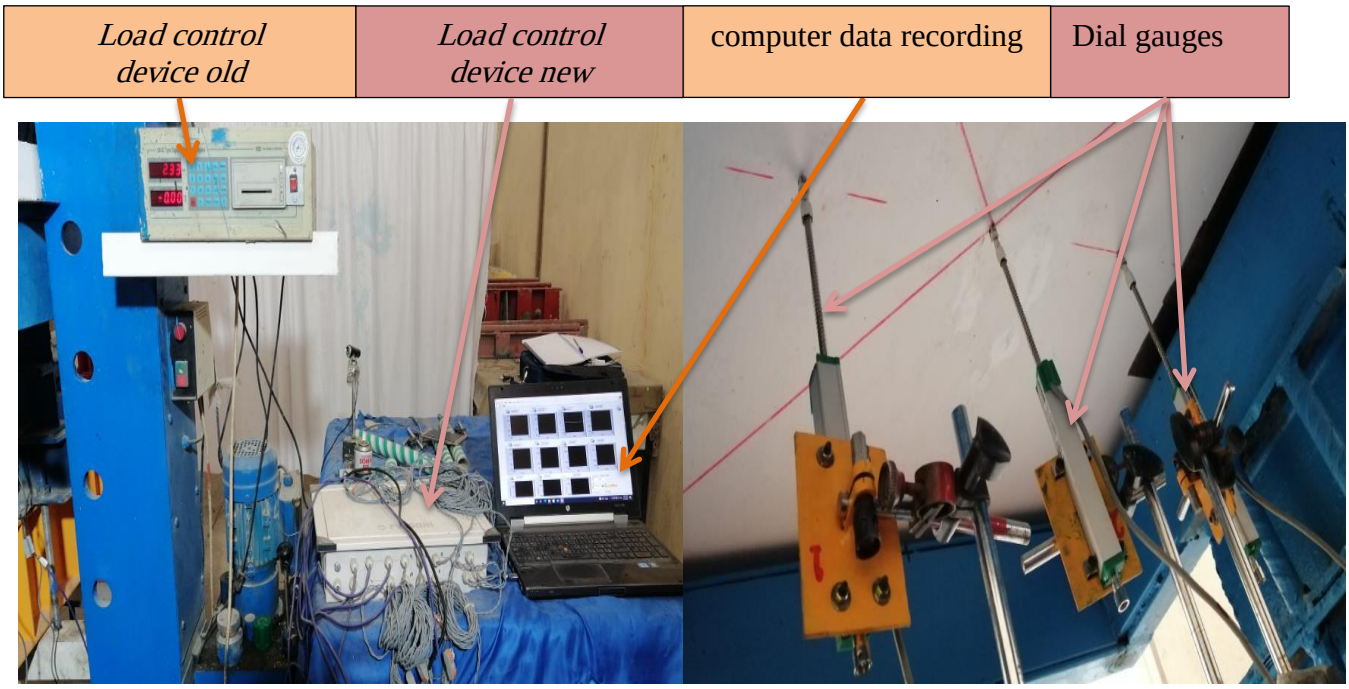

Plate (3-15): Instruments used in testing.

3-7-3 Test Procedure

All samples were painted white. At first, by testing the samples, the main characteristics of their structural behavior at each step of loading such as cracking load, cracking width, ultimate load, displacement, as well as failure mode were recorded.

In order to verify the accuracy and validity of the supports and devices used, one experimental sample was tested. At a loading rate of 0.1 kN/s, the load was applied in stages and the crack width was recorded at each increment of loading until approximately 80-85% of the expected final load for safety purposes. After each process of reading and showing the crack, which takes about two minutes, the loading process was resumed, and so on, until the sample fails. The signs of crack development on the concrete slabs were placed using a thick felt-tip pen in order to facilitate the identification of cracks and their locations during the examination.

The test began with a small preload cycle of about 5 kN to settle the slab and preserve its situation before the start of the test. Once the test was completed, the crack pattern was studied and further photographs were taken. Finally, the slab was removed from the test frame and the concrete surface was examined at different locations. Plates (3-16) and (3-17) show the details of the testing machine and the crack width measurement process.

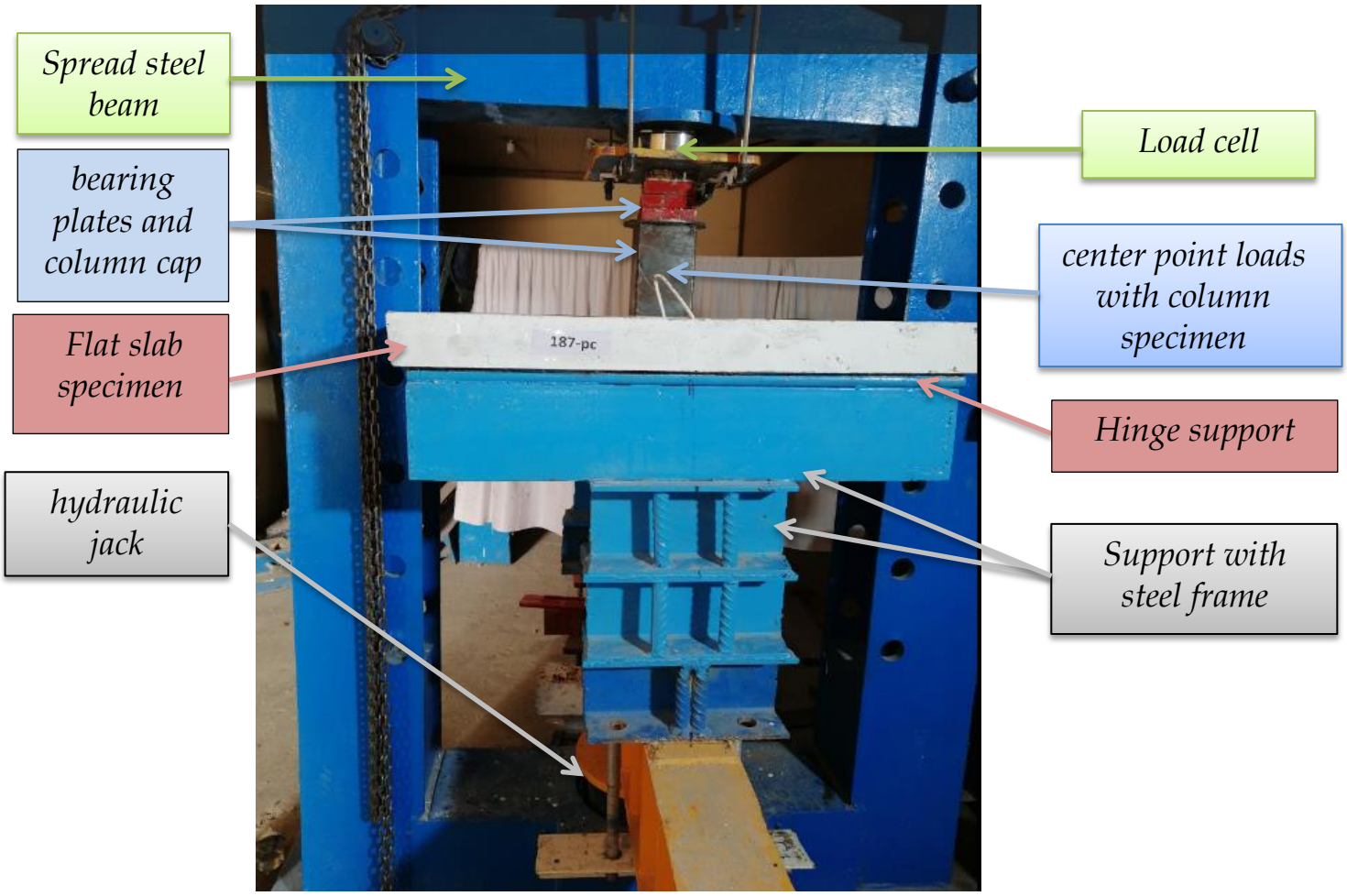

Plate (3-16): Specimen under testing.

Plate (3-17): Marking the cracks.

CHAPTER FOUR

EXPERIMENTAL RESULT AND DISCUSSIONS

4-1 Introduction

In this chapter, the most relevant results obtained from experimental program that described in previous chapter are summarized and discussed. First, the properties of concrete obtained from tests of the control samples (cubes, cylinders) are displayed. Then, test results obtained of flat slab specimens are presented and discussed including, Load-deflection response, cracking patterns, ultimate strength, failure modes, stiffness criteria, and ductility index.

4-2 Mechanical Properties of Concrete

After 28 days, three standard NSC cubes of (150×150×150) mm and three standard UHPC cubes from (50×50×50)mm and (70×70×70) mm for compressive strength and three standard concrete cylinders of (150×300) mm for NSC and (100 × 200) mm cylindrical for UHPC used for splitting tensile strength and modulus of elasticity were taken out of the container and tested according to **BS1881-116 [66]**, **ASTM-C496 [67]**, and **ASTM C469-2010 Standard [68]** respectively. The slump results for NSC are 87mm while, the fresh density for NSC is 23.15 kN/m3.

The mechanical properties of concrete samples are presented in Table (4-1). In this table, an average of three specimens for each reading is considered. The added values were deduced from the compressive strength of the cubes using the equations that follow the table below.

Table (4-1): Mechanical properties of the concrete (continue).

Slab specimen		Cube Compressive Strength fcu (MPa)	Cylinder Compressive Strength* fc' (Mpa)	Splitting Tensile Strength *fst* (Mpa)	Modulus of Elasticity** Ec (Mpa)
NSC	NC	28.875	23.1	2.54	24682
Sh.RN	NC	28.975	23.18	2.47	24461
1d-SC	NC	28.725	22.98	2.48	25482
	UHPC	125	125	9.375	46286.6
2d-SC	NC	28.8625	23.09	2.53	23983
	UHPC	123	123	8.854	45915
3d-SC	NC	28.8125	23.05	2.42	25433
	UHPC	126	126	9.1	46472
1d-SI C	NC	28.94	23.15	2.38	25568
	UHPC	127.4	127.4	9.8	46693
2d-SI C	NC	28.88	23.11	2.625	25499
	UHPC	127	127	9.8	46656
3d-SI C	NC	28.775	23.02	2.37	26378
	UHPC	125	125	9.5	46286.6
120-RC	NC	28.7	22.96	2.41	25325
	UHPC	126.8	126.8	9.6	46619
180-RC	NC	29	23.2	2.5	25590
	UHPC	122	122	9.15	45728
243-RC	NC	28.875	23.1	2.51	25460
	UHPC	121.5	121.5	9.2	45634
187-PF	NC	28.75	23	2.53	25310
	UHPC	120.8	120.8	8.7	45352
	NC	29.06	23.25	2.45	26400

Table (4-1): Mechanical properties of the concrete (continued).					
400-PC	NC	29.25	23.4	2.47	25988
	UHPC	126	126	10.1	46472
400-XC	NC	29.187	23.35	2.626	26310
	UHPC	126.6	126.6	10	46582

* $f\acute{c}$ (NSC) = 0.8 $f$cu (Mpa) according to (**BS8110-1-97 [69]**)
$f\acute{c}$ (UHPC) =1.0 $f$cu (Mpa) according to (**Larrard et al., 1994 [70]**)
** EC (UHPC) = 4140 $\sqrt{f\acute{c}}$ (Mpa) according to (**Adheem, 2016 [71]**)

4-3 Load-Deflection Response and Cracking Patterns

4-3-1 General Behaviour

In general, there are three phases of the load-deflection response: elastic uncracked, cracked elastic and inelastic up to the ultimate stages, where the first stage ends at the initiation of cracks and are shown in Figures (4-1) to (4-15). In the uncracked elastic phase, the deflection increased linearly in all samples with loading, because the materials in the stress and strain regions were elastic. In the elastic cracking stage, there was a linear relationship between load and deflection but with a decrease in slope. After this stage, the slope decreased dramatically and the increases in deflection worsened with a slight increase in the loading level until failure. The test results obtained for all samples are listed in Table (4-2) and discussed in the following sections. All the flat panels tested were free of cracks at the initial loading stages and responded elastically at low loading levels. The deflection was proportional to the applied loads. Later, as the load increased, more cracks developed. Generally, there were two types of cracks produced, radial cracks and tangential cracks. Radial cracks appeared and their width increased, and in the final stage, tangential cracks appeared and increased with expansion until

collapse occurs. Failure was defined as when the load could not be increased further.

Table (4-2): Cracking load, ultimate load and ultimate deflection of the tested samples.

Case study		Specimen designation	First crack KN	Deflection at service load* (mm)	Ultimate load pu (KN)	Ultimate Deflection Δu (mm)	Increasing in pu with respect to control %	Increasing in Δu with respect to control %
I		NSC	26	2.9	83.5	4.86	-----	-----
	G1	1d-SC	43	1.511	116.75	5.7	39.8	17.2
		2d-SC	47	1.067	154.5	6.77	85	39.3
		3d-SC	31	1.556	160	8.3	91	70.7
	G2	1d-SI C	33	1.38	137.5	6.44	64.6	32.5
		2d-SI C	33	2.94	158	10.03	89.2	106
		3d-SI C	30	1.965	166	8.85	98.8	82.1
	G3	120-RC	36	2.31	151	7.58	80.8	56
		180-RC	34	1.31	160.16	7.3	91.8	50.2
		243-RC	30	1.72	164	8.236	91.4	69.46
II		Sh.RN	35	2.065	98	4.84	-----	-----
	G4	187-PF	38	2.32	151.5	9.94	54.6	105.3
		187-XF	44	1.77	167	9.948	70.4	105.5
		400-PC	30	1.51	124	9.34	26.5	92.97
		400-XC	36	1.71	143	7.14	46	47.52

* Assumed service load = Ultimate load of reference slab/ 1.7 **[72]**

4-3-2 Pilot Flat Slab

This slab has been tested to verify the testing machine, adequacy of instruments, bearing and loading plates as well as to ensure that punching shear failure will occur before flexural failure. The failure occurred finally at a load of about (68 kN).

4-3-3 Control Flat Slab Specimen without Shear Reinforcement (NSC).

This specimen was made from normal-strength concrete (without shear reinforcement), which is regarded as a reference specimen for these test groups (G1, G2, & G3), as shown in Figure (3-4). An early first crack formed at load about (26 kN) (i.e. 31 % of the ultimate load) at a distance (1.5d) from the center of the slab approximately (d: represent average effective depth for all slab). After increasing the load level, as the load is increased to (42 kN), radial cracks are formed but it does not connect to the edges of the slab, then these cracks began to increase in width and length towards the edges of the slab. At load level (67 kN), tangential cracks are formed, then the punching shear failure occurred at the ultimate load of (83. kN), as shown in Plate (4-1). Figure (4-1), shows the Load-deflection curve.

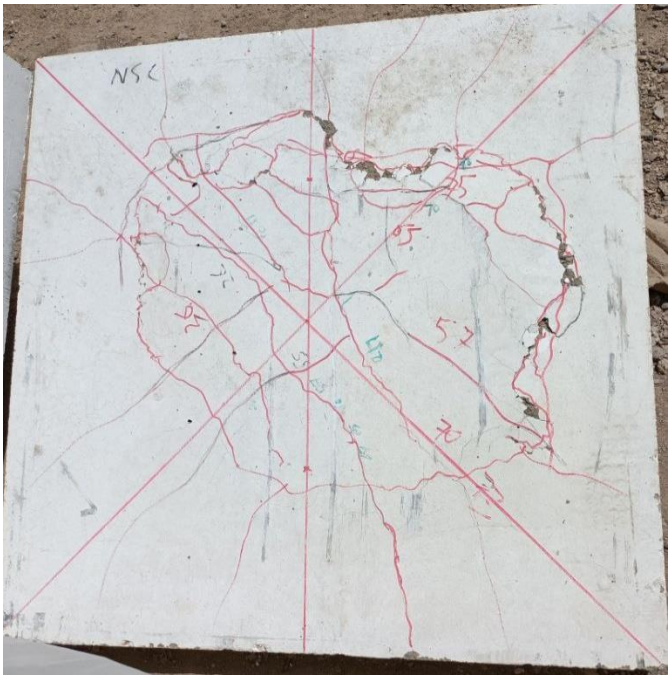

Plate (4-1): Cracking pattern specimen NSC at failure.

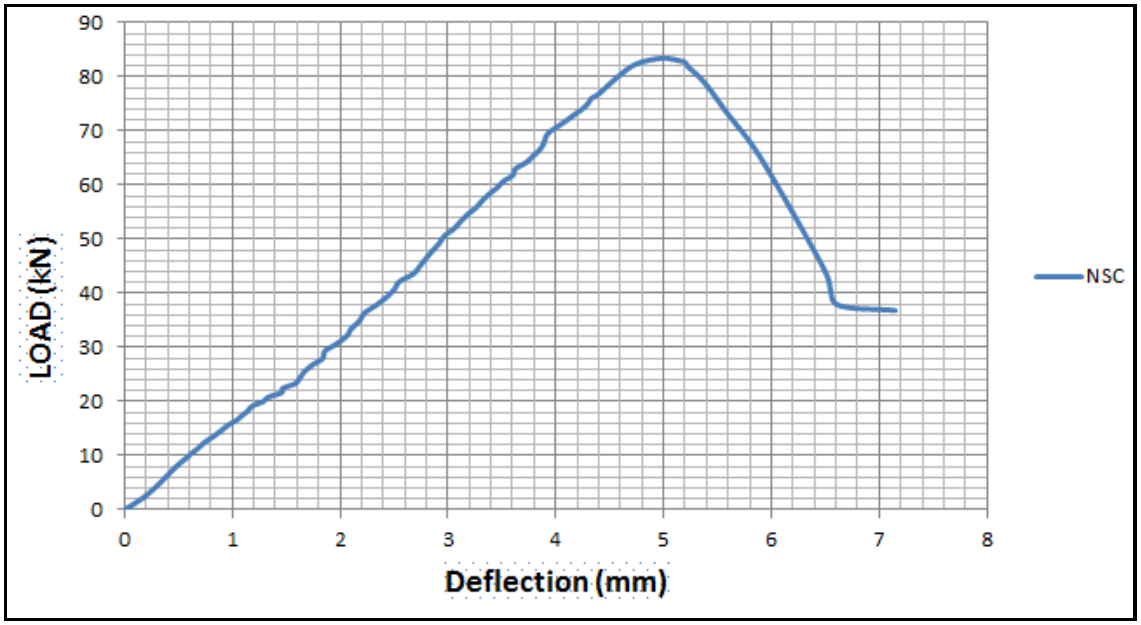

Figure (4-1): Load-deflection curve for specimen NSC.

4-3-4 Case Study (I) Groups (G1, G2, and G3):

All the flat slabs are hybrid concrete, ultra-high performance concrete casting in column-slab connection in different forms (G1: square shape, G2: rhombus shape and G3: circle shape). Each shape has three specimens (1d, 2d &3d) distance from the face of the column on each side, forming a strengthening region, with fixed thickness UHPC (40mm at compression face). The influence of these variables has been studied through cracking load, ultimate strength and failure mode and compared the results with those of reference specimen.

Specimen 1d-SC

Specimen 1d-SC is a flat slab with a square UHPC area of 210 * 210 mm. The first crack formed at a load of about (43 kN) (i.e. 36% of the ultimate load), and started from the projection angle of the column on the tension face. At the loading level (58 kN), the radial cracks started to extend from the column face towards the slab support.

When the load level was about (80%) of the final load, it was observed that no new cracks were initiated and the width of existing cracks increased in the NSC but cracks appeared in the tensile face at the edge of the UHPC region, as shown in Plate (4-2a). Then punching shear failure occurred at the ultimate load of (116.75 kN) as shown in Plate (4-2b). Figure (4-2) shows the load-deflection curve for this sample and its comparison with the NSC. It can be seen that the increase in the ultimate load is due to the presence of reinforcement by UHPC, but this reinforcement was not a good improvement and the decrease in the curve was somewhat sudden compared to the reference sample.

Specimen 2d-SC

The specimen 2d-SC (flat slab with square UHPC region of 320*320 mm). The first crack formed at the load of about (47 kN) (i.e. 30.4 % of the ultimate load) and started from the corner of the column-projection on the tension face. When the load increases, cracks began to form, similar to the first crack, radially from column projection and towards the edges of the slab.

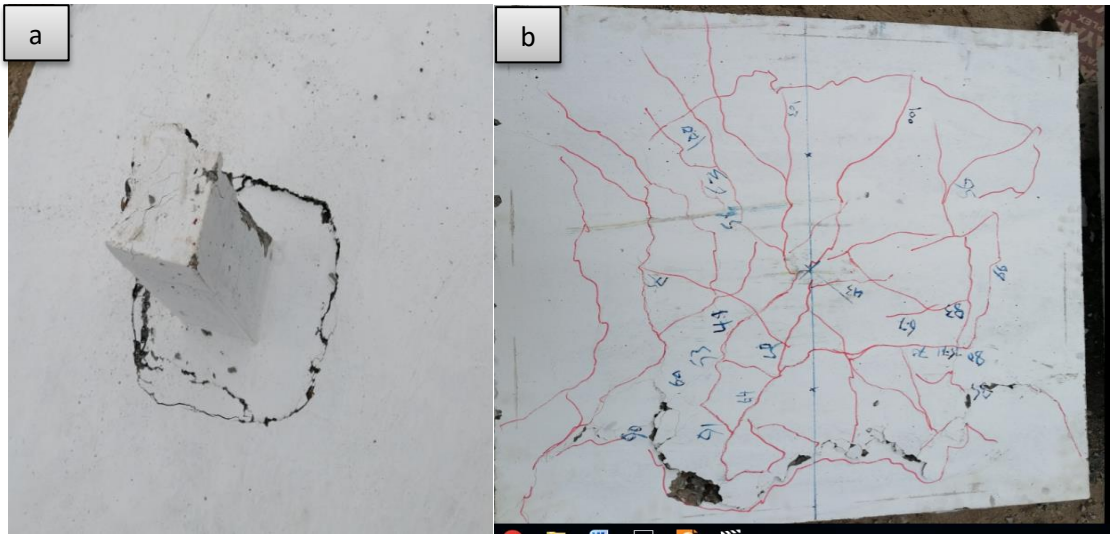

Plate (4-2): Cracking pattern for 1d-SC at failure, a: compression face b: tension face.

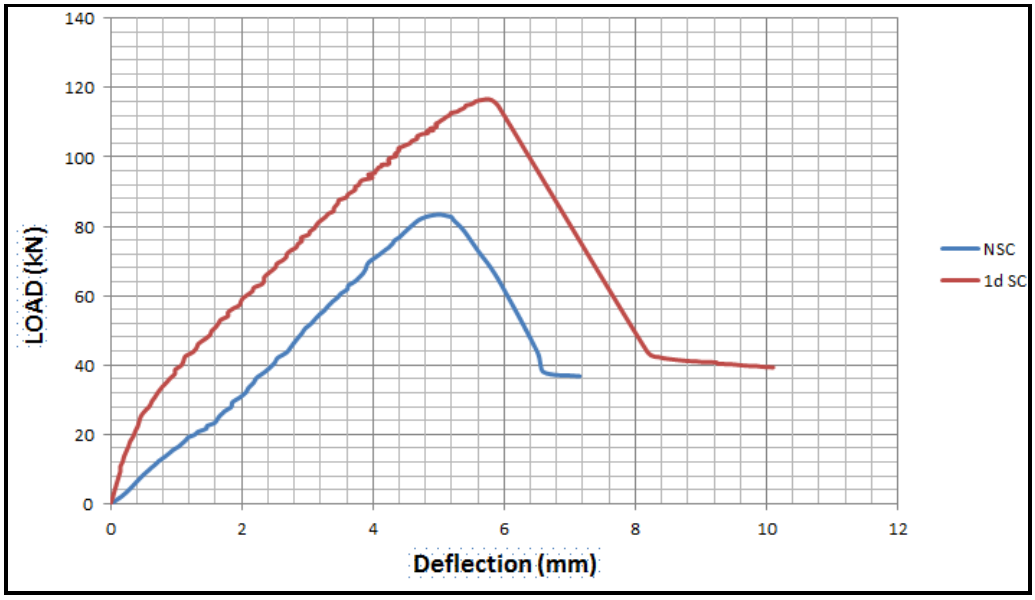

Figure (4-2): Load-deflection curve for Specimen 1d-SC.

It can be seen as illustrated in Plate (4-3), the cracks are marked in red and the numbers in green if we follow one of the cracks that started with 50 kN and then evolve (60, 65, 73, 88, and 91…etc.) towards the edge of the slab.

At load 125 kN cracks stopped generation in the tension face but were apparent around the area UHPC in the face of compression, as the load increased, these cracks developed, forming a failure of the punching shear and penetration deep into the slab at ultimate load (154.5 kN). The area UHPC for this specimen gave a strengthening ratio of about (85%) for the reference slab. Figure (4-3) shows the comparison between this specimen and the reference specimen and the amount of development in resistance by increasing the area of strengthening.

Specimen 3d-SC

The specimen 3d SC (flat slab with square UHPC region 430*430 mm). The first crack formed at the load of about (31 kN) (i.e. 19.5 % of the ultimate load), and started from the corner of the column-projection on the tension face, the first

crack was seen early approximately equivalent to its value in the reference specimen.

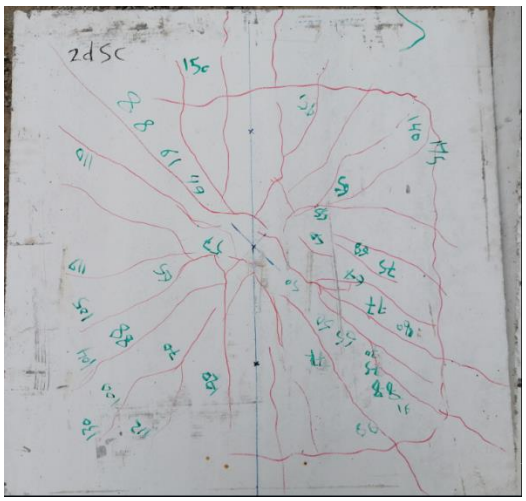

Plate (4-3): Cracking pattern for specimen 2d-SC at failure.

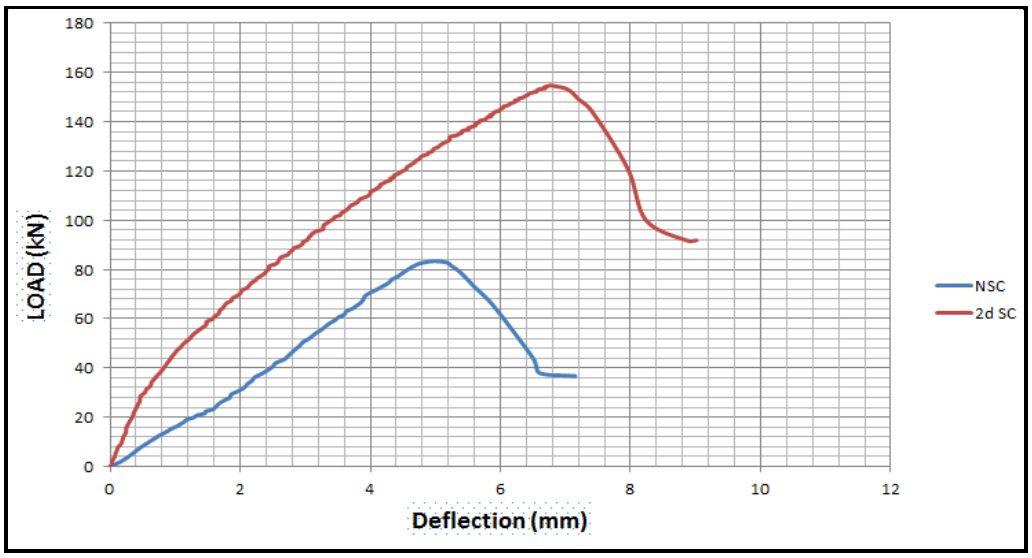

Figure (4-3): Load-deflection curve for specimen 2d-SC.

After that cracks began to form, similar to the first crack, radially from column projection and towards the edges of the slab.

Cracks developed in this slab similar to the previous two slabs (1d-SC & 2d-SC) at tension face, but it is completely different at compression face so that when

reaching the ultimate load (160 kN), the slab fails with a punching shear and the crack is around the perimeter of the column, an unfavorable place to fail, as in Plate (4-4a), and the failed area is in a semi-circular shape, as in Plate (4-4b).

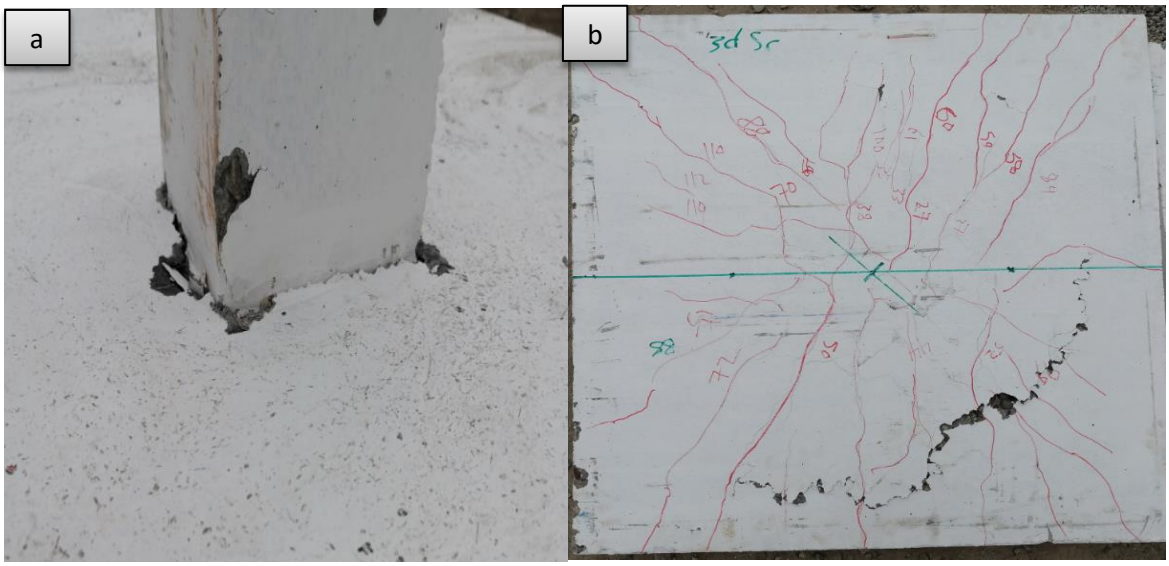

Plate (4-4): Cracking pattern for specimen 3d-SC at failure. a: compression face b: tension face.

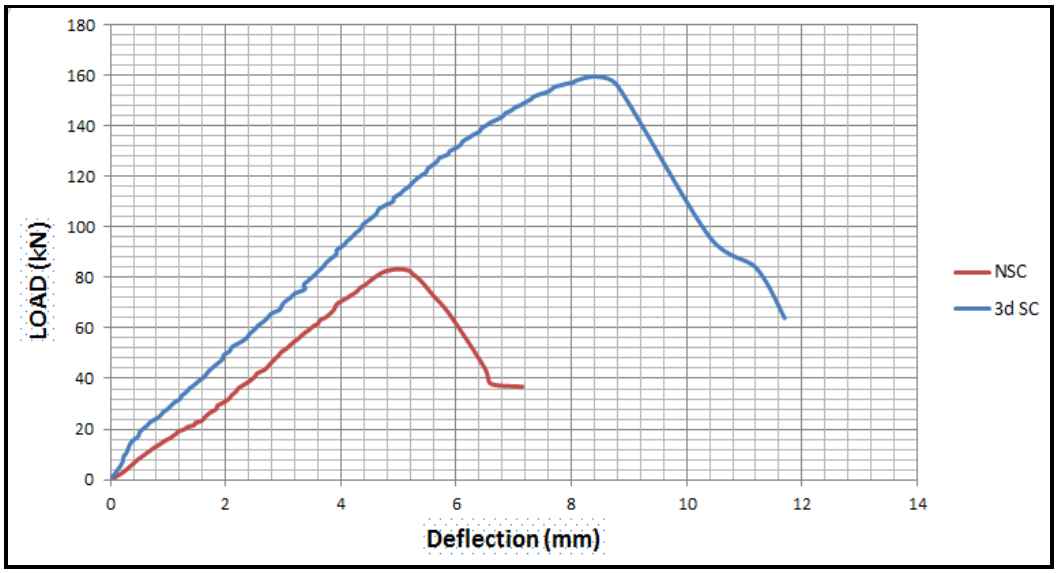

Figure (4-4): Load-deflection curve for specimen 3d-SC.

Specimen 1d-SIC

The specimen 1d-SIC (flat slab with rhombus shape UHPC region 210*210mm), the first crack formed at the load of about (33 kN) (i.e. 24 % of the ultimate load) the first crack appeared early started from the corner of column-projection on the tension face.

As the load is increased to (65 kN), radial shear cracks were formed and then the width of these cracks increased and developed extending towards the edges of the slab as the plate (4-5b), and with the load (108 kN) cracks stopped growing and cracks began to appear with an edge UHPC in the face of compression forming the failed space in the punching shear, its occurred at the ultimate load of (137.5 kN) as in Figure (4-5). As well as a crack through the space parallel to the face of the column as the plate (4-5a).

Specimen 2d-SIC

The specimen 2d-SIC (flat slab with rhombus shape UHPC region 320*320mm) has details as shown in Figure (3-4). The first crack formed at the load of about (33 kN) (i.e. 21 % of the ultimate load) the first crack appeared early and started from the corner of the column-projection on the tension face.

The behavior of the cracks is similar to the specimen 1d-SIC if it is radial cracks in the tension face up to the failure of the shear at the ultimate load (158 kN) as in Figure (4-6), but this failure of the punching shear occurs in this slab away from its center close to the edge of the slab as in the Plate (4-6).

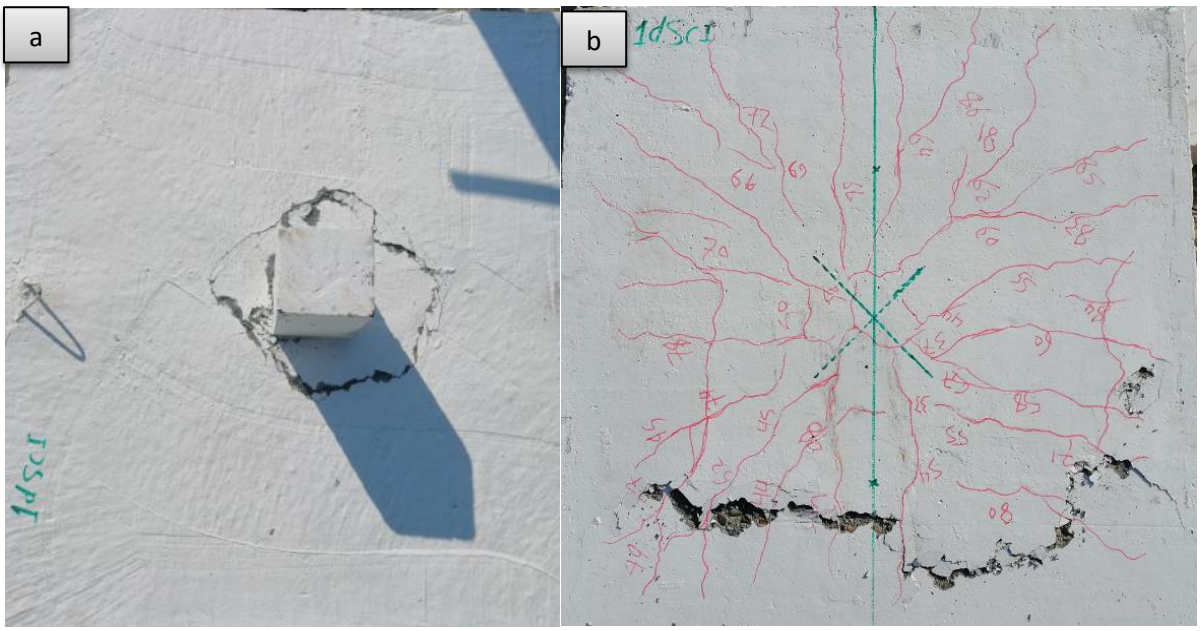

Plate (4-5): Cracking pattern for specimen 1d SIC at failure. a: compression face b: tension face.

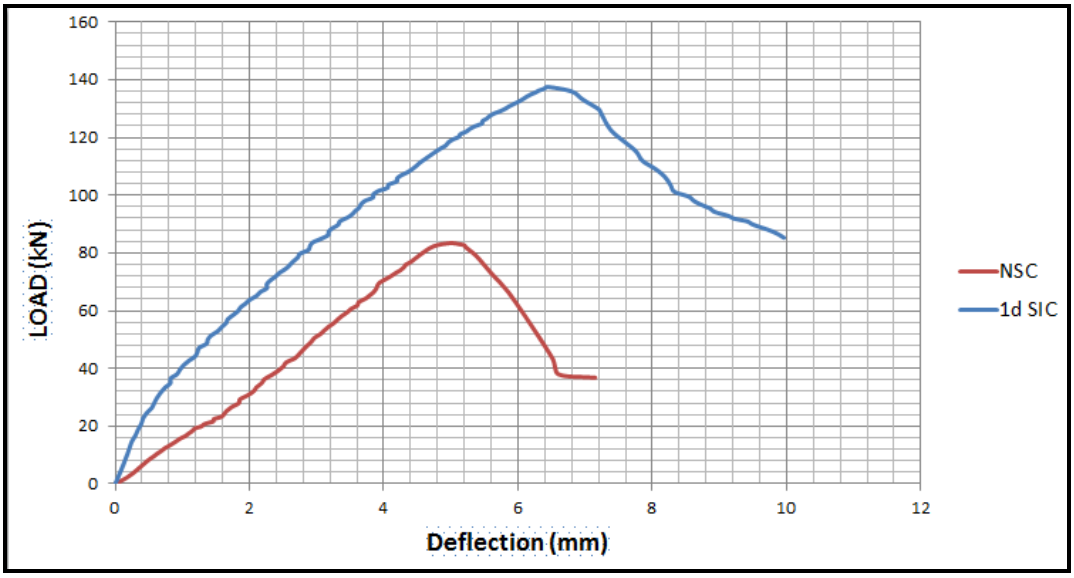

Figure (4-5): Load-deflection curve for specimen 1d SIC.

Specimen 3d-SIC

The specimen 3d-SIC (flat slab with rhombus shape UHPC region 430*430mm), has details as shown in Figure (3-4). The first crack formed at the load of about (30 kN) (i.e. 18 % of the ultimate load), the resistance of the slab to

failure up to the ultimate load after the first crack appeared early is due to the presence of high-performance concrete and the presence of steel fiber in it.

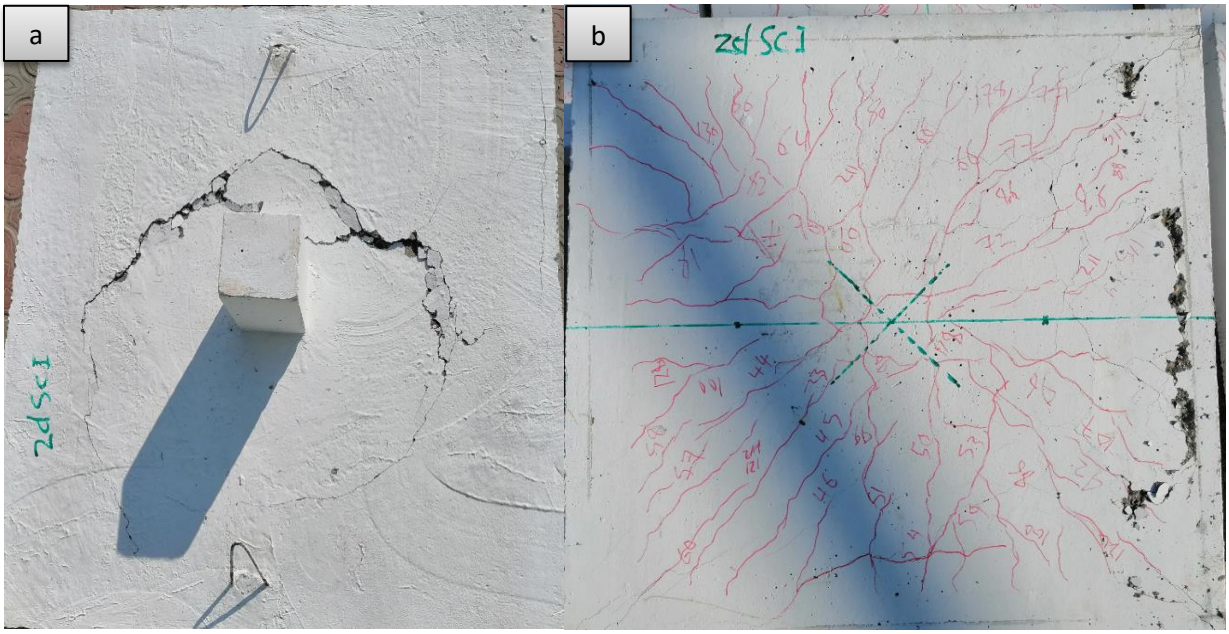

Plate (4-6). Cracking pattern for specimen 2d-SIC at failure. a: compression face b: tension face.

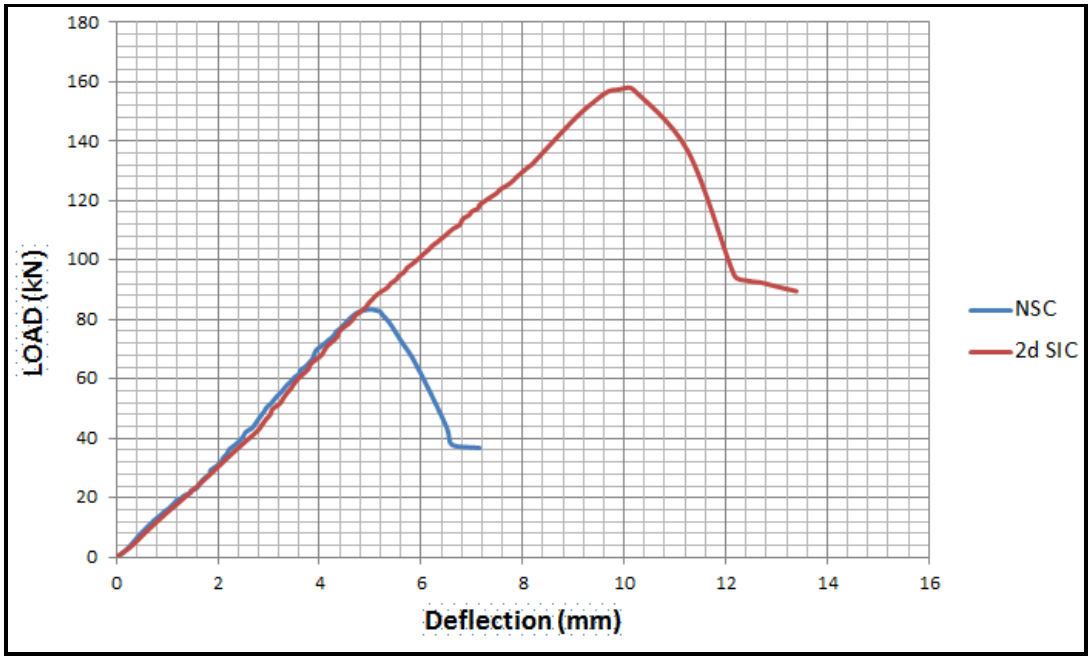

Figure (4-6): Load-deflection curve for specimen 2d-SIC.

The behavior of the cracks is similar to the specimens 1d-SIC and 2d-SIC, but what is noticeable in the crack pattern it is the occurrence of punching shear in the vicinity of the column in the compression face plate (4-7), and it is similar in its behavior to the specimen 3d-SC, which is considered equal to it in quantity UHPC. Because of the large area of UHPC the slab behaves as if it is made of the whole UHPC.

The similarity between (2d-SIC & 3d-SIC) was not only in the first crack and failure pattern, but the final load was close. Increasing the amount of UHPC by about (80%) did not lead to a noticeable increase in the final load, as it failed at (166 kN) as in Figure (4-7), through which we notice a sudden failure, as is the descending part of the curve.

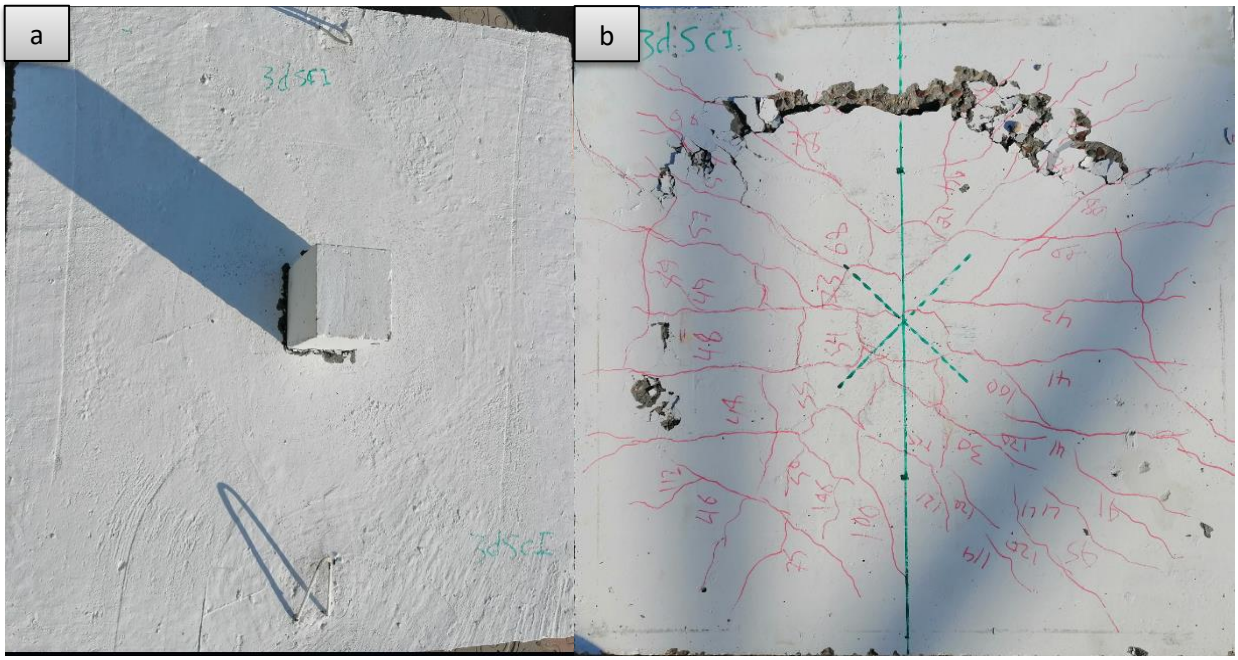

Plate (4-7). Cracking pattern for specimen 3d-SIC at failure. a: compression face b: tension face.

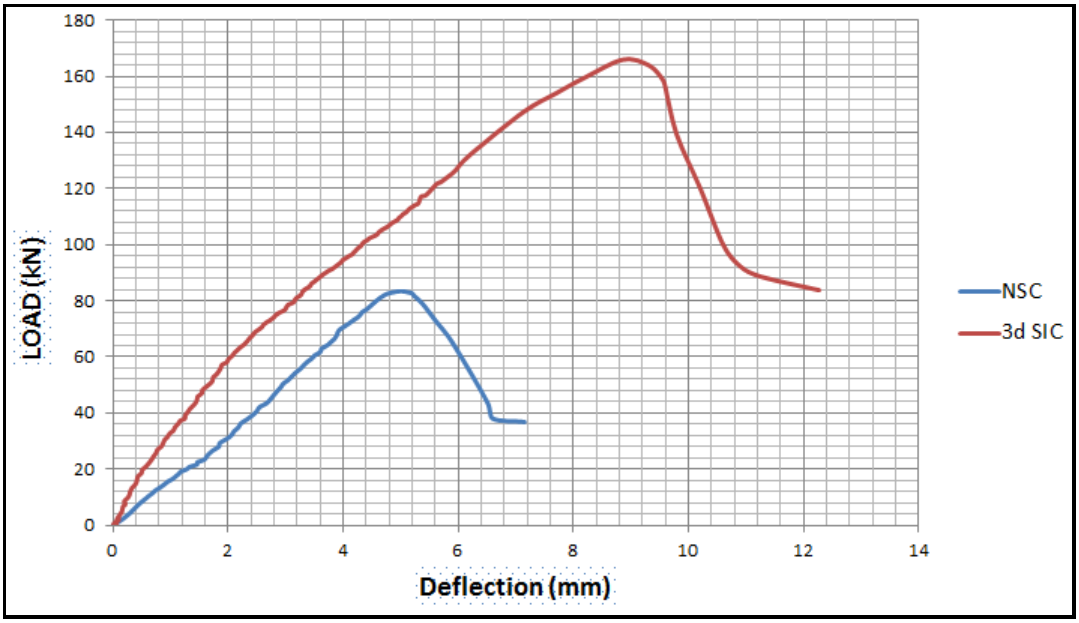

Figure (4-7): Load-deflection curve for specimen 3d-SIC.

Specimen 120-RC

The specimen 120-RC (flat slab with circular shape UHPC region radius 120mm) in a quantity UHPC equal to the quantity used in specimens 1d-SC & 1d-SIC, have details as shown in Figure (3-4). The first crack formed at a load of about (36 kN) (i.e. 24 % of the ultimate load) the first crack started from the column projection on the tension face.

Plate (4-8) shows that there is no difference in the failure pattern from the previous slabs, the growth of the radial cracks is the same as shown in the previous specimens, then the round cracks appear, which the specimen fails with the ultimate load (151 kN) as in Figure (4-8). This quantity of UHPC gives a good resistance reached (80%) of the reference sample.

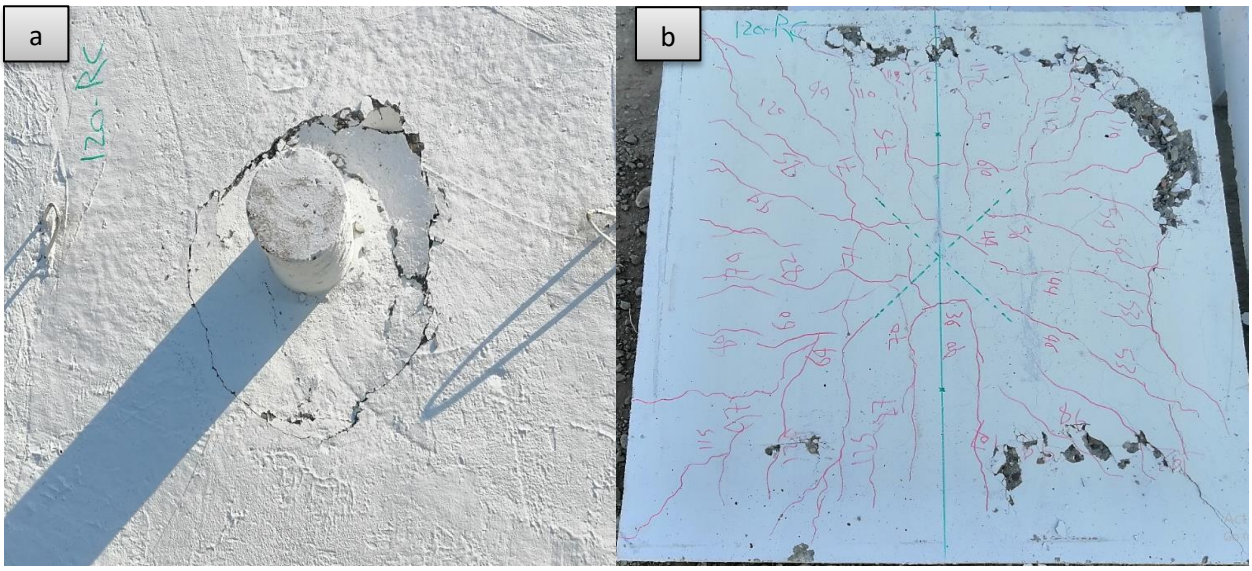

Plate (4-8). Cracking pattern for specimen 120-RC at failure. a: compression face b: tension face.

Specimen 180-RC

The specimen 180-RC (flat slab with circular shape UHPC region radius 180mm) in a quantity UHPC equal to the quantity used in specimens 2d-SC & 2d-SIC have details as shown in Figure (3-4). The first crack formed at the load of about (34 kN) (i.e. 21 % of the ultimate load) the first crack started from the column projection on the tension face.

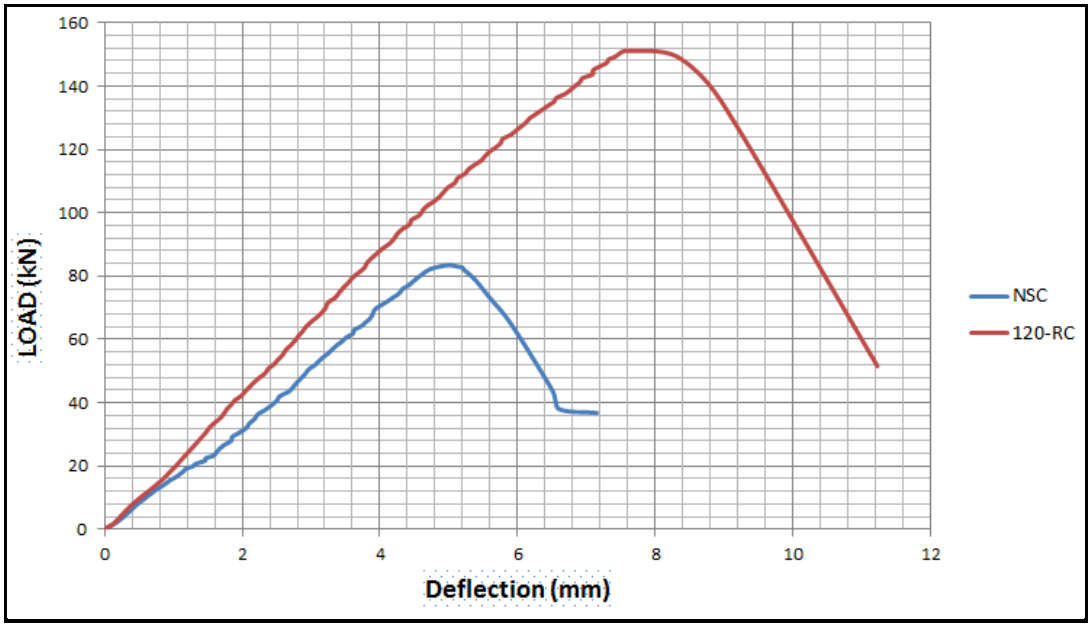

Figure (4-8): Load-deflection curve for specimen 120-RC

Plate (4-8) shows that there is no difference in the failure pattern from the previous groups, the growth of the radial cracks is the same as shown in the previous specimen, then the round cracks appear in the tension face, which the specimen fails with the ultimate load (160.16 kN) as in Figure (4-9). There is a difference in the pattern of cracks in the face of compression as in the plate (4-9a) that the failure of the punching is not circular and not within the region UHPC it is observed that the crack goes far.

Specimen 243-RC

The specimen 243-RC (flat slab with circular shape UHPC region radius 243mm) in a quantity UHPC equal to the quantity used in specimens 3d-SC & 3d-SIC has details as shown in Figure (3-4). The first crack formed at a load of about (30 kN) (i.e. 19 % of the ultimate load) the first crack started from the column projection on the tension face.

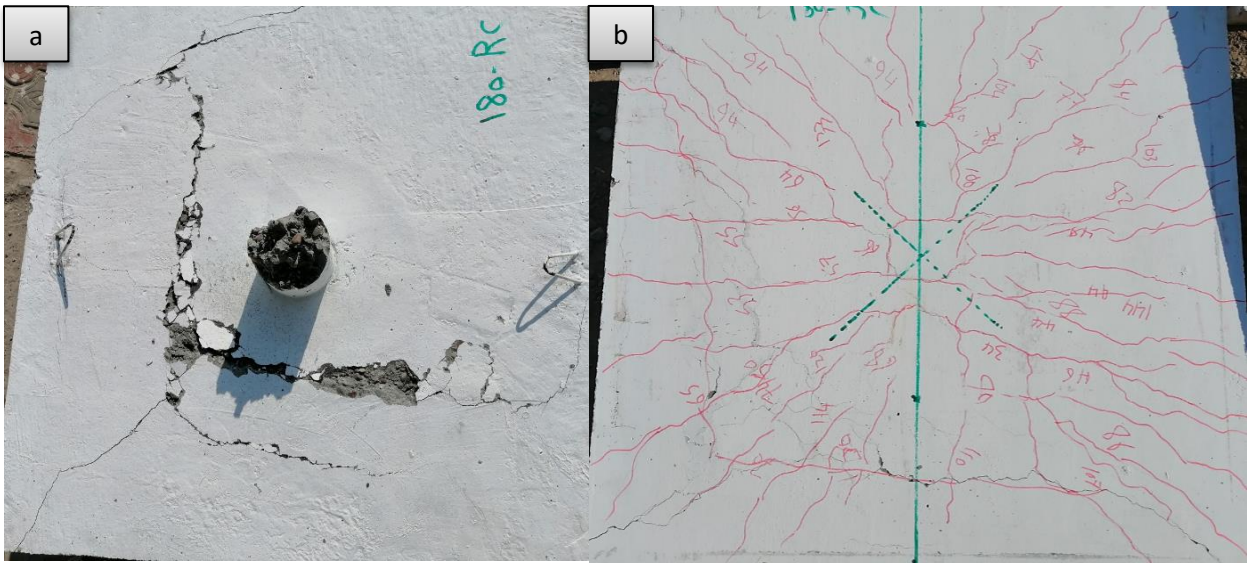

Plate (4-9). Cracking pattern for specimen 180-RC at failure. a: compression face b: tension face.

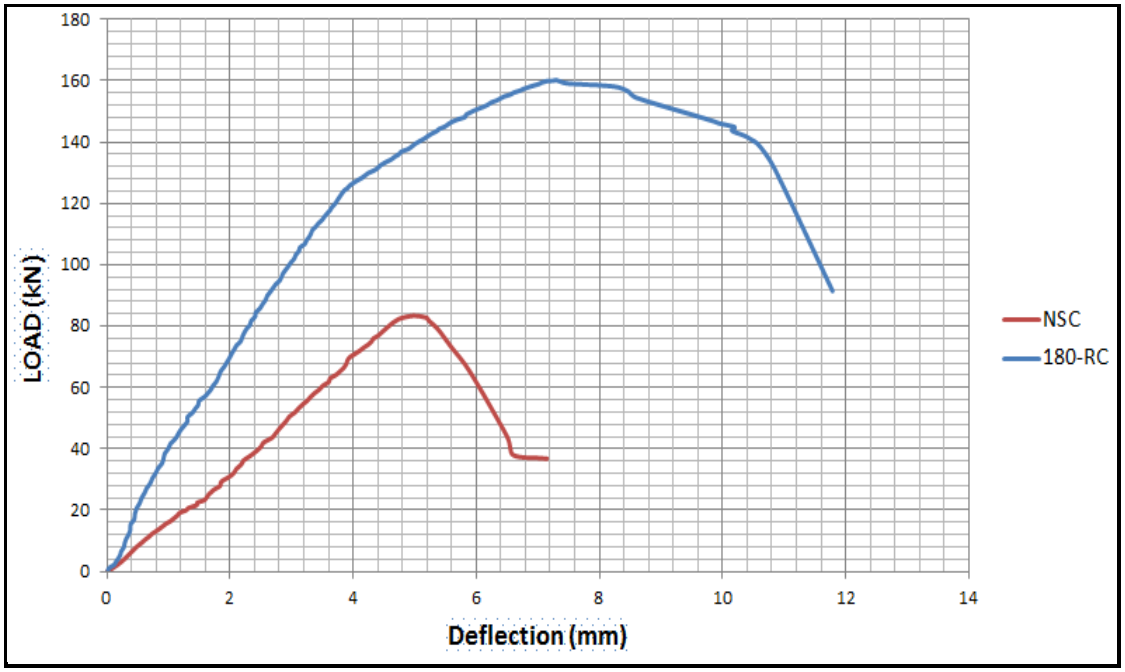

Figure (4-9): Load-deflection curve for specimen 180-RC.

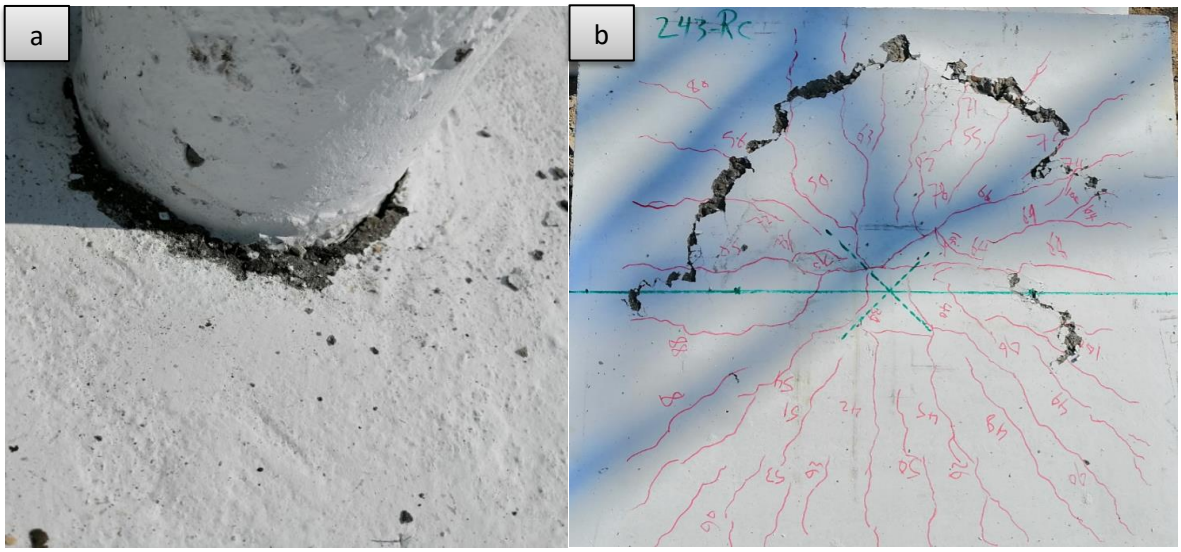

Plate (4-10). Cracking pattern for specimen 243-RC at failure. a: compression face b: tension face.

The failure pattern does not differ from the previous specimens except in the descending region of the punching failure, as it is small compared to the previous specimens as in Plate (4-10b). There is a difference in the pattern of cracks in the compression face as in the plate(4-10a) that the failure of the punching shear was circular in the circumference of the column, and no other cracks appeared. The same behavior specimens (3d-SC & 3d-SI C) the equivalent specimen with a quantity UHPC and this place of failure is unfavorable.

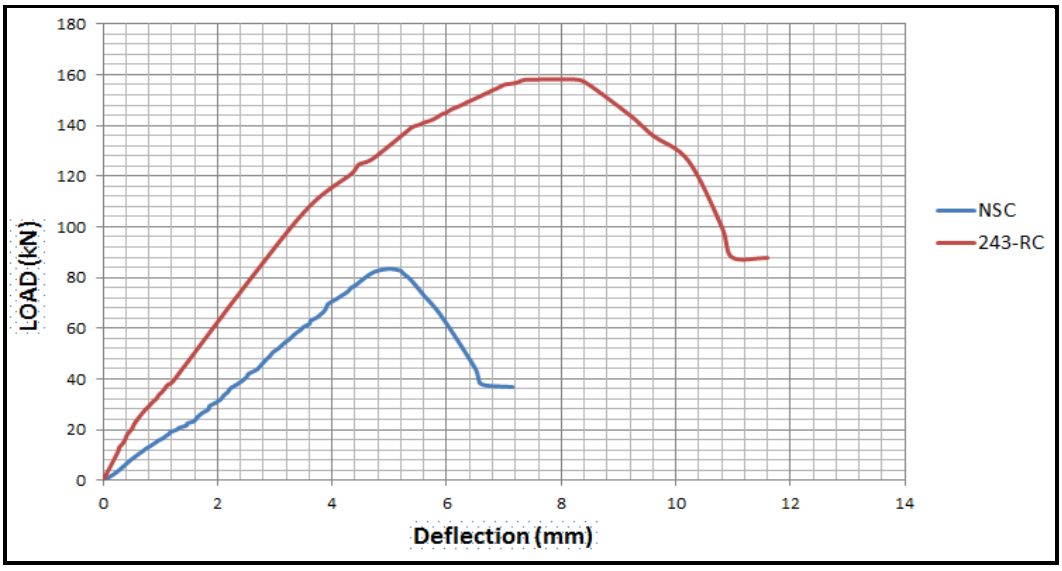

Figure (4-10): Load-deflection curve for specimen 243-RC.

4-3-5 Control Flat Slab Specimen with Shear Reinforcement (Sh.RN).

This specimen was made from NSC (with shear reinforcement). This slab was designed by punching shear reinforcement according to (ACI 318-19) which is regarded as a reference specimen for this test group (G4), see Figure (3-4). The first crack formed at a load of about (35 kN) (i.e. 35.7 % of the ultimate load) the first crack started from the corner of the column-projection on the tension face, away from punching shear reinforcement, as in Plate (4-11).

After increasing the load level, as the load is increased to (45 kN), Longitudinal cracks began to appear along the reinforcement area of the punching shear, as the load progressed, these cracks increased and similar ones appeared and then longitudinal cracks also appeared perpendicular to the previous one. At the load (80 kN) circular cracks appeared in more than one failure circumference until the slab failed with the ultimate load (98 kN) as in Figure (4-11).

Plate (4-11): Cracking pattern for specimen Sh.RN at failure.

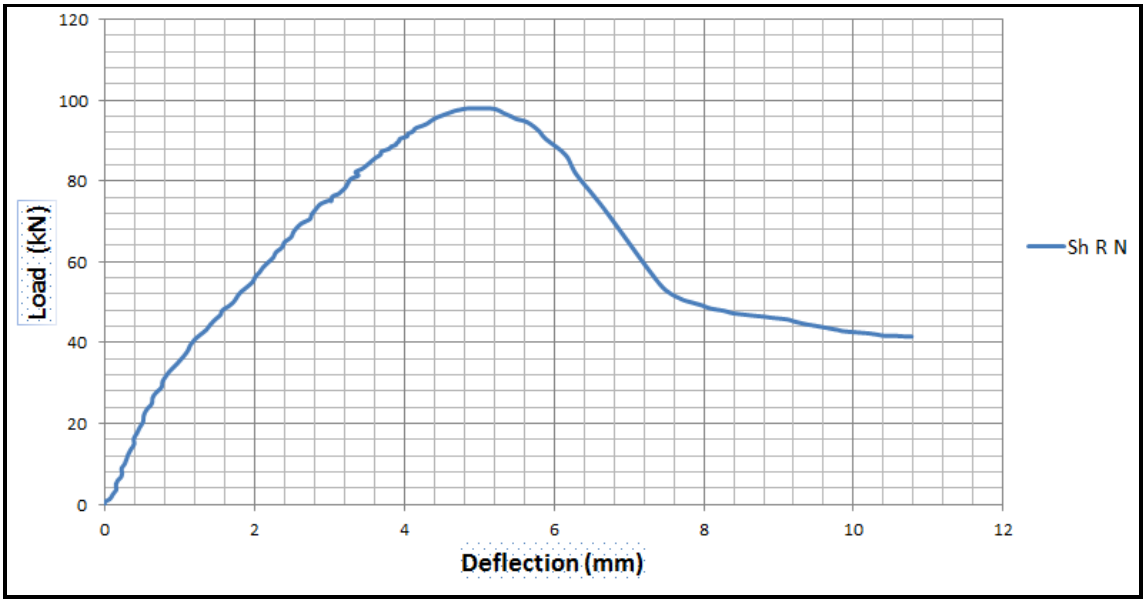

Figure (4-11): Load-deflection curve for specimen Sh.RN.

4-3-6 Second Test Case Study (II) Groups (G4):

All the flat slabs madding hybrid concrete, (NSC & UHPC) ultra-high performance concrete casting in column-slab connection, in this case of the study, the flat slab was strengthened by replacing the punching shear reinforcement with (UHPC) and because it is an expensive material, so we used the same amount of it in all specimens with different forms and different thickness. The influence of these variables has been studied through cracking load, ultimate strength and failure mode and compared the results with those of the reference slab.

Specimen 187-PF

The specimen 187-PF (flat slab with + shape of UHPC) is 187 mm from all faces of the column and width equal to section of column (100 mm) and full depth of slab (80mm), the 187 mm equal to 3.4d according to ACI 318-19 code where d: average effective depth (55mm), as shown in Figure (3-4). The first crack started

from the corner of column-projection extending into a contact area NSC/UHPC at load about (38 kN) (i.e. 25 % of the ultimate load) and the first crack in UHPC started at load (96 kN) (i.e. 63% of the ultimate load) as shown in Plate (4-12).

The radial cracks began to appear after the first crack and progressed in width and extension toward the edges of the slab with the progression of the load. After load (128 kN) cracks appeared in the face of tension until the slab failed to load the ultimate (151.5 kN) as in Figure (4-12), and the area of failure in the punching shear consists of UHPC plus a part of the normal concrete, as in plate (4-12a).

Specimen 187-XF

Specimen 187-XF (flat slab with X. shape of UHPC) same shape and dimensions as UHPC in specimen 187-PF but the shape of UHPC rotated at an angle of 45.

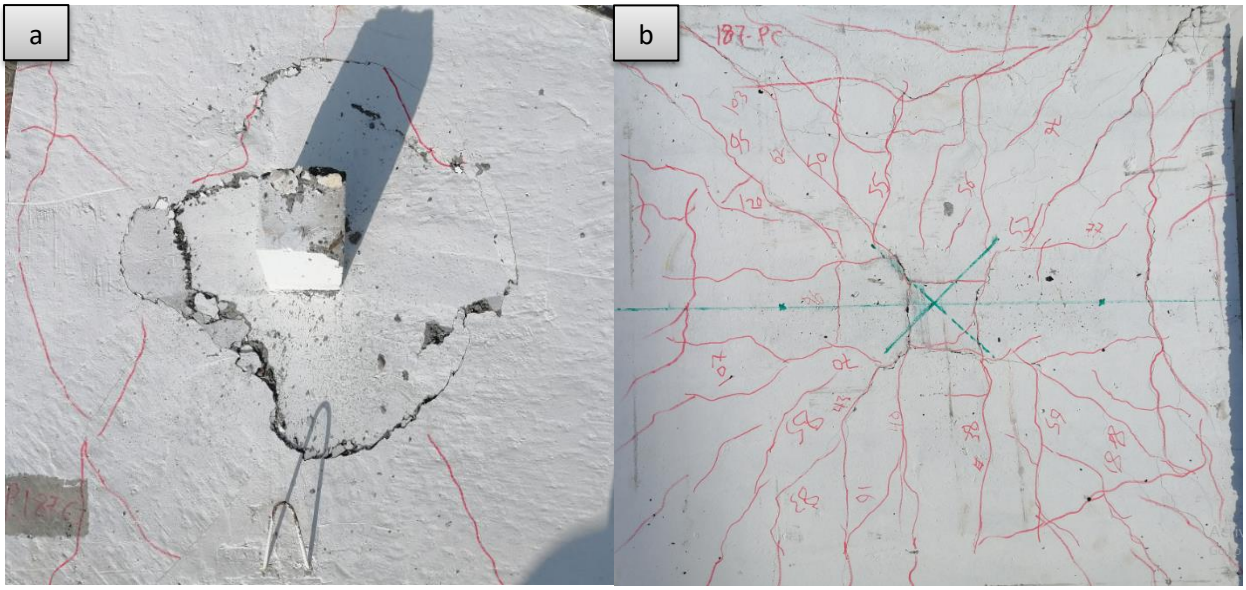

Plate (4-12).Cracking pattern for specimen 187-PF at failure. a: compression face b: tension face.

The first crack appeared far from the site of the column at the end of the UHPC area, and this is preferable, which is to move away from the area where the

column is connected to the slab at a load of about (44 kN) (i.e. 26.3 % of the ultimate load) and the first crack in UHPC started at load (75 kN) (i.e. 45 % of the ultimate load) as shown in Plate (4-13): The cracks behave similar to the previous slab, except that it gave a high resistance as it failed in ultimate load (167 kN) as in Figure (4-13).

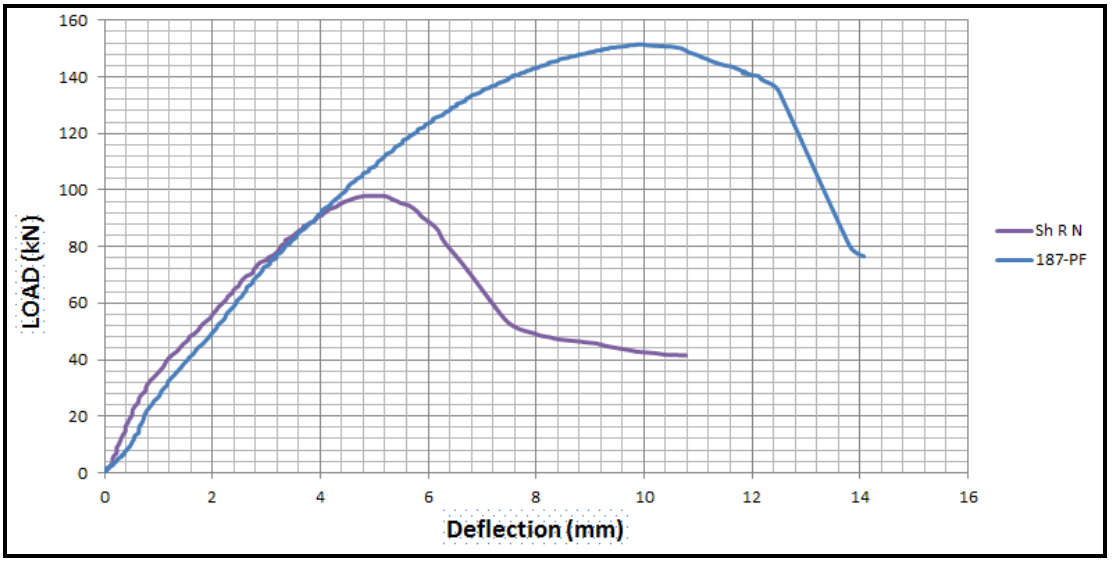

Figure (4-12): Load-deflection curve for specimen 187-PF.

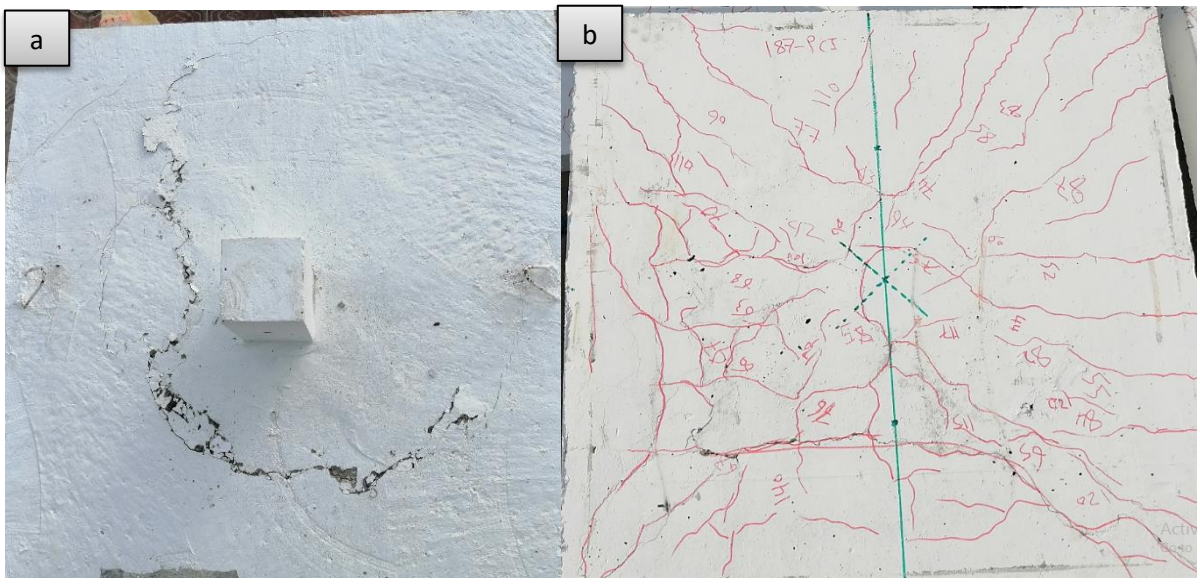

Plate (4-13): Cracking pattern for specimen 187-XF at failure. a: compression face b: tension face.

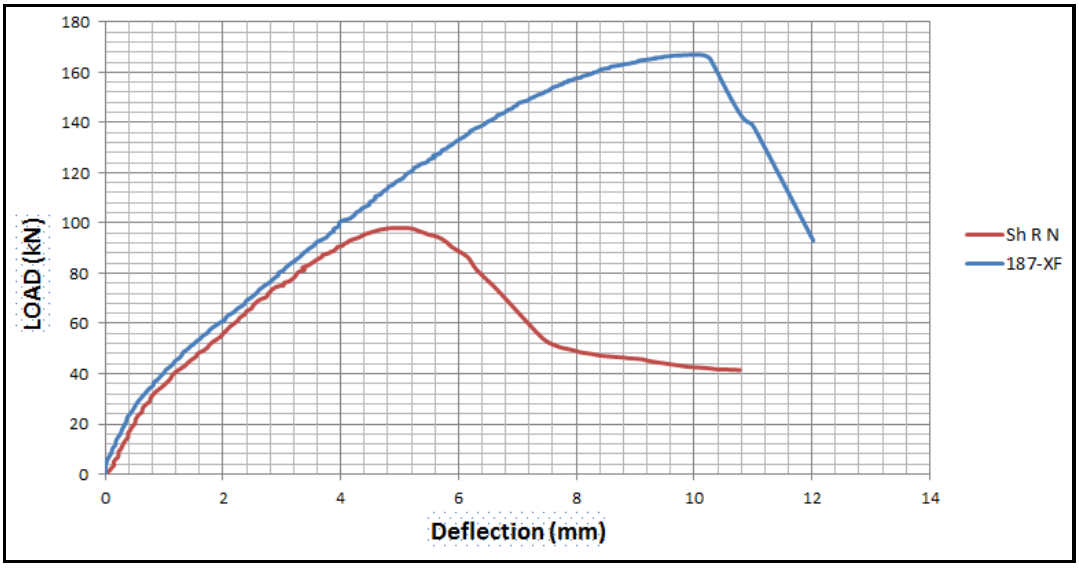

Figure (4-13): Load-deflection curve for specimen 187-XF.

Specimen 400-PC

The specimen 400-PC (flat slab with +. shape of UHPC) same shape and amount of UHPC as specimen 187-PF but with half the thickness of the slab (40 mm in compression face), so the dimension becomes (400 mm) from every side. The first crack started from the corner of the column projection extending into a contact area NSC/UHPC at load about (30 kN) (i.e. 24 % of the ultimate load) and the first crack in the bottom UHPC area started at load (80 kN) (i.e. 64% of the ultimate load) as shown in Plate (4-14).

The radial cracks began to appear (after load 30kN) symmetrically in the four quadrants of the slab and at each load. The growth of these cracks stopped after (75%) of the ultimate load, then the cracks appeared in the contact area, the two types of concrete in the face of the compression of the slab, then the slab failed with circumferential cracks as indicated in the red Plate (4-14), but they did not

appear in the tension face. Indeed, the resistance of the slab was not high as in Figure (4-14), but the type of failure changed to flexural failure.

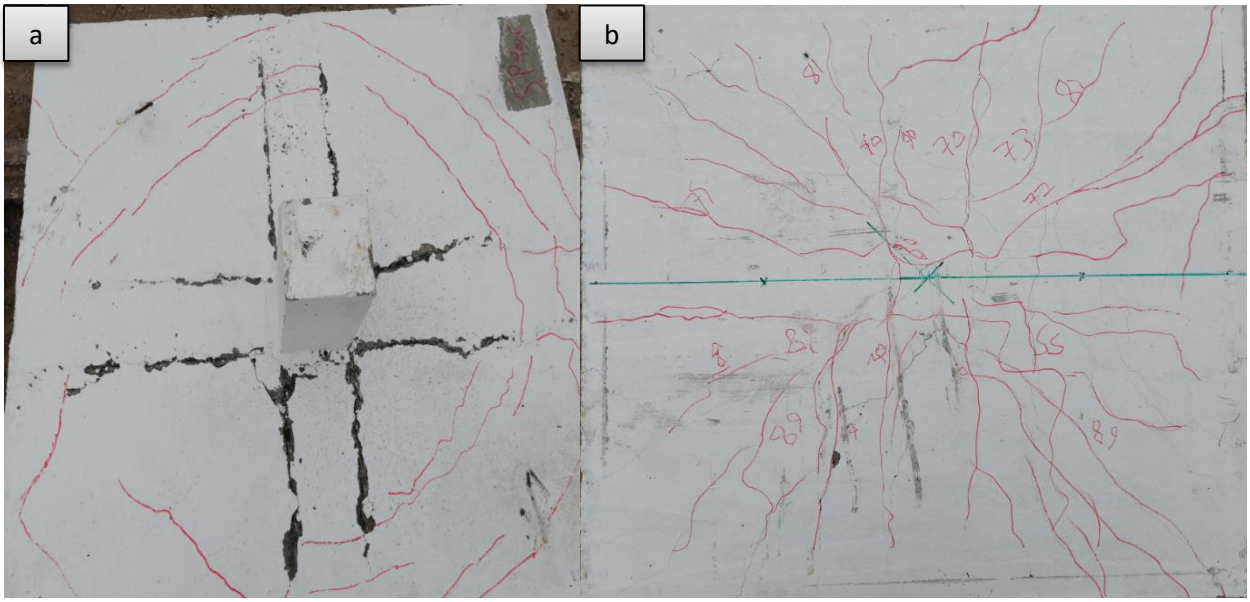

Plate (4-14).Cracking pattern for specimen 400-PC at failure. a: compression face b: tension face.

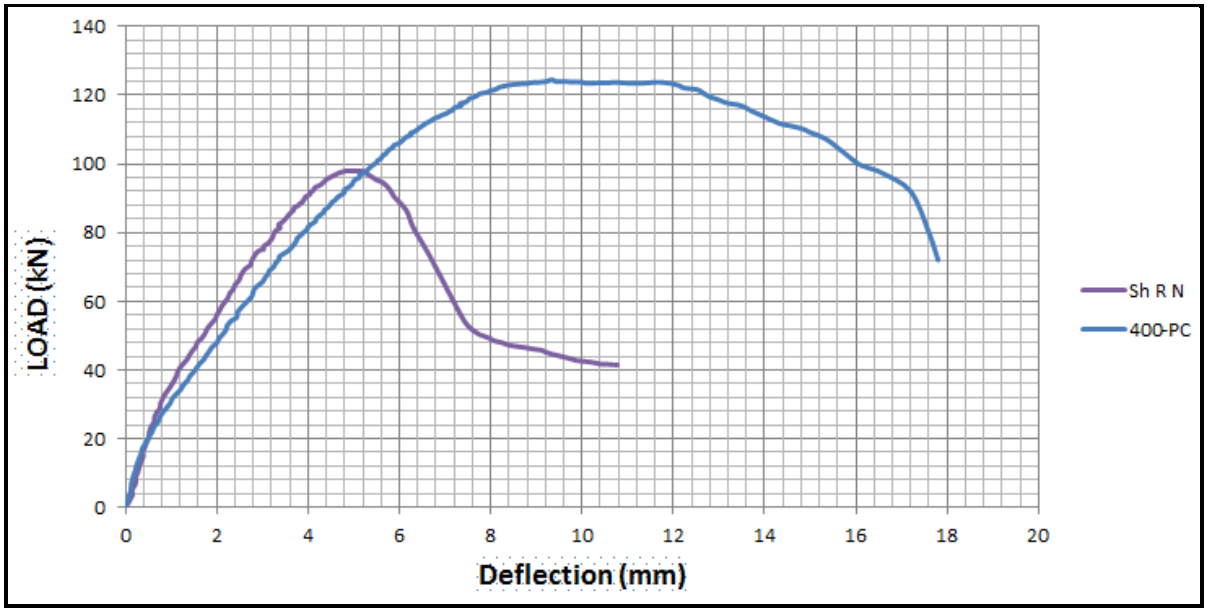

Figure (4-14) the Load-deflection curve for specimen 400-PC.

Specimen 400-XC

The specimen 400-XC (flat slab with X. shape of UHPC) same shape and dimensions as UHPC in specimen 400-PC but the shape of UHPC rotated at an angle of 45.

The first crack appeared a little away from the column due to the effect of the shape UHPC at load about (36 kN) (i.e. 25 % of the ultimate load) and the first crack in the bottom UHPC area started at load (60 kN) (i.e. 42% of the ultimate load) as shown in Plate (4-15). The development of radial cracks is similar to the previous slabs, but the failure of the punching occurred at the end of UHPC in the tension face, but in the face of compression it obtained a distance equal to the column section from the face of the column.

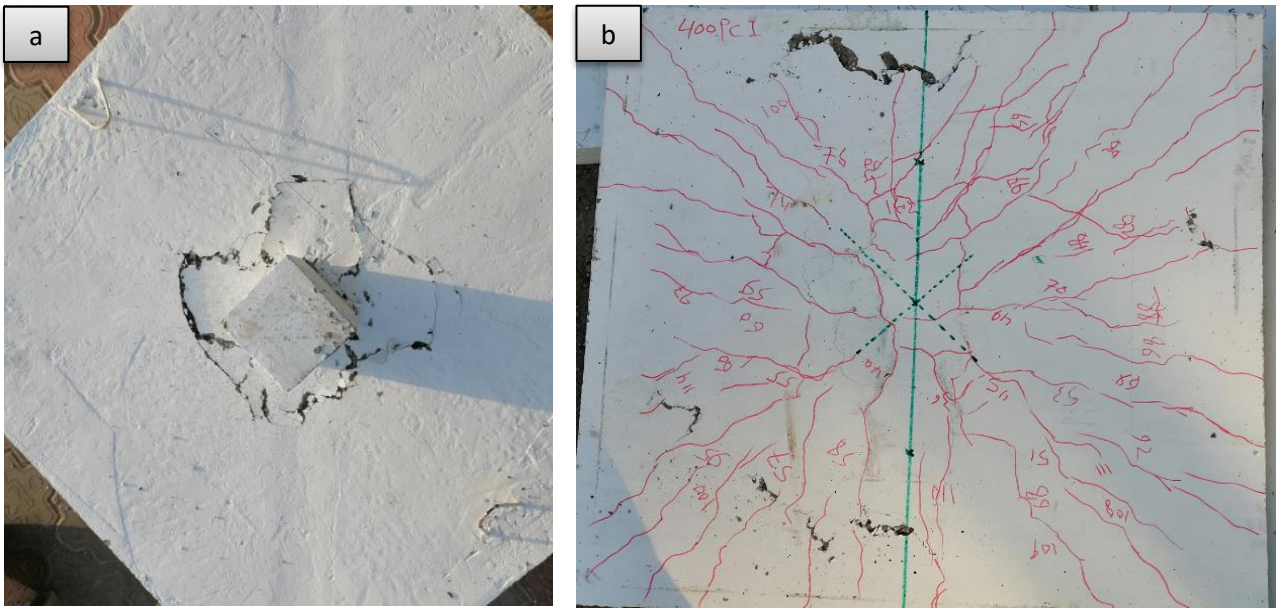

Plate (4-15).Cracking pattern for specimen 400-XC at failure. a: compression face b: tension face.

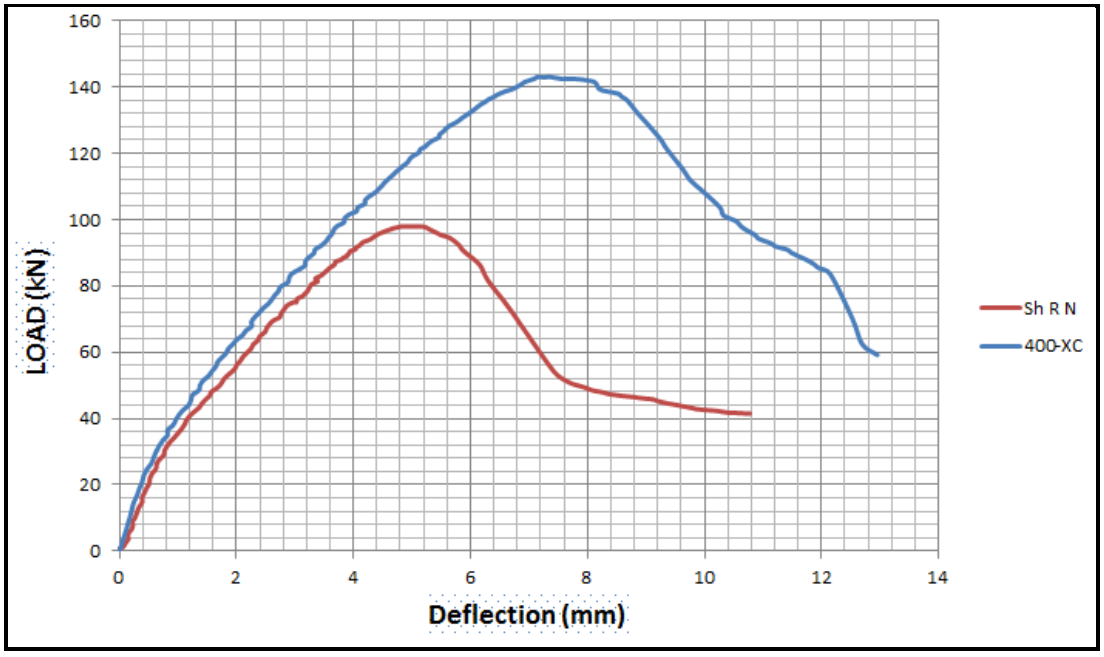

Figure (4-15): Load-deflection curve for specimen 400-XC.

4-4 Effect of Considered Variables on Structural Response.

A summary of the effect of considered variables (area UHPC, depth UHPC and its shape) will be discussed and devoted on the main structural response such as the first cracking loads of shear cracks, ultimate load, deflection at service load, failure mode as well as the best way to strengthen, as presented in Table (4-2).

4-4-1 Cracking Load

By reviewing the above specimens, we note that the first crack always occurs in normal concrete and started from the column projection on the tension face and growth toward the slab edge due to the concentration of stresses except in 187-XF it appears at the end of the UHPC region, and this may be one of the advantages of this application UHPC.

From the observation of Table (4-2), the value of the first crack ranges (26-48 kN) there is a clear discrepancy in the two groups (G1&G4) and convergence in

the two groups (G2&G3). As for the percentage of its appearance from the ultimate load, it ranged (from 19-36%). With further loading, additional cracks formed from the column face and moved in parallel to the first crack.

4-4-2 Ultimate Strength

For the results of the first case study (I) the ultimate load capacity (Pu) for each tested specimen and the comparison with the reference one NSC are listed in Table (4-2). In general, the ultimate load of the slab increases with the increase in the area of UHPC we notice this in groups (G1, G2, & G3.), so the percentages of increase in the group (G1) were 40%, 85%, & 91% for 1d-SC, 2d-SC, & 3d-SC, respectively. The percentages of increase in group (G2) were 64%, 89%, & 98% for 1d-SIC, 2d-SIC, & 3d-SIC respectively. The percentages of increase in group (G3) were 80%, 91%, & 91% for 120-RC, 180-RC, & 243-RC respectively.

We notice the effect of the UHPC shape, so the same quantity of UHPC gave a ratio (40%, 64%, & 80%) in the group (G1, G2, & G3) respectively, we conclude from this that the circular application in this quantity UHPC is ideal.

While the effect of the shape is small in the quantities of UHPC the rest in the three groups, if it ranges (from 85-98%), where was the highest percentage in the rhombic shape for specimen 3d-SIC.

On the other hand, for the second case study (II) the ultimate load capacity (Pu) for each tested specimen and the comparison with the reference one Sh.RN. In general, the ultimate load of the slab increases with the increase in the depth and shape of UHPC we notice this in group (G4) so the percentages of increase in this group were 55%, 70%, 27%, & 46% for 187-PF, 187-XF, 400-PC, & 400-XC respectively.

Although the same amount of UHPC was used in these specimens, the optimal use was in the 187-XF reached 70%, which is the same thickness UHPC in the specimen 187-PF, but it was rotated at an angle of 45.

4-4-3 Cracking pattern

Plates (4-1) to (4-15) explain the cracking pattern on the tension face for all specimens after failure. All specimens showed similar behavior in terms of cracking patterns and it can be summarized as follows. At the first stage of loading, the applied load was increased by a fixed increment up to the formation of the first crack. The first crack formed at the tension side of the specimen around the column according to the control (N.S.C) specimen. The first crack started from the corner of the column projection on the tension face, in the weaker material (normal strength concrete), then growth toward the slab corner.

At the second stage of loading, the spread of the cracks, as well as the corresponding load values on the slab surface detected and marked within each load increment up to failure. At this stage of loading, radial cracks began to extend from the face of the column toward the support of the slab. After more loading, this radial crack began to extend and then additional radial cracks were spread in the slabs in a different direction.

When the load level was approximately (80%) of the ultimate load, it was noted that no new cracks were initiated and the width of the cracks existing in NSC increased.

4-4-4 Deflection Response

Through Table (4-2) and Figure (4-16a), it is possible to know the effect of the presence of punching shear reinforcement on the ultimate deflection, so the deflection remains the same approximately (4.85mm) with the increase of the ultimate load by (14.5 kN).

In general, using UHPC gave an increase, in the central deflection but with varying proportions. The rate of increase, with respect to the control, for the first study case (ı) ranged from (17 to 106%), and for the second case study (II) ranged from (47.5 to 105%) as listed in Table (4-2). This increase in deflection is due to the high flexural strength of the UHPC that resulted from the presence of steel fiber and the good bond between fibers and the matrix. Where the fibers work on bridging the micro cracks growth. Therefore, when the distribution of fiber is good within the cross-section of the slab the proportion of deflection will be increased.

From the test results, can note that when increasing the area cast with UHPC as in Figure (4-16b), and can note that when changing the shape of UHPC for the same quantity changes the ultimate deflection, we notice an increase in the circular shape (56mm) with an increase in the load as well as in Figure (4-16d).

When comparing the casting of UHPC with all the thickness of the slab or half of it, the specimen 400-PC gave an ultimate deflection close to the specimen 187-PF despite the difference in the load as in Figure (4-16d), and this indicates the effectiveness of casting UHPC in the compression face.

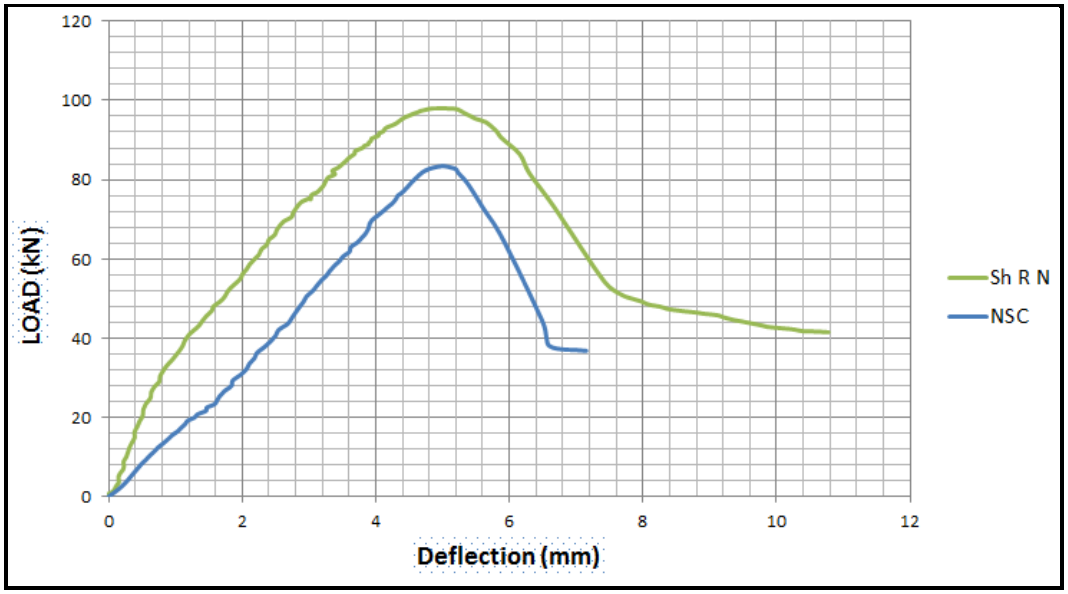

Figure (4-16): Load-deflection curves of the tested flat slabs (contines).

(a) Effect of the presence or absence of punching shear reinforcement.

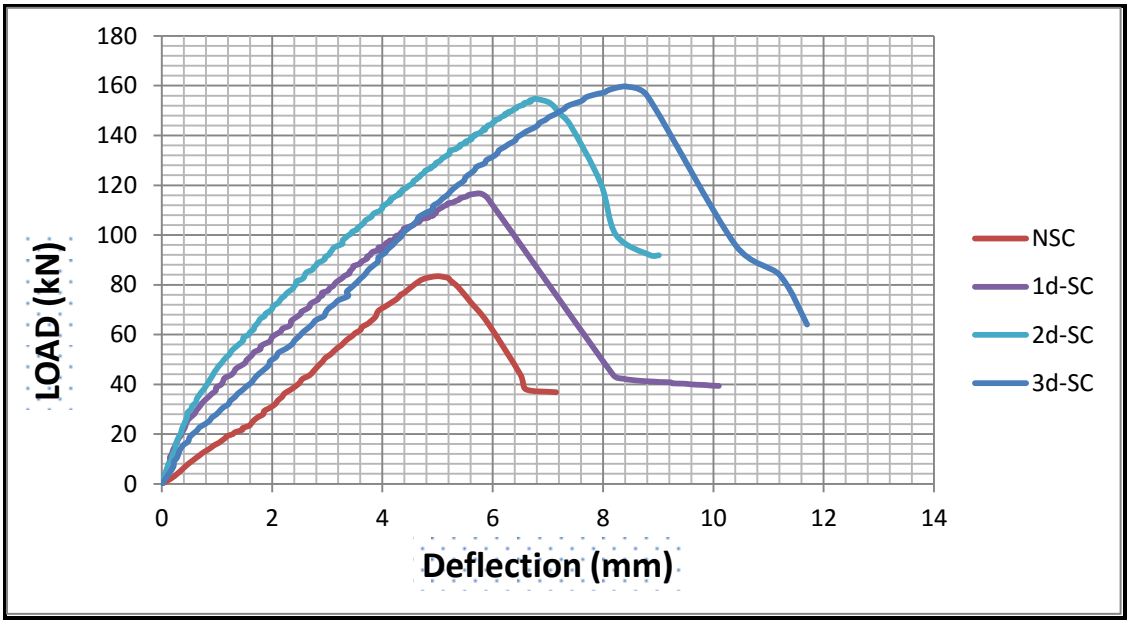

Figure (4-16): Load-deflection curves of the tested flat slabs (b) Effects of the area UHPC zone (contines).

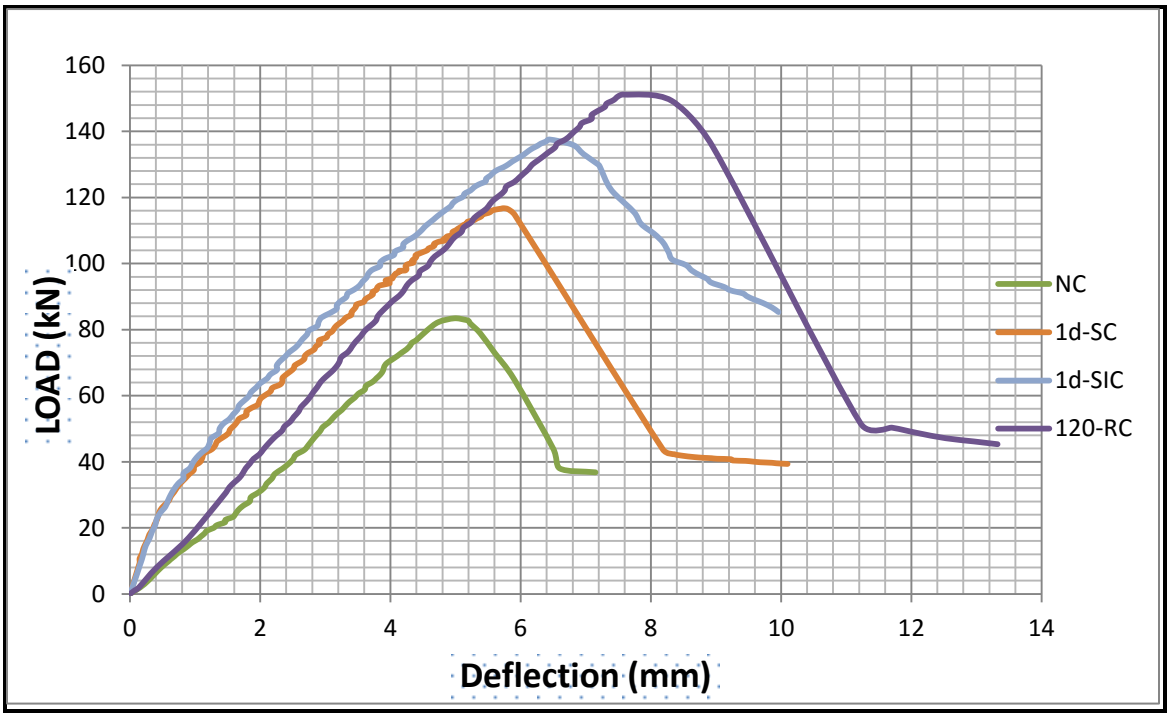

Figure (4-16): Load-deflection curves of the tested flat slabs (c) Effects of the shape UHPC area (contines).

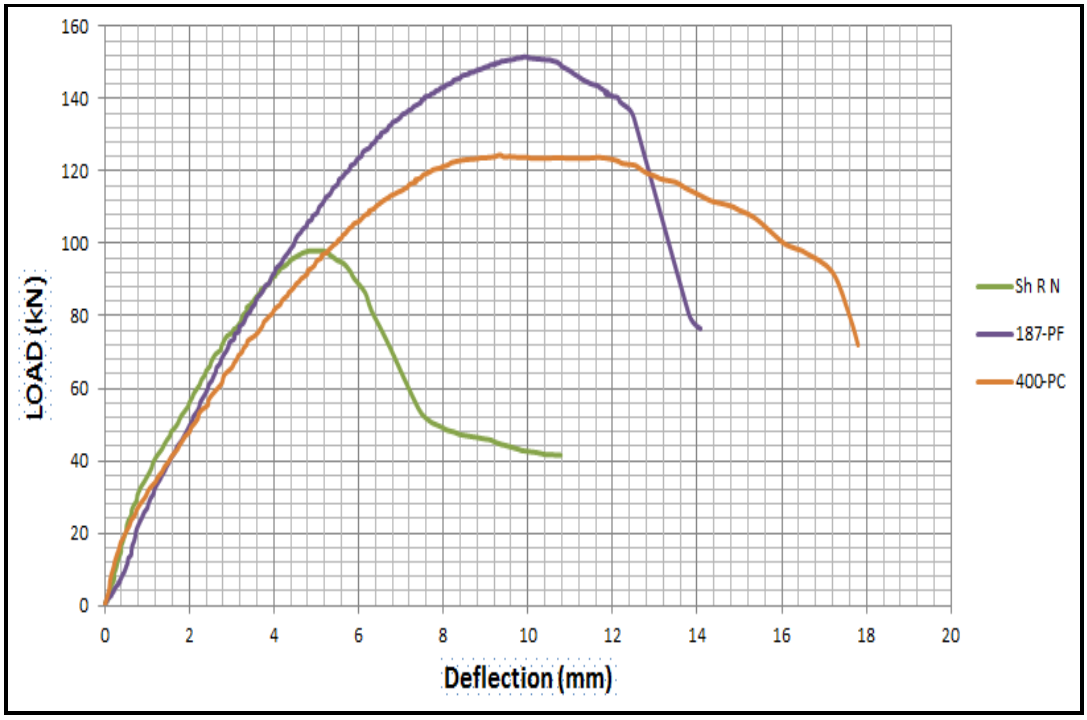

Figure (4-16): Load-deflection curves of the tested flat slabs (d) Effects of the thickness UHPC area (contines).

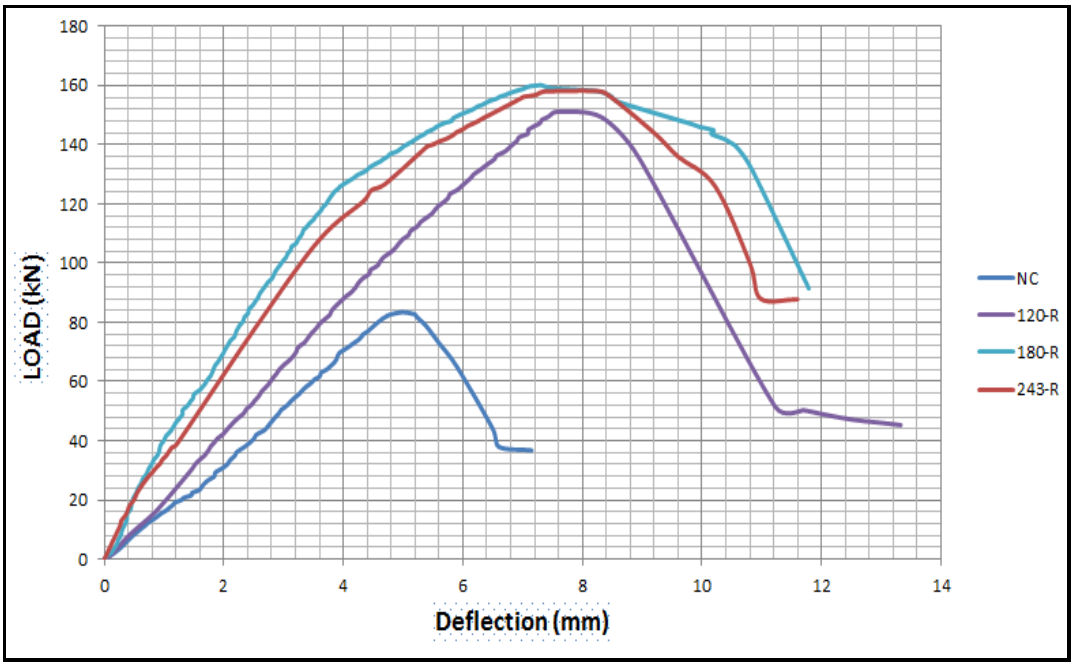

Figure (4-16): Load-deflection curves of the tested flat slabs (contined).

4-4-5 Stiffness Criteria

Stiffness is defined as the load required for producing unit deformation in the member. the stiffness criteria of any member can be determined as the slope of the secant which is drawn in the load-deflection curve at 0.75 of the ultimate load **[73]**. The stiffness criteria of the flat slabs are given in Table (4-3).

Table (4-3): Stiffness criteria of the tested flat slabs.

Flat Slab Symbol	0.75 Pu. (kN)	Deflection at 0.75 Pu. (mm)	Stiffness, K (kN/mm)*
NSC	62.625	3.62	17.3
1d-SC	87.56	3.477	25.18
2d-SC	115.875	4.277	27.09
3d-SC	120	5.366	22.36
1d-SIC	103.125	4.06	25.4
2d-SIC	118.5	7.1493	16.575
3d-SIC	124.5	5.83	21.35
120-RC	113.25	5.283	21.436
180-RC	120.12	3.72	32.29
243-RC	118.6	4.197	28.25
Sh.RN	73.5	2.84	25.88
187-PF	113.625	5.313	21.386
187-XF	125.25	5.518	22.698
400-PC	93	4.88	19.05
400-XC	107.25	4.261	25.17

*Stiffness (K)=0.75Pu/0.75 δu

The stiffness of the flat slabs was enhanced with the use of ultra-high performance concrete in column-slab connection, because often the use of UHPC

increases the stiffness of concrete and reduces its damage, but not by a large percentage and not always, some specimens did not give strong stiffness and perhaps less than the reference specimen such as 2d-SIC. In the second case study, the stiffness is lower in all specimens that do not contain shear steel reinforcement, because the use of internally reinforced steel leads to an increase in the moment of inertia and thus increases the stiffness.

4-4-6 Ductility Index of the Tested Slabs.

Ductility has an important role in reinforced concrete members, and this importance is prominent in those designed for seismic areas. Where these members are supposed to have the ability to bear high loads to allow people to be evacuated when earthquakes occur. The ductility, according to **[74]**, can be defined as the ratio between the displacement corresponding to the final load (Δu) and the displacement corresponding to the first yield of bending reinforcement (y). As for the ductility of the slabs, it can be calculated using the method developed by **[75]** and **[76]**. This method was also recommended by **[77]** who considered the displacement factor as an indicator. Often, the determination of yield displacement makes it difficult when calculating ductility factors from experimental data because the load-deflection relationship may not have a well-defined yield point. This may occur, the deflection at yielding which is the intersection of the tangent drawn to the beginning of the curve with the horizontal line at the ultimate, when a vertical line is projected from this point on the curve **[78]**. Figure (4-17) explains the considered approach in that determination of the specimens (2d-SC) calculating procedures of the ductility index from the load-deflection curves.

Because the yield in a different part of the structure starts at a different loading level or as a result of the nonlinear behavior of the material. The ductility of all the tested slabs is illustrated in Table (4-4).

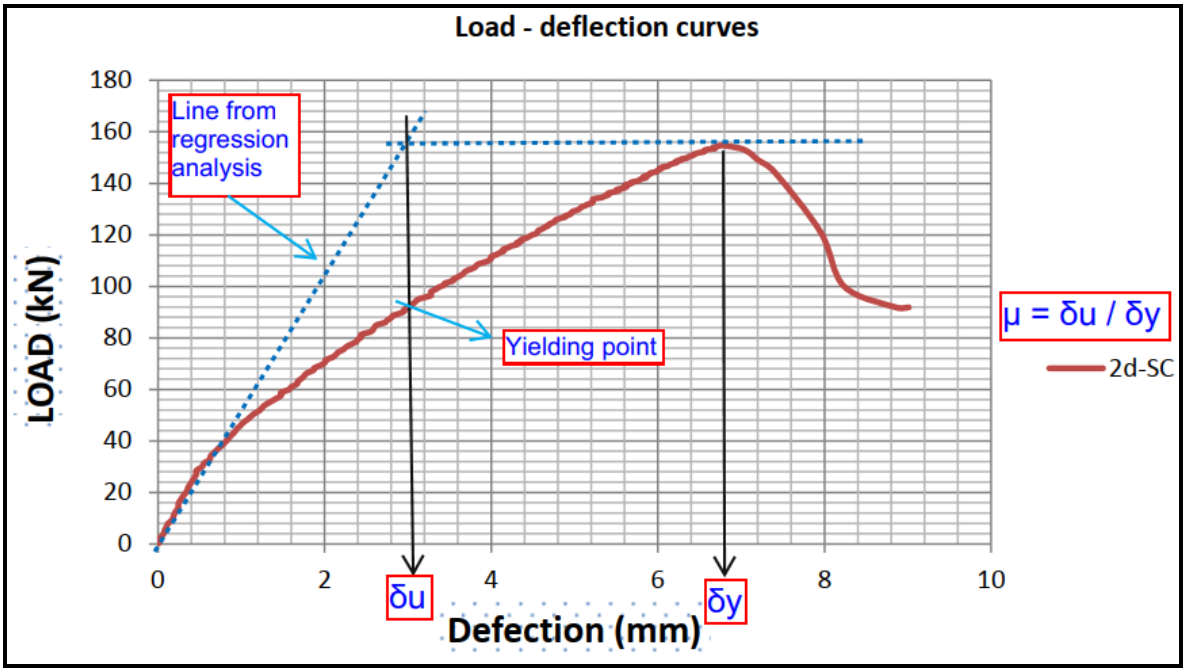

Figure (4-17): Determination of the ductility index [78].

Table (4-4): Ductility factor (μ) for the tested flat slabs.

Flat Slab designation	Ultimate deflection δu (mm)	Yielding deflection δy (mm)	Ductility index(μ)*
NSC	4.86	3.38	1.44
1d-SC	5.7	2.4	2.375
2d-SC	6.4	3.1	2.065
3d-SC	8.3	3.3	2.51
1d-SI C	6.44	2.38	2.7
2d-SI C	10.03	5	2
3d-SI C	8.85	4.9	1.8

Table(4-4) continues			
120-RC	7.58	5.1	1.5
180-RC	7.3	3.3	2.2
243-RC	8.236	3.8	2.16
Sh.RN	4.84	2.1	2.3
187-PF	9.94	4.1	2.42
187-XF	9.948	3.6	2.76
400-PC	9.34	3.7	2.54
400-XC	7.14	4.15	1.72

* Ductility index (μ) = δu / δy

Through the test result table (4-4), all specimens gave a ductility index greater than that index of the control slab, because it contains UHPC which is characterized by high ductility, the reason for this is that it contains steel fibers. The ductility index is convergent for almost all slabs, and the reason may be due to the lack of effect of increasing the area of UHPC in addition to its lack of effect on the shape of UHPC.

4-4-7 Energy Absorption index of the Tested Slabs (Toughness).

Energy absorption capacity can be defined as that area under the load-deflection curve of the tested slabs. This area was calculated up to the ultimate load and corresponding displacement. **[79]** Identified the energy absorption capacity of reinforced concrete members as a measure of absorbed energy up to its ultimate state. The authors supposed that the energy absorption capacity up to the final status of the slabs is the most appropriate index in the structural response against ground motions. Energy absorption capacity is defined by **[80]** as the ratio of the total area under the Load-deflection curve to that under the ascending portion only,

as explained to the specimen (1d-SCI) in Figure (4-18). According to **[80]** the result of the energy absorption capacity was determined for all tested slabs and tabulated in Table (4-5).

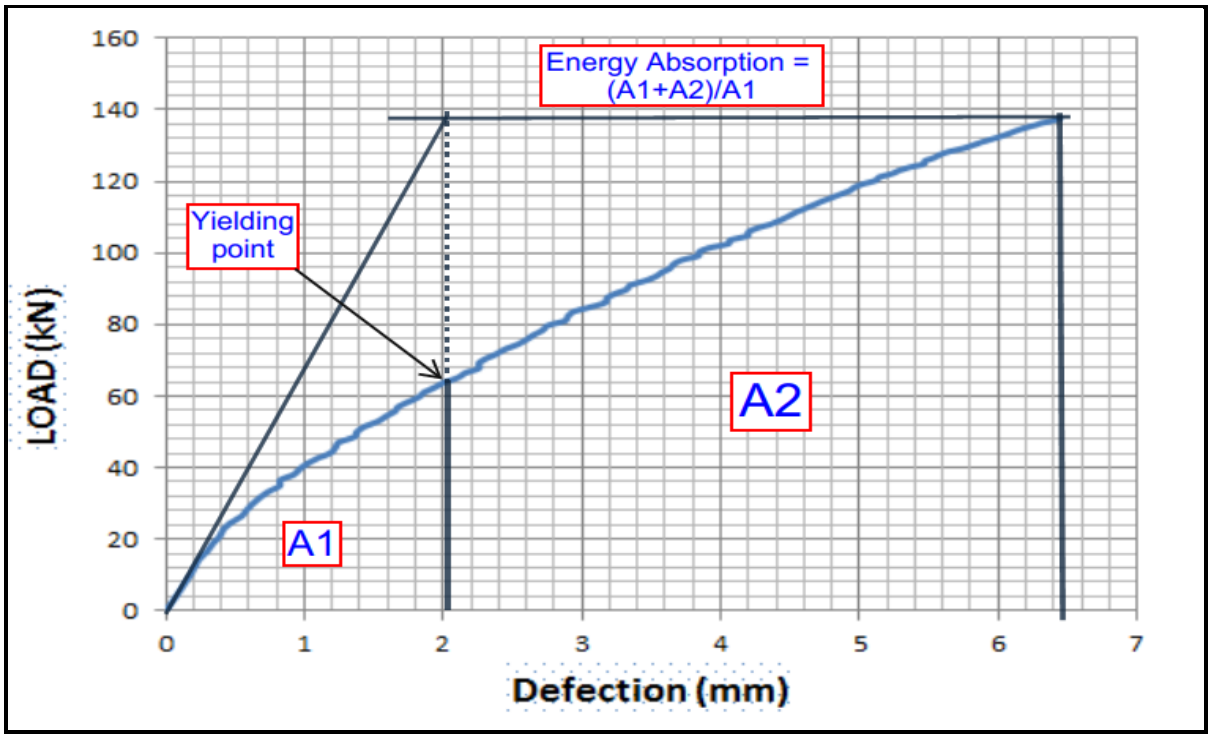

Figure (4-18): Determination of the energy absorption capacity.

From the test results, the energy absorption capacity for all the specimens is increased with a different percentage according to the area cast with UHPC, the shape of UHPC, and the distribution of UHPC within the cross-section. Also, it provides additional strengthening advantages for buildings in areas vulnerable to extreme earthquakes.

Table(4-5): Energy absorption capacity for the tested flat slabs.

Flat Slab Designation	Area Under Ascending Part A1 kN.m	Area Under Descending Part A2 kN.m	Energy Absorption EAI*
NSC	90	118.93	2.32
1d-SC	105.15	447	5.25
2d-SC	202.143	970.28	5.8
3d-SC	129.1141	640.789	5.96
1d-SI C	154.77	811	6.24
2d-SI C	207	652.05	4.15
3d-SI C	310.3	557.11	2.8
120-RC	278.84	468.45	2.18
180-RC	193.81	563.7835	3.9
243-RC	203.9	654	4.2
Sh.RN	67.249	245.6268	4.65
187-PF	197	771.927	4.91
187-XF	199.95	882.81	5.415
400-PC	244.9	528	3.15
400-XC	250	388	2.55

*Energy Absorption = (A1+A2)/A1

It is also illustrated that UHPC exhibited good values of energy absorption capacity, this is due to the content of steel fibers in UHPC that significantly enhances energy absorption.

In general, using steel fiber caused an increase in energy absorption capacity because that fiber reduces the microcracks firmly and needed additional forces to

slip it from the matrix or cut off it as in Table (4-5) for groups G1 and G2. Therefore, when increasing the area that was cast with UHPC led to the need for more energy to reach the failure. This increase in the energy absorption capacity difference in percent compared to the control specimen is due to the influence of the anisotropy nature of UHPC.

Distribution of UHPC in the cross-section of the specimen has an important effect on improving the energy absorption capacity from the results, we notice that in group G4 where the two specimens with UHPC each thickness of slab gave good results compared to the two specimens with half the thickness, although all specimens are equal in quantity UHPC.

4-4-9 Evaluation of the Best Case of Improvement Punching Shear

Before selecting the perfect method for improving punching shear, the first set

the limitation that was adopted for selection. Here the author adopted this parameter to choose the most effective way to improve punching shear (punching shear strength, deformation capacity, and cost).

4-4-9-1 Case Study (I) Groups (G1, G2, and G3):

The specimens (3d-SC, and 3d-SIC,) give a higher resistance of punching shear, but the amount of UHPC used in them is more (80%) than the specimens (2d-SC, and 2d-SIC) so it is considered uneconomical, as for the latter, in the optimal use of UHPC, the rhombic form of UHPC is considered better, as it gives good engineering properties in addition to high resistance. As for the circular shape UHPC in the specimen (120-RC), it gave high shear strength at a lower cost.

4-4-9-2 Case Study (II) Group G4:

The specimens in this group are equal in quantity UHPC, we noticed that the use of UHPC for all thicknesses of the slab gave a high resistance to shear compared to the specimens with half thickness, the slab 187-XF is considered the best application of UHPC due to the high strength and other properties such as ductility, energy absorption.

4-4-10 Discussion and comparison

Strengthening flat slabs using ultra-high performance concrete (UHPC) gives high resistance to punching shear, and this is what we observed in this practical study. In the first group of specimens (1d-SC, 2d-SC & 3d-SC), the resistance increased compared to the reference sample, and the specimens of the second group (1d-SCI, 2d-SCI & 3d-SCI), developed more resistance than the first. Also in the third group, the circular shape of the area was used, as well as the circular shape of the column (which is the area equivalent to the square section column used in the first and second groups). Despite the stabilization of the amount of (UHPC) in the coupled specimens, for example, the sample (1d-SC) quantity (UHPC) is the same for the sample (1d-SCI) from the second group and the sample (120-RC) from the third group, but the resistance increased and this proves the importance of the form of strengthening. Where the study proved that the rhombic and circular shape is better than the square.

In the second case of the study, which is replacing reinforcement steel shear with (UHPC) it gave great results, and the resistance developed by a greater percentage than (70%). We also noticed an improvement in other engineering

properties, especially in the two specimens with a full slab thickness of (187-PF & 187-XF). The results of the sample (187-XF) proved that rotating the figure at an angle (45) significantly improves the resistance compared to the sample (187-PF).

CHAPTER FIVE
THEORTICAL AND PARAMETRIC STUDY

5-1 GENERAL

Finite element analysis (FEA) is an economical and effective procedure that can be used to study the behavior of structural members, principally those that behave structurally in a nonlinear manner, such as reinforced concrete structures. Among the most commercially available finite element analysis software used to perform parametric studies and to understand the structural response is ABAQUS. In the present study, ABAQUS/CAE 2017 **[81]** is used to simulate numerically the behavior of reinforced concrete flat slabs with and without strengthening made of homogenous or hybrid concrete. Experimental testing is the most reliable method for studying the behavior of concrete structures. However, the study of variables in the practical study remains relatively limited. In addition to the fact that pilot testing is time-consuming and expensive, its results may be different for many reasons. Thus, FEM simulation is a method of great interest not only to verify the experimental results but also to implement a parametric study of many variables that are not considered in the experimental program **[82]**.

In this chapter, the FEM analysis are validated by comparing the numerical results with the experimental results for some tested samples. Details of the developed FEM model are given first, which comprises the material constitutive model, element types, size of the mesh, and boundary conditions for each element. Finally, a parametric study of several variables are performed.

5-2 Element Type and Material Properties

To model the actual behavior of the reinforced concrete slab column connection, it is recommended to model the concrete with a three-dimensional linear eight-headed rigid element with low integration (C3D8R) (meaning one point of integration corresponding to the center of the element) **[83]** as shown in Figure (5-1-a). This type of element provides a reliable solution for most applications. Eight nodes with three degrees of freedom for each node, are contained in each 3D solid. It can be used for linear analysis as well as for nonlinear analysis including large deformations and plasticity. On the other hand, two-headed linear truss elements (T3D2) as indicated in Figure (5-1-b) were used to model the reinforcement of the steel bars. Similar to the concrete beam, the 3D steel element (C3D8R) was chosen to model the steel bar which is used as a simple support (border support).

Among the formative models for simulating the behavior of concrete, the concrete damaged plasticity (CDP) model offered by ABAQUS was choosen. Details of the CDP model, including the behavior and properties of concrete and other materials used in this study are given in **Appendix B**.

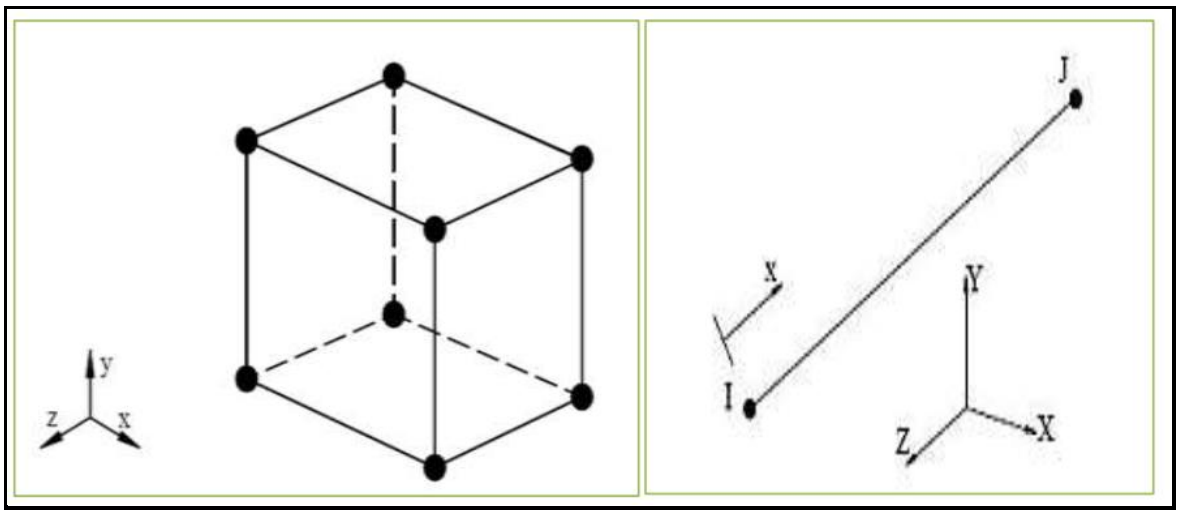

(a) C3D8R element (b) T3D2 truss element

Figure (5-1).C3D8R, and T3D2 elements used in the present study **[83]**.

5-3 Model Geometry and Boundary Conditions

This section includes two parts, the first describing the geometry of the tested samples and the second part explaining the boundary conditions and load utilized in this study. The boundary conditions and applied geometric load were simulated to be similar to those in the experimental analysis.

5-3-1 Model Geometry

Generally, three parts were involved in modeling the slab-column connections. These three parts were the slab and concrete column, reinforcing slabs, and finally, the simply supported rods along the perimeter of the slab. These parts were drawn separately and then assembled and combined to form modeling samples.

Symmetry was used in two directions (X and Z), which greatly minimized the number of nodes. This has facilitated and accelerated the work of the program. Figure (5-2) shows the assembly of these three parts.

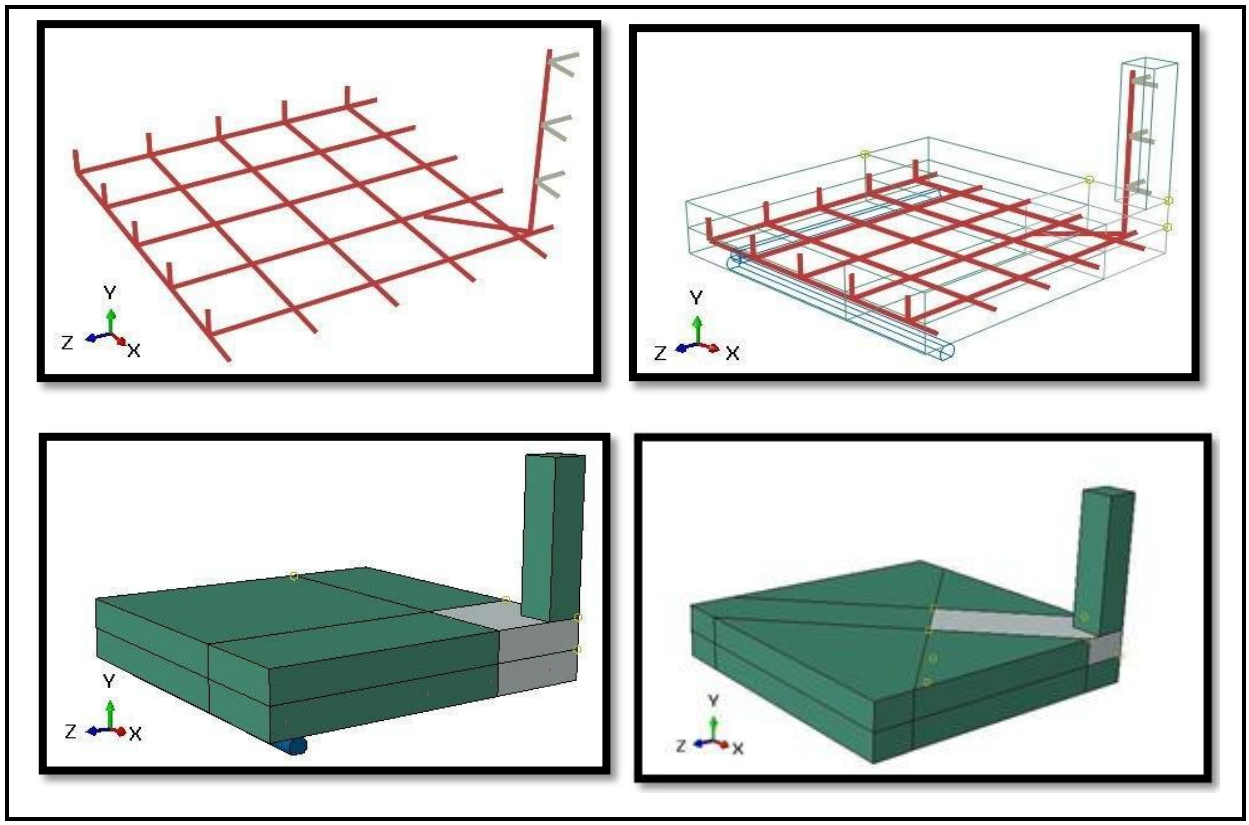

Figure (5-2): The assembly of the model parts.

After the assembly step, some of the parts must be interacted together to form a composite system. All elements have been combined to form the model. An ideal bond between UHPC and normal-strength concrete was assumed to simulate the experimental work. The combined method was adopted to simulate the bond between concrete and reinforcement. In this limitation, the concrete served as the host region while the reinforcing steel bars were chosen as the embedded region. This constraint mimics the perfect steel-concrete bond. Steel plates in both loading and supporting positions are connected to the beam specimen using the ‘‘mechanical fraction’’ option, with a frictional coefficient of 0.3 **[84].**

5-3-2 Loading and Boundary Conditions

The overall dimensions of the square slab were (900 * 900 * 80 mm). The cross-section of the column was a square with side lengths (100*100 mm) and a height of 200 mm. The clear span between supports was (800 mm).

All slabs are simply supported, thus, the slabs are supported by a rod with a diameter of 25 mm delivered at 50 mm from the outer perimeter. The constraint is applied at support lines to get a unique result. Boundary conditions must be chosen carefully as similar to that in the experimental test set-up.

The FE model was loaded at similar locations in the experimental test for all slabs. The RC flat slabs had been analyzed using static analysis in ABAQUS/Standard. In the static analysis, the load was applied as a displacement along the width of the beam on the centerline of the upper plates. The applied displacement was 12 mm for the specimens. Figure (5-3) presents details of the typical boundary conditions for the samples employed in the simulations.

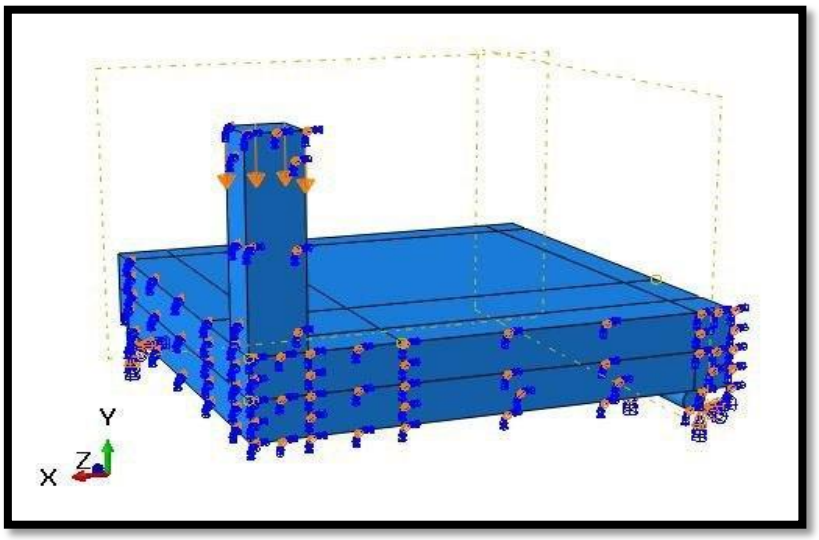

Figure (5-3): The boundary conditions of the modeled slabs.

5-4 Convergence Study

Choosing a mesh size is an important step in finite element modeling before starting the analysis. An appropriate pre-analysis was carried out for different mesh densities to determine the best density that gives the necessary accuracy according to the degree of complexity of the analysis. When the slab is divided into a satisfactory number of elements, a good convergence of results is achieved. This is realized when a decrease in the mesh size has a slight effect on the result. Therefore, in the present FEM, a convergence analysis was performed on the slab-column connection model to secure the suitable mesh size.

The main objective of the convergence survey is to determine the convenient mesh size for the model with a minimum number of elements and maximum convergence with the experimental test results.

The convergence study was made by decreasing the element size of the model (NSC) from 80, 40, 26.6, 20, 16, 13.3, and 11.4 to 10 mm. The mid-span deflection for the mentioned specimen with different mesh sizes was observed at the same applied load level of 70 KN. As shown in Figure (5-4) convergence study, shows the accuracy of adopting 4077 elements (mesh size of 16 mm), therefore; the 16 mm model is adopted for all tested specimens as shown in

Figure (5-5). **[5]** stated that the chosen mesh size should be greater than the maximum aggregate size (10 mm in the current study).

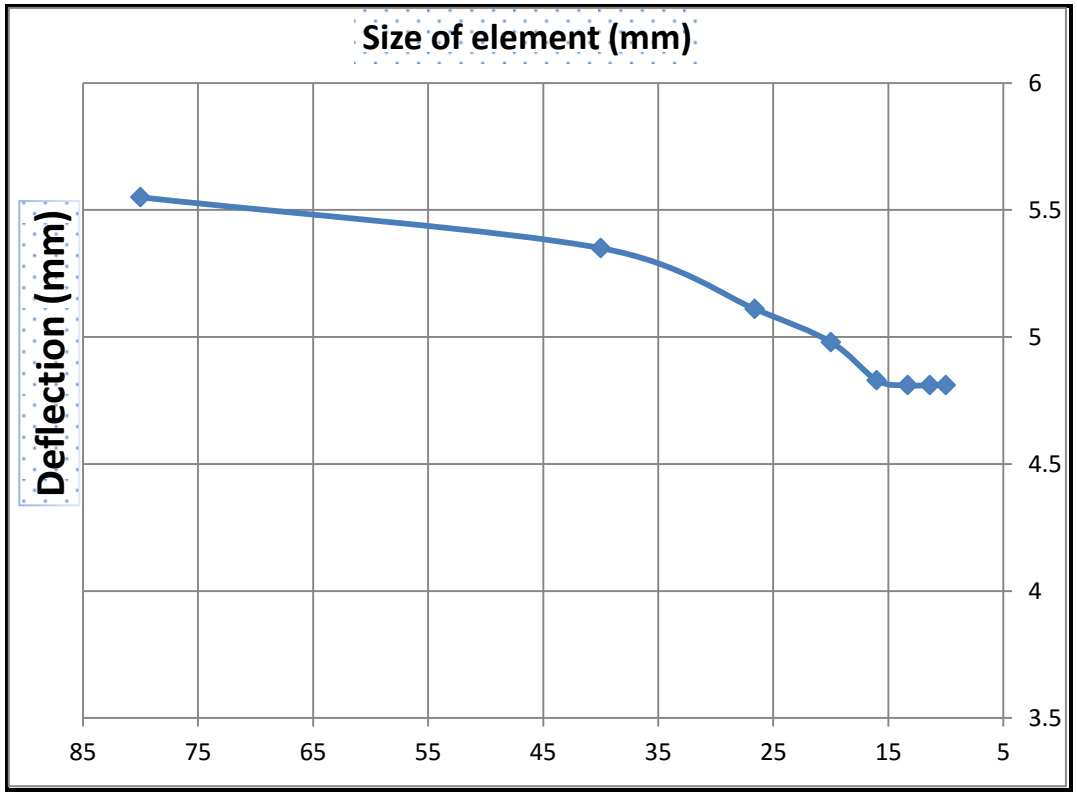

Figure (5-4): Convergence analysis, imposed load equal to 100 kN

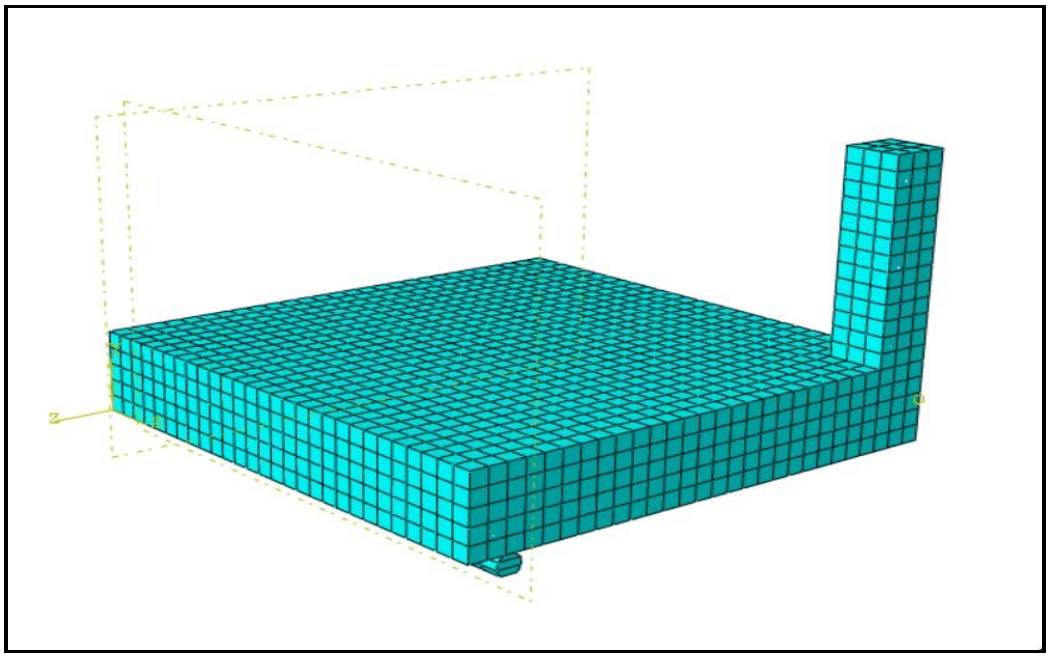

Figure (5-5): Typical mesh applied for the (N.S.C) specimen.

5-5 Comparison Between Finite Element and Experimental Results

In this part, the finite element analysis results were compared with the experimental results. This comparison was made in terms of final load, and load deflection curve behavior.

5-5-1 Ultimate Load and Central Deflection

The comparison between the ultimate loads and the central deflection (ultimate loads) obtain from the numerical FE models and the experimental tests are listed in Table (5-1). A good agreement was observed between the result of FEA and that of experimental data. Therefore, the model proposed is accurate and can be used confidently. It is noticed from the results in Table (5-1) that all the numerical data of punching load of the tested slabs were convergent with the experimental values, and the rate of difference ranged between (1 to 6 %). Whereas the maximum difference in the central deflection ranged between 1.5 % (increase) to 14 % (redaction). And the maximum difference in the ultimate load ranged between 6% (increasing) and 6.8 % (reduction) is about 1.3%. An average of 5% decrease in first cracking loads was observed.

Table (5-1): Summary of comparison of FEM and experimental results.

Specimen designation	Cracking load Pcr (KN)		P.D* of Pcr %	Ultimate load (KN) Pu		P.D of Pu%	Deflection at ultimate load (mm)		P.D of δ_u %
	Exp	FEM		Exp	FEM		Exp	FEM	
NSC	26	28.3	+8	83.5	87	+4	4.86	4.6	-5
2d-SC	47	40.8	-13	154.5	144	-6.8	6.77	6.15	-9
2d-SIC	33	34	+3	158	156	-1	10.03	8.61	-14
180-RC	34	32	-5.8	160	170	+6	7.3	7.12	-2.5

	Table (5-1): continues.								
Sh.RN	35	32	-8.5	98	103	+5	4.84	4.91	+1.5
187-PF	38	34	-10.5	151.5	150	-0.99	9.94	9.49	-4.5
187-XF	44	40	-9	167	172	+3	9.948	9.05	-9
Average			≈ -5%			≈1.3%			≈ -6%

*P.D is Percentage difference % = $\frac{\text{FEM}-\text{Exp}}{\text{Exp}} * 100\%$

5-5-2 Load-Deflection Curves

The comparison between the numerical and the experimental results in terms of load-deflection curves for all samples are shown in Figures (5-6) to (5-12). The analytical results of the tested samples (NSC, 2d-SC, 2d-SIC, 180-RC, Sh.RN, 187-PF and 187-XF) are in good agreement with the experimental results as in the central deflection and the final punching shear capacity. The FEA results also show a good agrement compared to the experimental load-deflection curves for the non-cracked stage and nearly the same behavior in the cracked stage, but with a lower difference.

In finite element analysis, there are many factors represented the reasons for the varying in the results between the numerical finite element models and the experimental tests. Some of these factors have been found:

1. In the simulations, FEM does not include the development of micro-cracks caused due to concrete curing, environmental influences, dry shrinkage, etc., in the experimental cases.
2. It has been assumed that concrete is a homogeneous material in the FEA, but the fact is that it is a heterogeneous material.
3. The embedded area constraints that were utilized in (ABAQUS) program to model the interaction of concrete with reinforcing steel assumed a ideal bond. While the actual bond is not perfect in real practice.

4. The equilibrium and model level as well as the application of the load where all these variables are ideally applied in FEM differ from the experimental work.

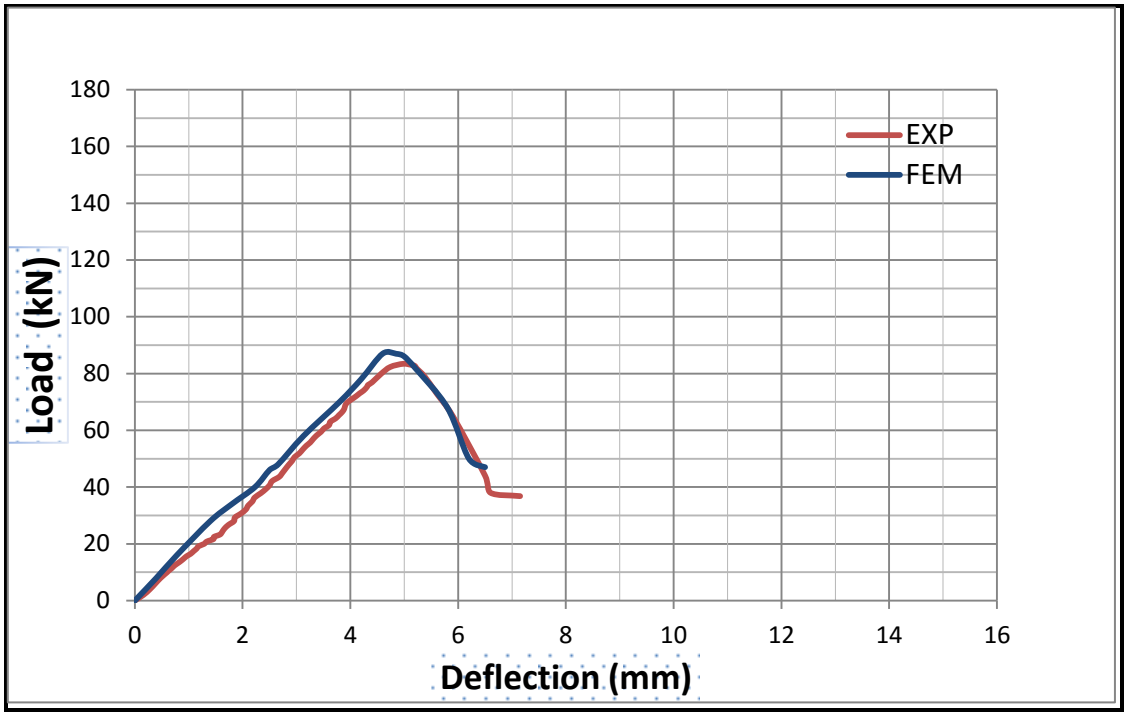

Figure (5-6): Experimental and numerical load-center slab deflection curves for NSC.

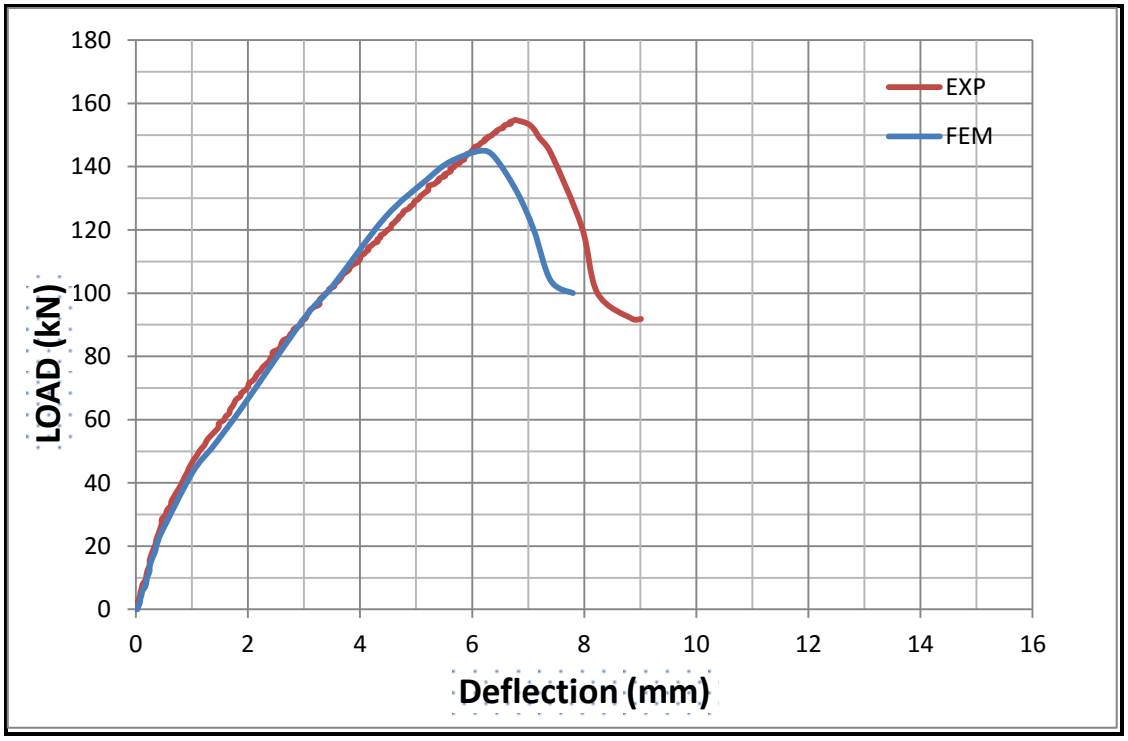

Figure (5-7): Experimental and numerical load-center slab deflection curves for 2d-SC.

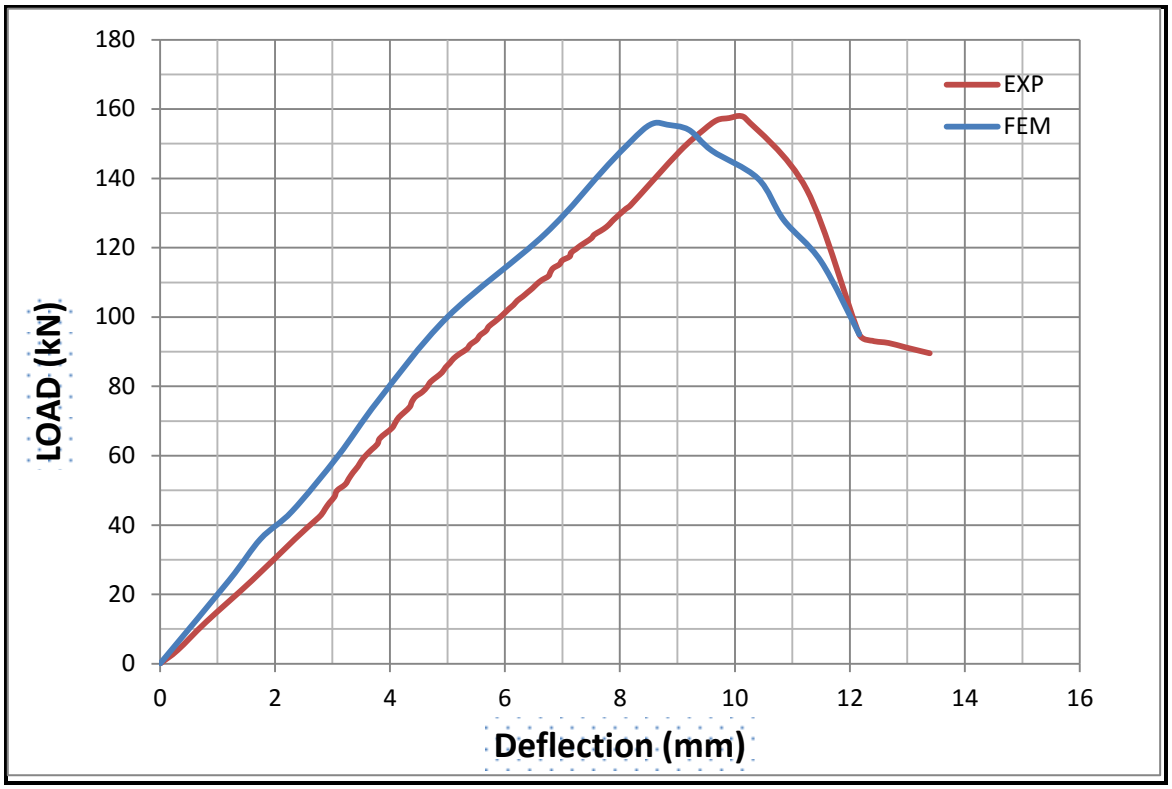

Figure (5-8): Experimental and numerical load-center slab deflection curves for 2d-SIC.

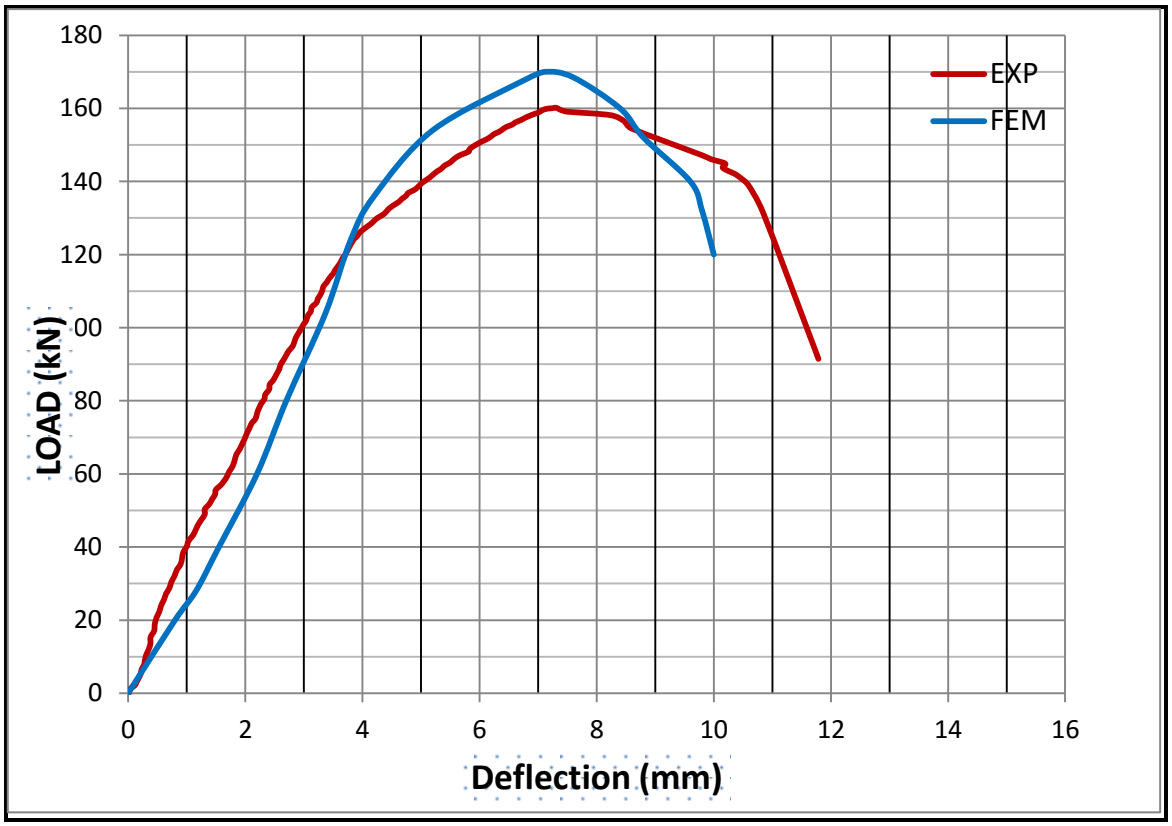

Figure (5-9): Experimental and numerical load-center slab deflection curves for 180-RC.

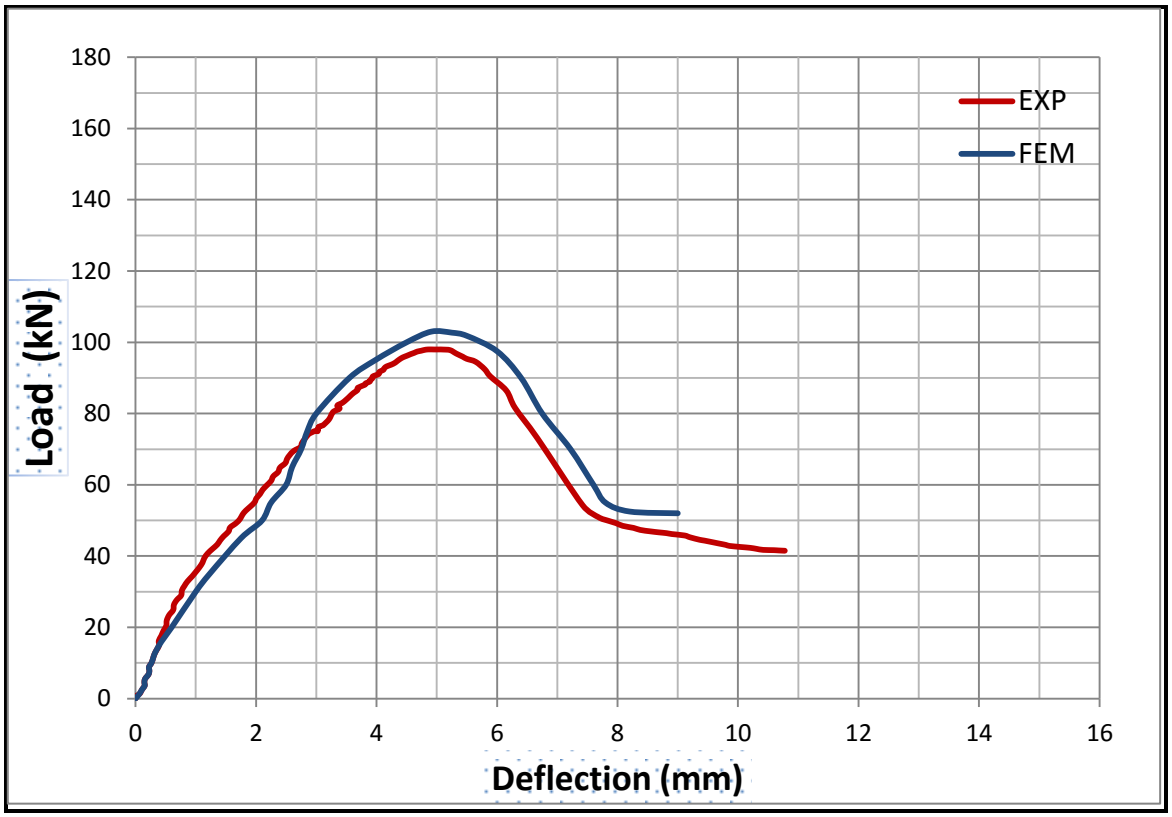

Figure (5-10): Experimental and numerical load-center slab deflection curves for Sh.RN.

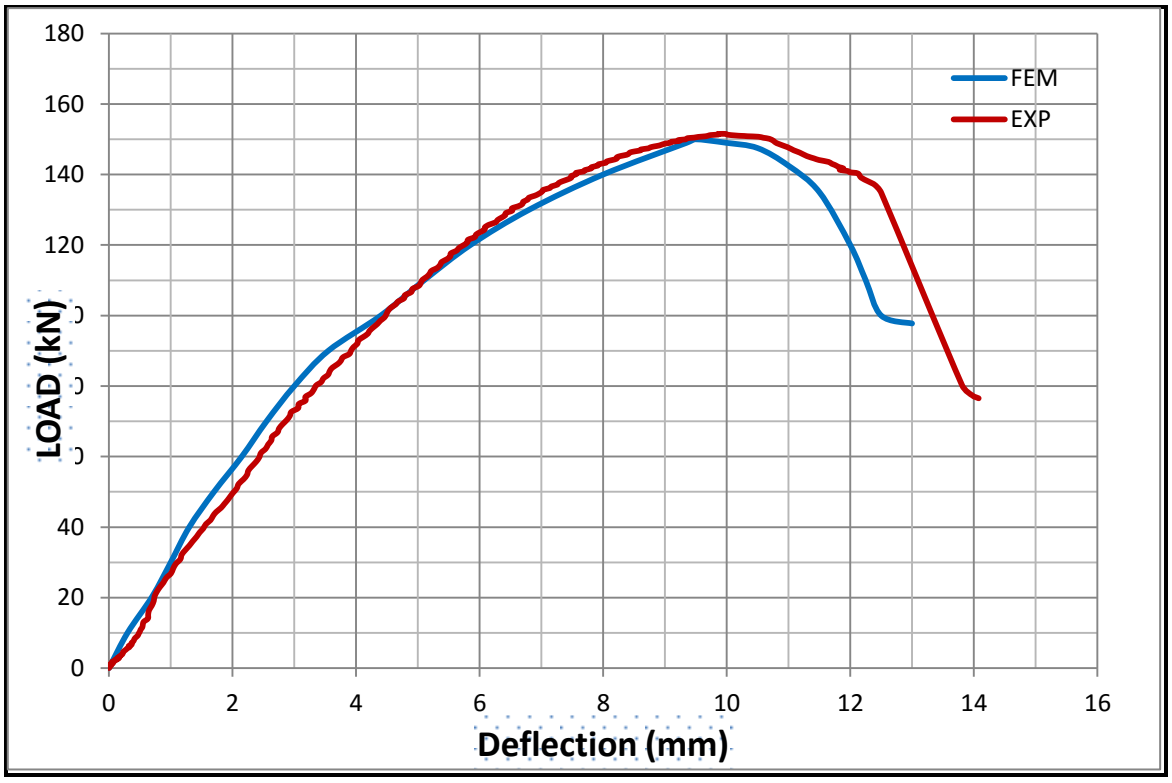

Figure (5-11): Experimental and numerical load-center slab deflection curves for 187-PF.

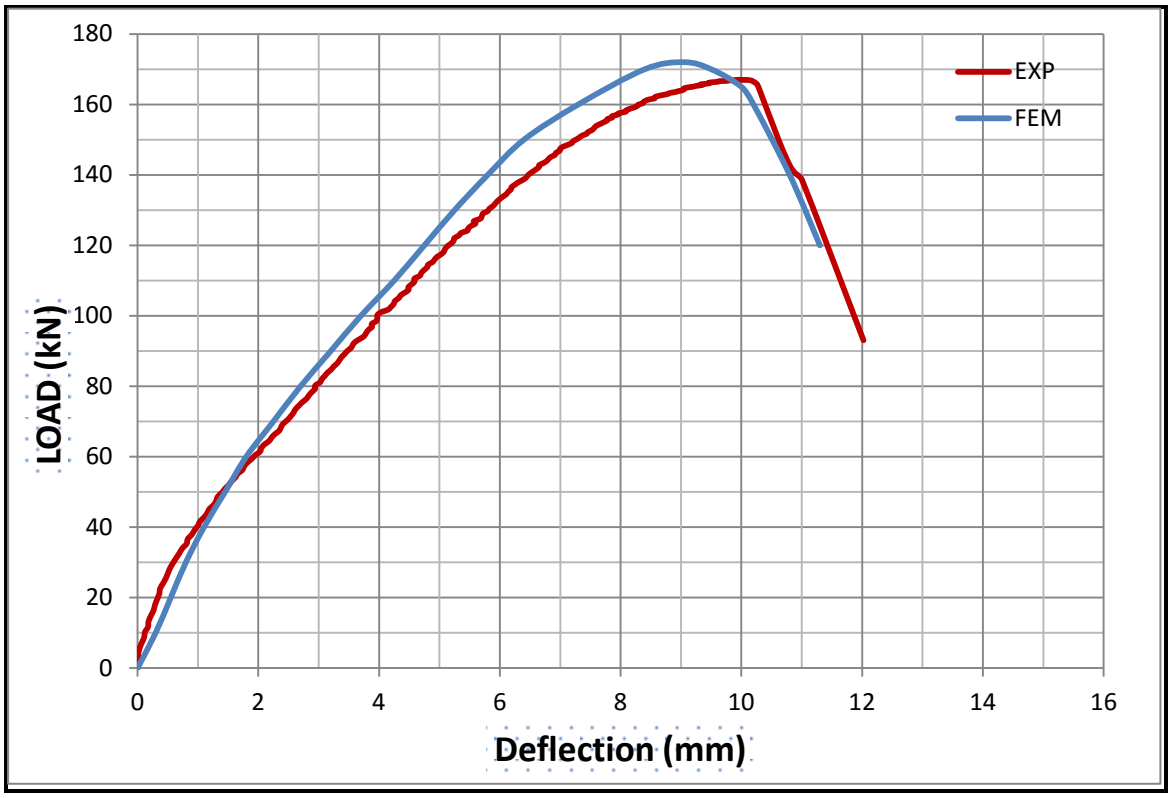

Figure (5-12): Experimental and numerical load-center slab deflection curves for 187-XF.

5-6 PARAMETRIC STUDY

Parameters examined in the pilot study include UHPC area, UHPC shape, UHPC thickness, and replacement of shear reinforcement with UHPC. The use of the FEA model developed in the current study is in reasonable agreement in predicting fracturing load, ultimate load, ultimate deflection and damage states. Therefore, a parametric study was performed to form a more accurate and detailed understanding of the behavior of the hybrid flat plate slab-column connections with UHPC. In the parametric study, there is no change in the load location, support condition, and reinforcement ratio. The parameters that were varied to search their possible impacts were as follows: column dimensions, UHPC compressive strength, NSC and UHPC area dimensions. The thickness of the slab for the above cases was 80 mm, except for the column dimensions cases, where a thickness of 120 mm was selected to represent more practical dimensions.

5-6-1 Impact of the zone dimensions of UHPC

In the practical part of this research, three dimensions of UHPC area were tested with UHPC area of equal effective depth (UHPC perimeter equal to 1d (210*210 mm) from the column face) where d: average effective depth of the slab and other reinforcement areas by UHPC equal to 2d (320 * 320mm), and 3D (430*430mm). When other factors remain constant, the dimensions of the different auxiliary UHPC areas are 4d and 5d, that is, the UHPC area is 540*540, and 650*650mm respectively. Figure (5-13) shows the deflection curves between load and average span acquired from the FEA model, and the ultimate load and first cracking load for each case gained from the FEA model are summarized in Table (5-2).

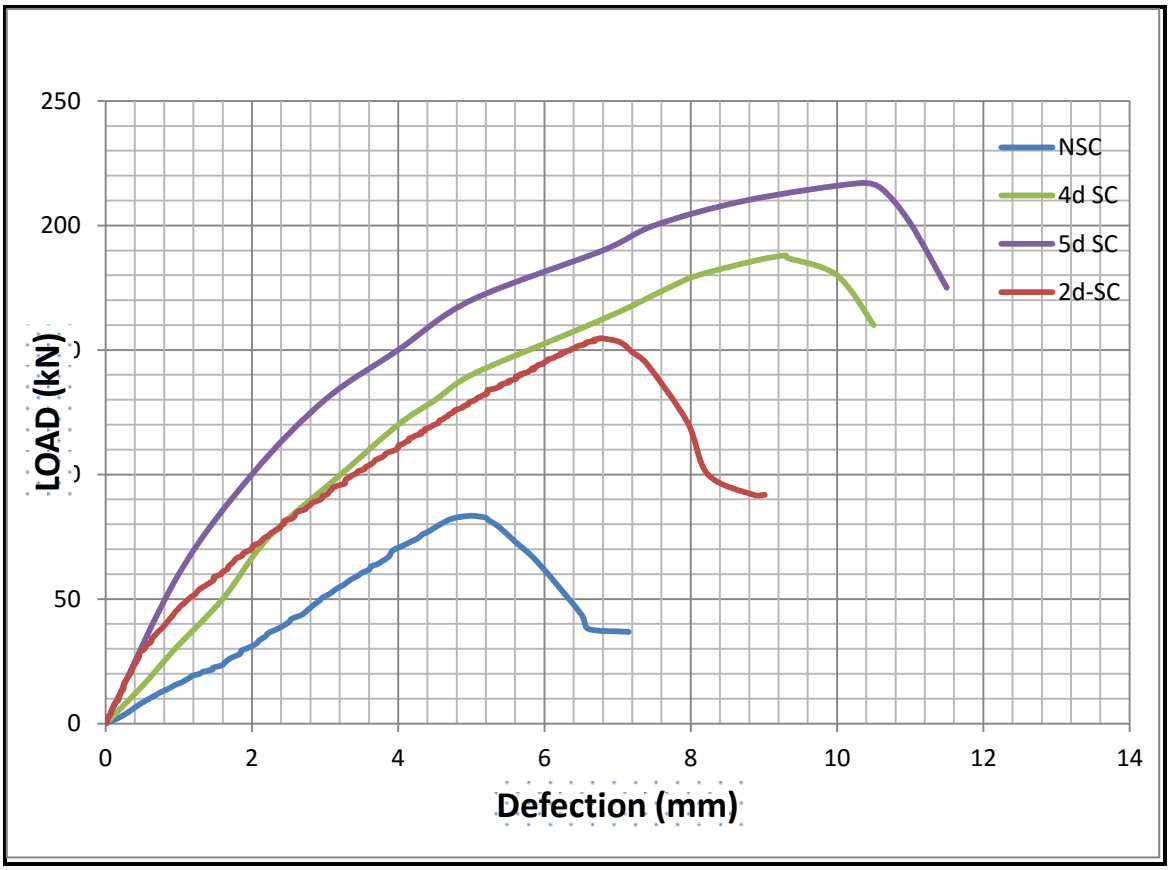

Figure (5-13): The load-deflection curve of FEM for different UHPC zones.

Table (5-2). Comparison between the UHPC zone effects by the FEA analysis.

FEA model	UHPC area dimension (mm*mm)	Cracking load Pcr (kN) FEM	Increasing the Cracking load relative to the reference (%)	Numerical ultimate load Pu (kN)	Increasing in the ultimate load relative to the reference (%)
NSC	----	26	----	87	----
4d-SC	540	46	77	188	116
5d-SC	650	54	108	212	143

From Figure (5-13) and Table (5-2), it is cleared that the ultimate load growes with increasing UHPC area, as well as the first crack. It is also noticed that by increasing the area UHPC cracks appear within the UHPC zone forming a mixed failure punching and flexural. The reason for the increase in slab resistance and the appearance of cracks in the area UHPC and also the transformation of failure into a composite failure may be caused by the increase in the area of UHPC and UHPC engineering properties, including high resistance to tensile stress because it contains steel fiber.

5-6-2 Influence of the compressive strength of concrete

The compressive strength value used in the practical samples fu/fc = 5.6 (22.5 MPa for NSC and 126 MPa for UHPC), where, fu: compressive strength of ultra-high-performance concrete and fc: compressive strength of normal concrete. To realize the compressive strength effects of NSC (fc) and UHPC (fu), another compressive strength amount is proposed for each type of concrete, that is fu/fc = 2.8 (45 MPa for NSC and 126 MPa for UHPC) and fu

/fc = 4 (45 MPa for NSC and 180 MPa for UHPC). The above values were tested for hybrid flat slabs with the same UHPC area dimensions (430 * 430 mm) provided in the 3d-SC specimen.

Boosting the ratio of fu/fc arising the bearing capacity of the slab for punching shear as in Figure (5-14) and it is noted through it that the lower the ratio, the more common failure of shear and flexure occurs, and it can be noted through it the increased fu/fc ratio, which is a common failure in punching shear.

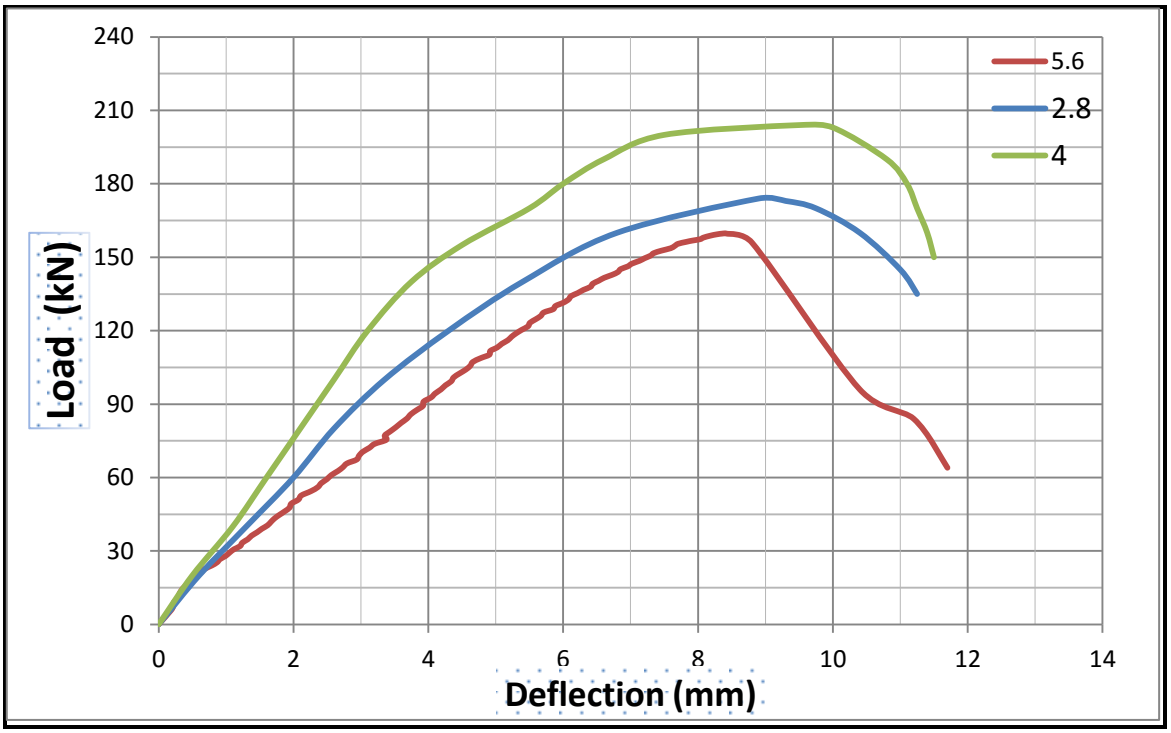

Figure (5-14): The load-deflection curve of FEM for different fu/fc ratios.

Where fu/fc: The ratio of compressive strength of UHPC to NSC.

5-6-3 influence of the column dimensions

The coefficient of the effect of column section dimensions on slab resistance to punching shear failure is one of the many studies of slabs made of normal concrete. But few have studied the effect of this modulus on slabs made

of hybrid concrete. In the current experimental study, the dimensions of the column section of (100*100 mm) are used.

In this section of the study, two different sections were selected, one of them with dimensions (80*80 mm) smaller than the section used in the practical specimens, and the other with dimensions (120*120 mm) which is larger than the one used in the practical specimens.

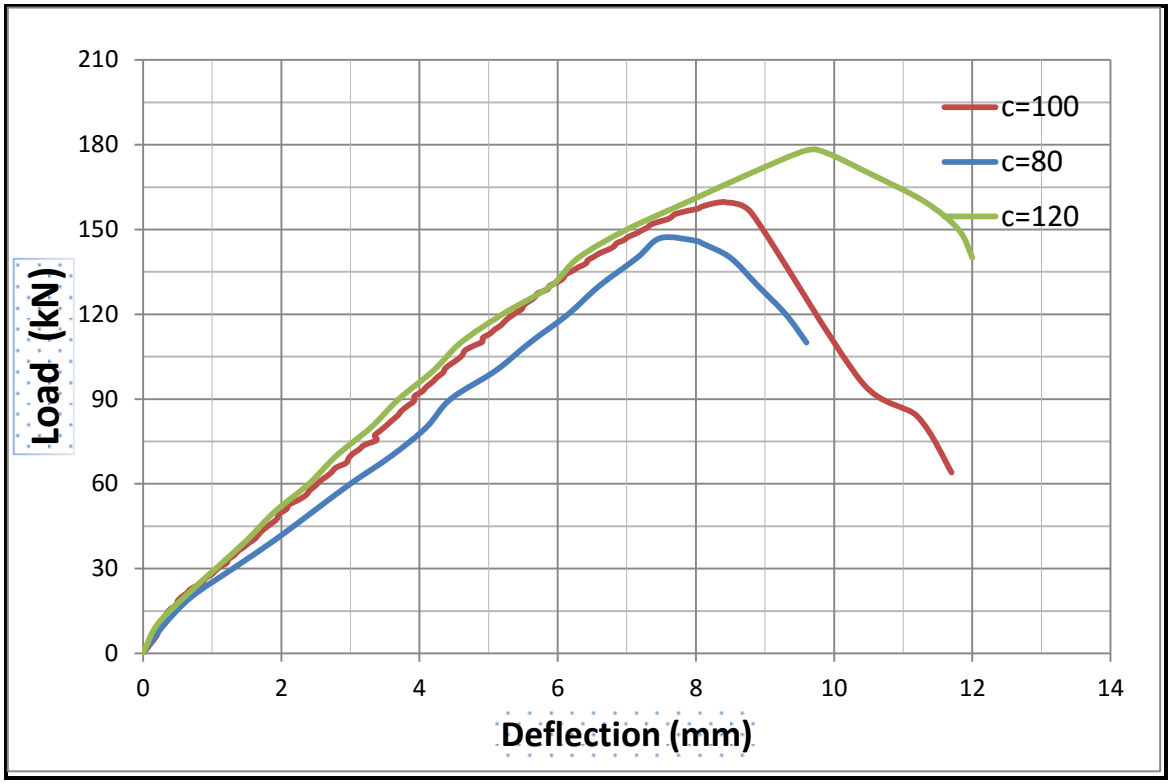

Figure (5-15): The load-deflection curve of FEM for different dimension sections of the column.

One can notice in the deflection versus load diagram that the slab's resistance to shear failure increases with the increase in the column section (c=120 mm), the reason for this is due to the increase in the cross-sectional area of the column where it supports the slab and also gives a longer path to failure by increasing the failure cone. It gives an increase in deflection capacity before failure occurs. And resistance to shear failure decreases with the decrease in the

column dimensions (c=80 mm). Also noted is that the load-deflection curve has a sudden failure whenever the dimensions of the column section decrease.

CHAPTER SIX

CONCLUSIONS AND RECOMMENDATIONS

6-1 Summary

In the previous chapters, experimental work with finite element analysis and a parametric study of the RC flat slab with reinforcement against shear failure using hybrid concrete (normal and ultra-high-performance concrete) explained and reached the optimal use of (UHPC) in terms of depth, location and shapes. Both experimental and numerical results using ABAQUS software showed that providing RC slabs Reinforced panels have a varying effect on overall behavior and the ultimate strength depends on many parameters. From the experimental and numerical results, many conclusions can be drawn in this field as well as some suggestions for future works are presented.

6-2 Conclusions from Experimental Work

1. Ordinary concrete is weak to resist punching shear failure despite the slab being reinforced with the highest percentage of flexure reinforcement.
2. The slab resistance increases to the failure of the punching shear using hybrid concrete, and UHPC has good engineering properties, including its tensile resistance because it contains steel fiber.
3. The increaser the strengthing area, the increased the model's susceptibility to shear failure, down to twice the resistance in the reference model.
4. Ultra-high-performance concrete increases the ultimate deflection, thus increasing the area under the curve, which in turn absorbs energy and plasticity.

5. Rotating the stiffening shape at an angle of 45 is the optimal use for the square shape of the same amount (UHPC).
6. The slabs with UHPC total depth (replacing the reinforcement shear by UHPC) imparted a high punching shear bearing capacity which amounted to 70% of the specimen containing the punching shear reinforcement.
7. Post-punching capacity is the remaining strength of the slab which can be measured as the load after the punching failure at which the load-deflection response tends to flatten and grows in UHPC with the rising of steel fiber percentage.
8. The experimental results conclude that the energy absorption index of the specimens with UHPC increased from (20 to 168 %) compared with the control specimens.
9. The experimental findings conclude that the ductility index of the specimens with UHPC increased from (4 to 91%) compared with the control specimens.
10. Slabs made of Hybrid NSC and UHPC often fail in punching and flexural composite as a result of the higher initial ductility and stiffness of UHPC.
11. The technique of replacing the shear reinforcement with another suitable strengthening is considered an important matter that designers may resort to in the rebar engagement areas.
12. Using UHPC led to changing the failure mode from sudden to gradual failure.
13. From the test results can be concluded that the distribution of UHPC around the column instead of the punching shear reinforcement provided a good ability to control the spread of the diagonal shear cracks, which improved the whole behavior of the specimen as compared with the control specimen.

6-3 Conclusions from Finite Element Analysis

The following conclusions are derived from the 3D Finite Element Analysis based on the CDP model of the ABAQUS package as follows:

1. The constructed model by the ABAQUS program predicts a good simulation for the real behavior of the slab-column connections in terms of punching capacity, and load-deflection curves with reasonable accuracy.
2. A high agreement was observed between the analysis result and experimental data; therefore, the model suggested is reliable and can be used with dependability. All the numerical data of the punching load of tested slabs have a good agreement with the experimental values.
3. The results obtained from the ABAQUS program explain that the increase in the area cast with UHPC led to an increase in the ultimate load.
4. Increasing the dimensions of the column section increases the shear resistance due to the large failure path.
5. Increasing the compressive strength of the two types of concrete increases the shear resistance, but the economy must be taken into account in the quality of special concrete because it is very expensive.

6-4 RECOMMENDATIONS FOR FUTURE WORKS

Based on the findings of this study, several suggestions for future research are listed below. These suggestions may lead to more understanding of the performance of flat slabs:

1. The present study focuses on the inner slab-column connections. Therefore, it is suggested to investigate (experimentally and numerically) the behavior of corner or edge slab-column connections.
2. The numerical and experimental studies were performed, in the current research, taking into account the static loads only. Thus, the influence of cyclic load must also be examined in order to better understand the punching shear behavior of the slab-column connections.
3. More parameters are necessary to be investigated such as the effect of different ratio (ρ) of flexural reinforcement, openings, slab thickness, column aspect ratio, and different compression strength for the normal strength concrete and replace the normal strength concrete with other types of concrete like high-strength and reactive powder concrete.
4. Proposal to replace the reinforcing steel with a punching sheer and make it inclined at an angle other than 45, after proving in this study that its effectiveness is more than that in the code.

REFERENCES

[1] J. K. Wight, S. H. Chien, and L. Dovich, “Evaluation ofR/C Slab-ColumnSystems for Seismic Strengthening,” 1994.

[2] A. E. Zaghloul and A. G. Razaqpur, “Punching shear behavior of CFRP reinforced concrete flat plates,” Proc. Int. Conf. on, Compos. Constr., 2003.

[3] Venkata, R. N., Gnaneswar, K., Sashidhar, C. and Naresh, K. T., 2012 "Behavior of High Performance Concrete Two Way Slabs in Punching Shear", International Journal of Science and Advanced Technology, Volume.2, No.3, pp. 122-126.

[4] “SHEAR STRENGTH OF REINFORCED CONCRETE FLAT SLABS,” 1970.

[5] L. J. Mensch et al., “Discussion on Reinforced Concrete Flat Slab Floors,” Trans. Am. Soc. Civ. Eng., vol. 77, no. 1, pp. 1682–1730, 1914.

[6] T. L. Condron, “Principles of Design and Results of Tests on Girderless Floor Construction on Reinforced Concrete,” in Journal Proceedings, 1913, vol. 9, no. 12, pp. 116–126.

[7] E. Smulski, “A Test of the SMI System of Flat-Slab Construction,” in Journal Proceedings, 1918, vol. 14, no. 6, pp. 206–232.

[8] D. P. Billington, “Robert Maillart and the art of reinforced concrete,” 1991.

[9] A. R. Whitson, W. J. Geib, C. Thompson, C. B. Post, L. R. A. Schoenmann, and A. E. Taylor, Reconnoissance Soil Survey of North Eastern Wisconsin, no. 47. The State, 1916.

[10] A. Sayed, "Punching shear behaviour of FRP-reinforced concrete interior slab-column connections," 2015.

[11] R. Park and W. L.Gamble, Reinforced concrete slabs. John Wiley & Sons, 1999.

[12] C.-L. Chiang, "Punching shear strength of reinforced and post-tensioned concrete flat plates with spandrel beams," 1994.

[13] R. A. Joseph and P. Lakshmi, "Study on Effect of Concrete Compressive Strength and Column Shape on Punching Shear Stress in Flat Plate Systems."

[14] N. W. Hawkins and W. G. Corley, "Moment transfer to columns in slabs with shearhead reinforcement," Spec. Publ., vol. 42, pp. 847–880, 1974.

[15] S. Islam and R. Park, "Tests on slab-column connections with shear and unbalanced flexure," J. Struct. Div., vol. 102, no. 3, pp. 549–568, 1976.

[16] B. A. Graybeal, "Material property characterization of ultra-high performance concrete," United States. Federal Highway Administration. Office of Infrastructure …, 2006.

[17] M. Lopez, L. F. Kahn, and K. E. Kurtis, "Effect of internally stored water on creep of high-performance concrete," ACI Mater. J., vol. 105, no. 3, p. 265, 2008.

[18] C. Wu, J. Li, and Y. D. Su, Development of ultra-high performance concrete against blasts: from materials to structures. Woodhead Publishing, 2018.

hien, and L. Dovich, "Evaluation ofR/C Slab-ColumnSystems for Seismic Strengthening," 1994.

[19] A. Setiawan, R. L. Vollum, L. Macorini, and B. A. Izzuddin, "Punching shear design of RC flat slabs supported on wall corners," Struct. Concr., vol. 21, no. 3, pp. 859–874, 2020.

[20] N. Hammil and A. Ghali, "Punching shear resistance of corner slab-column connections," Struct. J., vol. 91, no. 6, pp. 697–707, 1994.

[21] N. K. Oukaili and T. S. Al-Gasham, "Punching Shear Strength of Reinforced Concrete Flat Plates with Openings," Volume 20 January 2014

[22] N. K. Oukaili and T. S. Al-Gasham, "Shear strengthening with CFRP sheets applied in reinforced concrete flat plates with openings," FRPRCS-12/APFIS-2015 - Jt. Conf. 12th Int. Symp. Fiber Reinf. Polym. Reinf. Concr. Struct. FRPRCS 2015 5th Asia-Pacific Conf. Fiber Reinf. Polym. Struct. APFIS 2015, no. April 2017, 2015.

[23] P. Y. Yan and Y. C. Wang, "Hybrid steel tubular column/flat slab construction - Development of a shearhead system to improve punching shear resistance," J. Constr. Steel Res., vol. 119, pp. 154–168, 2016, doi: 10.1016/j.jcsr.2015.12.024.

[24] M. H. Meisami, D. Mostofinejad, and H. Nakamura, "Strengthening of flat slabs with FRP fan for punching shear," Compos. Struct., vol. 119, pp. 305–314, 2015.

[25] M. Lapi, A. P. Ramos, and M. Orlando, "Flat slab strengthening techniques against punching-shear," Eng. Struct., vol. 180, no. May 2018, pp. 160–180, 2019, doi: 10.1016/j.engstruct.2018.11.033.

[26] E. F. El-Salakawy, M. A. Polak, and K. A. Soudki, "New shear strengthening technique for concrete slab-column connections," Struct. J., vol. 100, no. 3, pp. 297–304, 2003.

[27] A. Muttoni, "Punching shear strength of reinforced concrete slabs without transverse reinforcement," ACI Struct. J., vol. 105, no. ARTICLE, pp. 440–450, 2008.

[28] M. Fernández Ruiz, A. Muttoni, and J. Kunz, "Strengthening of flat slabs against punching shear using post-installed shear reinforcement," ACI Struct. J., vol. 107, no. ARTICLE, pp. 434–442, 2010.

[29] M. H. Meisami, D. Mostofinejad, and H. Nakamura, "Punching shear strengthening of two-way flat slabs using CFRP rods," Compos. Struct., vol. 99, pp. 112–122, 2013.

[30] B. Binici and O. Bayrak, "Punching shear strengthening of reinforced concrete flat plates using carbon fiber reinforced polymers," J. Struct. Eng., vol. 129, no. 9, pp. 1173–1182, 2003.

[31] H. R. Taresh, M. Y. M. Yatim, and M. R. Azmi, "Punching shear behaviour of interior slab-column connections strengthened by steel angle plates," Eng. Struct., vol. 238, no. February, p. 112246, 2021, doi: 10.1016/j.engstruct.2021.112246.

[32] A. H. Jasim and H. K. Ammash, "Effect of using column capital on the punching shear strength of flat slab-edge column connection under eccentric loading," J. Phys. Conf. Ser., vol. 1895, no. 1, 2021, doi: 10.1088/1742-6596/1895/1/012060.

[33] Z. A. Neamah and M. A. Al-Ramahee, "Punching shear strength of flat slab strengthened with reinforced concrete column capital under bi-axial loading," IOP Conf. Ser. Mater. Sci. Eng., vol. 1067, no. 1, p. 012005, 2021, doi: 10.1088/1757-899x/1067/1/012005.

[34] F. B. D. Oliveira, A. S. C. Oliveira, G. F. Rizatto, and B. S. Denadai, "Resistance training for explosive and maximal strength: effects on early and late rate of force development," J. Sports Sci. Med., vol. 12, no. 3, p. 402, 2013.

[35] A. Committee, "318M-19: Building Code Requirements for Concrete and Commentary," p. 628, 2019.

[36] S. Nayef, W. Zaki, and M. Rabie, "Effect Of Reinforcement On Punching Shear Behavior Of Flat Slabs," Int. J. Civ. Eng. Technol., vol. 10, no. 2, pp. 2403–2418, 2019.

[37] S. Rasheed Abass and H. Jameel Abd, "Punching Shear Strengths of Hybrid Reinforced Concrete Flat Plate Slabs," J. Eng. Sustain. Dev., vol. 2018, no. 04, pp. 101–115, 2018, doi: 10.31272/jeasd.2018.4.8.

[38] M. M. Kadhum, S. M. Harbi, S. S. Khamees, M. S. Abdulraheem, and E. N. Farsangi, "Punching Shear Behavior of Flat Slabs Utilizing Reactive Powder Concrete with and without Flexural Reinforcement," Pract. Period. Struct. Des. Constr., vol. 26, no. 1, p. 04020060, 2021, doi: 10.1061/(asce)sc.1943-5576.0000551.

[39] K. T. Azoom and R. M. R. Pannem, "Punching strength and impact resistance study of sifcon with different fibres," Int. J. Civ. Eng. Technol., vol. 8, no. 4, pp. 1123–1131, 2017.

[40] A. S. I. Shwalia, N. H. A. Al-Salim, and H. M. Al-Baghdadi, "Enhancement punching shear in flat slab using mortar infiltrated fiber concrete," Civ. Eng. J., vol. 6, no. 8, pp. 1457–1469, 2020, doi: 10.28991/cej-2020-03091560.

[41] P. Kumar, S. Chaudhary, and R. Gupta, "Behaviour of adhesive bonded and mechanically connected steel-concrete composite under impact loading," Procedia Eng., vol. 173, pp. 447–454, 2017.

[42] B. A. Graybeal, “Material property characterization of ultra-high performance concrete,” United States. Federal Highway Administration. Office of Infrastructure …, 2006.

[43] P. Richard and M. Cheyrezy, “Composition of reactive powder concretes,” Cem. Concr. Res., vol. 25, no. 7, pp. 1501–1511, 1995.

[44] Ş. Yazıcı, G. İnan, and V. Tabak, “Effect of aspect ratio and volume fraction of steel fiber on the mechanical properties of SFRC,” Constr. Build. Mater., vol. 21, no. 6, pp. 1250–1253, 2007.

[45] S. Allena and C. M. Newtson, “Ultra-high strength concrete mixtures using local materials,” J. Civ. Eng. Archit., vol. 5, no. 4, pp. 322–330, 2011.

[46] W. I. Khalil, “Some properties of modified reactive powder concrete,” J. Eng. Dev, vol. 16, no. 4, pp. 66–87, 2012.

[47] H. Kim, P. Hadl, and V. T. Nguyen, “A New Mix Design Method for UHPC based on Stepwise Optimization of Particle Packing Density,” in International Interactive Symposium on Ultra-High Performance Concrete, 2016, vol. 1, no.

[48] M. Pourbaba, E. Asefi, H. Sadaghian, and A. Mirmiran, “Effect of age on the compressive strength of ultra-high-performance fiber-reinforced concrete,” Constr. Build. Mater., vol. 175, pp. 402–410, 2018.

[49] H. H. Muteb and D. M. Hasan, “Ultra-high-performance concrete using local materials and production methods,” IOP Conf. Ser. Mater. Sci. Eng., vol. 870, no. 1, 2020, doi: 10.1088/1757-899X/870/1/012100.

[50] X. Wu, S. Yu, S. Xue, T. H. K. Kang, and H. J. Hwang, "Punching shear strength of UHPFRC-RC composite flat plates," Eng. Struct., vol. 184, no. January, pp. 278–286, 2019, doi: 10.1016/j.engstruct.2019.01.099.

[51] A. P. Lampropoulos, J. N. Duncan, and O. T. Tsioulou, "Punching shear resistance of UHPFRC," 20th Congr. IABSE, New York City 2019 Evol. Metrop. - Rep., pp. 867–872, 2019, doi: 10.2749/newyork.2019.0866.

[52] L. Moreillon, "Shear strength of structural elements in high performance fibre reinforced concrete (HPFRC)." Université Paris-Est, 2013.

[53] M. M. A. Kadhim, A. R. Saleh, L. S. Cunningham, and A. A. Semendary, "Numerical investigation of non-shear-reinforced UHPC hybrid flat slabs subject to punching shear," Eng. Struct., vol. 241, p. 112444, 2021.

[54] P. Zohrevand, X. Yang, X. Jiao, and A. Mirmiran, "Punching Shear Enhancement of Flat Slabs with Partial Use of Ultrahigh-Performance Concrete," J. Mater. Civ. Eng., vol. 27, no. 9, p. 04014255, 2015, doi: 10.1061/(asce)mt.1943-5533.0001219.

[55] A. S. I. Shwalia, N. H. A. Al-Salim, and H. M. Al-Baghdadi, "Enhancement punching shear in flat slab using mortar infiltrated fiber concrete," Civ. Eng. J., vol. 6, no. 8, pp. 1457–1469, 2020, doi: 10.28991/cej-2020-03091560.

[56] Iraqi Specification No.5, "Portland Cement", Baghdad, 1984.

[57] Iraqi Specification No.45, "Natural Sources for Gravel that is used in concrete and construction", Baghdad, 1984.

[58] ASTM C1240-04, "Standard Specification for the Use of Silica Fume as a Mineral Admixture in Hydraulic Cement Concrete, Mortar and Grout", Vol.4.2, 2004, 6p.

[59] ASTM C494-05, "Standard Specification for Chemical Admixtures for Concrete", Annual Book of ASTM Standards, American Society for Testing and Materials, Vol.04.02., 2005.

[60] ASTM 615/A 615M-15a, "Standard Specification for Deformed and Plain Carbon Steel Bars for Concrete Reinforcement", Annual Book of ASTM Standards, American Society for Testing and Materials, Vol.01.02, 2015.

[61] ACI Committee 211.1-91, "Standard Practice for Selecting Proportions for Normal Heavyweight, and Mass Concrete (ACI 211.1-91) Reapproved 1997", Manual of Concrete Practices, American Concrete Institute, 1991, pp. 1-38.

[62] ASTM C192, "Standard practice for making and curing concrete test specimens in the laboratory," Annual Book of American Society for Testing Materials Standards, vol. 4, 2007.

[63] BS1881-116, "Method for Determination of Compressive Strength of Concrete Cubes", British Standards Institute, London, 1989.

[64] ASTM C496-11, "Standard Test Method for Splitting Tensile Strength of Cylinder Concrete Specimens", Annual Book of ASTM Standards, American Society for Testing and Materials, Vol.04.02, 2011.

[65] ASTM C469-10, "Standard Test Method for Static Modulus of Elasticity and Poisson'sRatio of concrete in Compression," ASTM International, West Conshohocken, PA, 2010.

[66] BS-1881:116, ―Testing concrete Part 116. Method for determination of compressive strength of concrete cubes‖ London: British Standards Institution. (1989).

[67] ASTM C496-11, "Standard Test Method for Splitting Tensile Strength of Cylinder Concrete Specimens", Annual Book of ASTM Standards, American Society for Testing and Materials, Vol.04.02, 2011.

[68] ASTM C469-2010 Standard Standard Test Method for Static Modulus of Elasticity and Poisson's Ratio of Concrete in Compression

[69] BS-8110, ―Structural Use of Concrete‖, British Standards Institution, London,1997.

[70] Larrard, F., Belloc, A., Renwez, S., and Boulay, C., ―Is the Cube Test Suitable for High Performance Concrete‖, Materials and Structures, Vol.. 27, No. 174, 1994, pp. 3,

[71] Adheem, A.H., ―Structural Behavior of Composite Prestressed Concrete Beams with RPC Slabs under Repeated Loads‖, Ph.D. Thesis, University of Babylon, Babylon, Iraq, 2016.

[72] Mansur, M.A., Design of reinforced concrete beams with web openings. in Proceedings of the 6th Asia-Pacific structural engineering and construction conference (ASPEC 2006), 2006: p. pp. 5–6.

[73] Muthuswamy, K. and G. Thirugnanam, Structural behaviour of hybrid fibre reinforced concrete exterior Beam-Column joint subjected to cyclic loading. International journal of civil structural engineering,2014. 4(3): p. 262.

[74] Marzouk, H., and A. Hussein. (1991) "Punching Shear Analysis of Reinforced High-Strength Concrete Slabs." Canadian Journal of Civil Engineering 18, no. 6 (December 1, 1991): 954–963. doi:10.1139/l91-118. Marzouk, H., Emam, M. and Hilal, M. S. (1998). "Effect of High-Strength.

[75] Priestley and R. Park, (1987). “Strength and ductility of concrete bridge columns under seismic loading,” Struct. J., vol. 84, no. 1, pp.61–76.

[76] Park, R., (1988). “Ductility evaluation from laboratory and analytical testing”. In Proceedings of the 9th world conference on earthquake engineering, Tokyo-Kyoto, Japan (Vol. 8, pp. 605-616).

[77] Robertson and Durrani, (1991). “Gravity load effect on seismic behavior of exterior slab-column connections”. Struct. J., vol. 88, no. 3, pp. 255–267.

[78] Park, R., (1989). “Evaluation of ductility of structures and structural assemblages from laboratory testing”. Bull. New Zeal. Natl. Soc. Earthq. Eng., vol. 22, no. 3, pp. 155–166.

[79] Ohno and Nishioka, (1984) “An experimental study on energy absorption capacity of columns in reinforced concrete structures,” Doboku Gakkai Ronbunshu, vol. 1984, no. 350, pp. 23–33.

[80] Husain M., A. S. Eisa, and R. Roshdy, (2017). “Alternatives to enhance flat slab ductility”. Int. J. Concr. Struct. Mater., vol. 11, no. 1, pp. 161–169.

[81] Simulia ,DS. "ABAQUS/standard User's manual, version 2017." Providence, RI: Simulia (2017).

[82] Meng, Xianzhe. “Shear strengthening of prestressed hollow core slabs using externally bonded Carbon Fiber Reinforced Polymer sheets.", M.Sc. Thesis, Windsor’s University, Canada, 2016.

[83] Bahij, S., Adekunle, S. K., Al- Osta, M., Ahmad, S., Al- Dulaijan, S. U., & Rahman, M. K. “Numerical investigation of the shear behavior of reinforced ultra- high-performance concrete beams,’’ Structural Concrete, PP. 305-317, 2018.

[84] Jawdhari, A.and I. Harik. "Finite element analysis of RC beams strengthened in flexurewith CFRP rod panels ". Constr Build Mater 2018;163:751–66.

[85] Lubliner, J., Oliver, J., Oller, S., & Oñate, E. "A plastic-damage model for concrete‖. International Journal of Solids and Structures, 25(3), pp. (299-326), (1989).

[86] Kmiecik, P., and M. Kamiński. "Modelling of reinforced concrete structures and composite structures with concrete strength degradation taken into consideration." Archives of civil and mechanical engineering 11.3 (2011): 623-636.

[87] Malm, R., "Shear cracks in concrete structures subjected to in-plane stresses," Lic. thesis, Royal Institute of Technology (KTH) (2006), Stockholm, Sweden.

[88] Hibbitt, Karlsson, & Sorensen, "ABAQUS User's Manual". Pawtucket, 6th Edition, (2010).

[89] Jankowiak, Tomasz, and Tomasz Lodygowski. "Identification of parameters of concrete damage plasticity constitutive model." Foundations of civil and environmental engineering6.1 (2005): 53-69.

[90] Birtel, V., and P. Mark. "Parameterised finite element modelling of RC beam shear failure." ABAQUS users' conference. 2006.

[91] Zheng, W., Li, H., and Wang, Y., ―Compressive Stress-Strain Relationship of Steel Fiber-reinforced Reactive Powder Concrete after Exposure to Elevated Temperatures‖, Construction and Building Materials, Vol. 35, 2012, pp. 9.

[92] Hannawayya, S.P., ―Behavior of Reactive Powder Concrete Beams in Bending‖, Ph.D. Thesis, University of Technology, Baghdad, Iraq, October 2010, pp.239.

[93] Fujikake, K., Senga, T., Ueda, N., Ohno, T., & Katagiri, M., "Effects of strain rate on tensile behavior of reactive powder concrete". Journal of Advanced Concrete Technology, 2006.

[94] S. Popovics, “A numerical approach to the complete stress-strain curves ofconcrete,” Cement and Concrete Research, vol. 3, no. 5, pp. 583-599, 1973.

[95] Dere, Y., & Koroglu, M., A. “Nonlinear FE Modeling of Reinforced Co ncrete,”International Journal of Structural and Civil Engineering Research, Vol.(6), No.1,pp.(71-74), (2017).

Appendix-A

SLAB DESIGN

By using ACI code 318-2019:

Design of Flexural Reinforcement:-

Material and section properties:

fy = 460 *MPa*	fc'=22.5 MPa
Es = 200 GPa	εcu=0.003
εs=0.0023	b = 900 mm
t = 80 mm	da = 55 mm

Using $\rho = \rho max$=0.85×β1× $\frac{fc'}{fy}$× $\frac{\varepsilon cu}{\varepsilon cu+0.004}$

fc'< 28 $MPa \rightarrow \beta$1=0.85

ρmax= 0.85 × 0.85 × ($\frac{22.5}{460}$) × [$\frac{0.003}{0.003+0.004}$] = 0.0152

As= $\rho \times b \times d$ =0.0152 × 900 × 55 = 750 mm^2

Using $\emptyset 10mm$ $A_s)\ bar = \pi/4 \times 10^2 = 78.54mm^2$

No. of bars = $\frac{As)\ required}{As)\ one\ bar} = \frac{750}{78.54} = 9.58$ bars

In this study (10Ø10) *bars will be used in two directions.*

$\rho)\ provided = \frac{\text{As) provided}}{\text{b}\times\text{d}} = \frac{10\times 78.54}{900\times 55} = 0.0158$

$Spacing\ (S) = \frac{900}{10} = 90$ mm

S).=78.54

1450 ×900 =48.75$mm\ using\ S$=50 $mm\ in\ each\ direction$

Check length of development:-

Bar in tension:-

For $d_b \leq \emptyset 35mm$

l_d =0.02$A_b(f_y/\sqrt{f_{c-}}) \times factor \geq 0.06 d_b f_y \times factor \geq 300mm$

Cases of factor:-

$A_s)req/A_s)pro.$< 1=1450/1492= 0.972<1

l_d =(0.02×78.54×422/√28.5) ×0.972= 120.7mm

0.06×10×422×0.972=246mm

$\therefore\ l_d$ = 300mm <430$mm\ \therefore\ o.k.$

Design of column:-

Distance between two vertical bars = Smax = max(40mm or 1.5 db)

$\therefore S_{max}$ = 40mm ($pure\ compression\ for\ tied\ column$)

A_c =150×150 =22500mm^2

$\therefore using$ 4Ø10mm

Design of ties:-

d_{tie} ≥ 1/50 ($max.destance\ of\ the\ section$ = 150 ×150=3mm

Or d_{tie} =10$mm\ if\ d_b$ ≤32$mm\ and\ d_{tie}$ =12$mm\ if\ d_b$ >32mm

$\therefore using\ d_{tie}$ =4mm

$Spacing\ (S)ween\ two\ ties$=min (48$d_{tie}or$ 16d_bor0.5($small\ length\ of\ the\ section$))

S = 48 x 4 = 192mm

S = 16x10 = 160mm

S = 0.5x150 = 75mm

$\therefore S$=75mm

Appendix B

MODELING OF MATERIAL PROPERTIES IN FINITE ELEMENT ANALYSIS

B.1 INTRODUCTION

There are three material models for analyzing concrete in ABAQUS: (1) Smeared crack concrete model, (2) Brittle crack concrete model, and (3) Concrete damaged plasticity (CDP) model. Out of the three concrete models, the concrete damaged plasticity model is selected in the present study. Details of the CDP model used in ABAQUS, in addition to the behavior and properties of the concrete and the other material used in this study are described below.

B.2 CONCRETE DAMAGED PLASTICITY IN ABAQUS

Concrete damaged plasticity is capable of modelling all structural types of reinforced or unreinforced concrete or other quasi-brittle materials subjected to monotonic, cyclic, or dynamic loads, this model is based on a coupled damage plasticity theory and the multi-axial behavior of concrete in damaged plasticity model governs by a yield surface, which proposed by **(Lubliner et al.) [85]**. Tensile cracking and compressive crushing of concrete are two assumed main failure mechanisms in this model. Furthermore, the degradation of material for both tension and compression behavior have been considered in this model. Degradation of concrete in cyclic and dynamic loadings is taken into account by defining two scalar parameters; tensile damage parameter (dt) and compressive damage parameter (dc).

B.2.1 Concrete Damaged Plasticity Parameters in Triaxial Loading State

In order to describe strength with the equation for triaxial stress as input to the finite element program ABAQUS, a set of five parameters are required to completely describe the plastic behavior of concrete;

Ψ, Dilation angle: The angle of inclination of the failure surface toward the hydrostatic axis, measured in the meridional plane. Physically, dilation angle Ψ is interpreted as a concrete internal friction angle. Maximum value of it equal (56.3^{o}) and minimum value is close to (zero) **[86]**.Through many trials of geometry with the aim of achieving proper failure to be compatible with the observed experimental failure mechanism, the value of dilation angle was taken as (45^{o})for NSC and (50^{o}) for UHPC.

ϵ: Plastic potential eccentricity, it is a small positive value which expresses the rate of approach of the plastic potential hyperbola to its asymptote. It is recommended to assume ϵ = 0.1 in the CDP model **[86]**.

F_{b0}/f_{c0}: is the proportion of initial uniaxial compressive yield stress and initial uniaxial compressive yield stress **[86]**. The default value in ABAQUS is (1.16) for NSC and UHPC.

K: is the ratio of the second stress invariant in the tensile meridian to compressive meridian for any defined value of the pressure invariant at initial yield. It is used to define the multi-axial behavior of concrete and is ($0.5<Kc\leq1$) **[86]**.The default value in ABAQUS is (0.667) for NSC and UHPC.

μ: is the viscosity parameter. It does not affect the ABAQUS/Explicit analysis but contribute to converge in an ABAQUS/Standard analysis. According to (Malm) **[87]** $\mu=10^{-5}$ for NSC and UHPC is recommended because in comparison with characteristic time increment it should be small.

B.3 UNIAXIAL BEHAVIOR OF CONCRETE

B.3.1 Uniaxial Behavior of normal strength Concrete

B.3.1.1 Uniaxial Tensile Behavior for normal strength Concrete

Under uniaxial tension, as can be seen in Figure B-1, the stress increases with a linear elastic relationship with strain up to the ultimate tensile strength, and then micro-cracks form microscopically with a tension softening response. There are three different methods to define tension softening response in ABAQUS; stress-strain, stress-displacement or by use of fracture energy, Gf **[88]**.

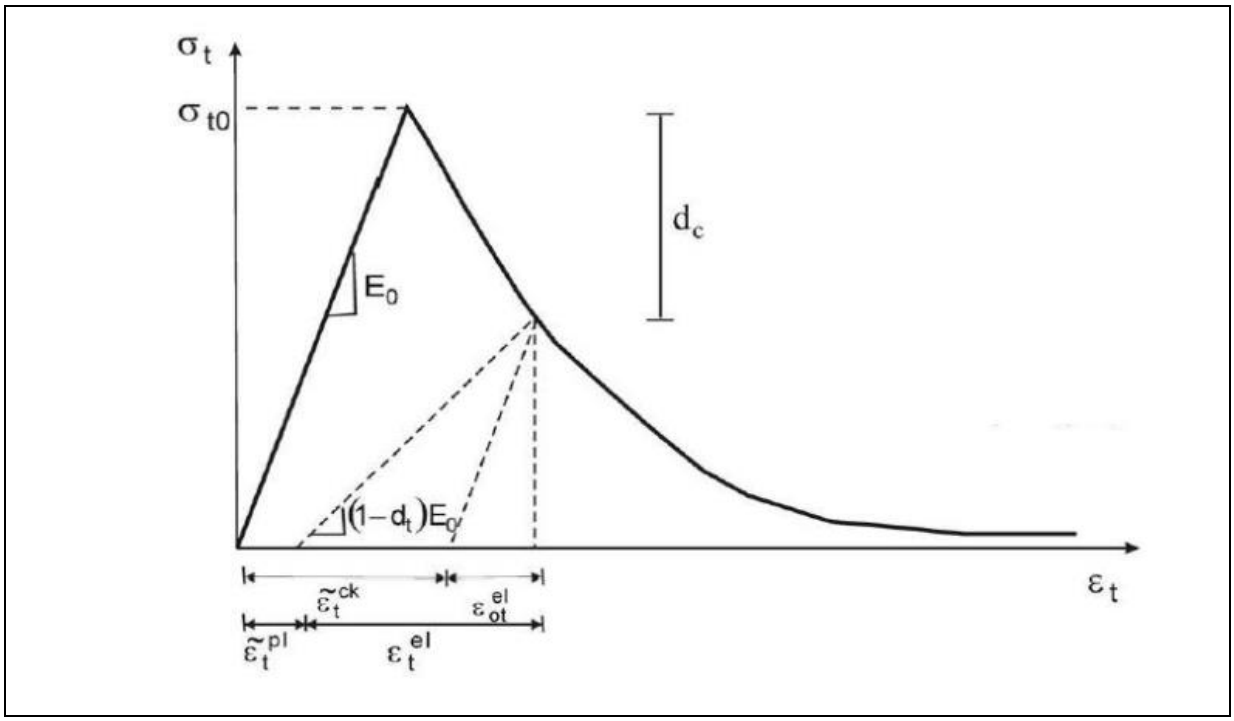

Figure (B-1). Uniaxial tensile behavior of concrete [96].

To define the tensile stress-strain relation of concrete in ABAQUS, user should input young's modulus (E_0), stress (σ_t), cracking strain ($\tilde{\varepsilon}_t^{ck}$) values and the damage parameter values (dt) for the relevant grade of concrete. The cracking strain ($\tilde{\varepsilon}_t^{ck}$) should be calculated from the total strain using Eq. (B-1) below:

$$\tilde{\varepsilon}_t^{ck} = \epsilon_t - \varepsilon_{ot}^{el} \qquad \text{(B-1)}$$

Where, $\epsilon_{ot}^{el} = {}^{\sigma_t}/_{E_o}$, the elastic strain corresponding to the undamaged material, and $\varepsilon_t = \text{total tensile strain}$

B.3.1.2 Uniaxial Compression Behavior for normal strength Concrete

Under uniaxial compression, there is a linear elastic relationship between stress - strain until initial yield. After losing stiffness due to bond failure between the aggregates and the cement paste, the behavior becomes non-linear. In stresses greater than ultimate strength, stress hardening and strain softening define plastic response. In other words, compressive stress decreases while the corresponding strain increases. The uniaxial compressive behavior of concrete is depicted in Figure (B-2).

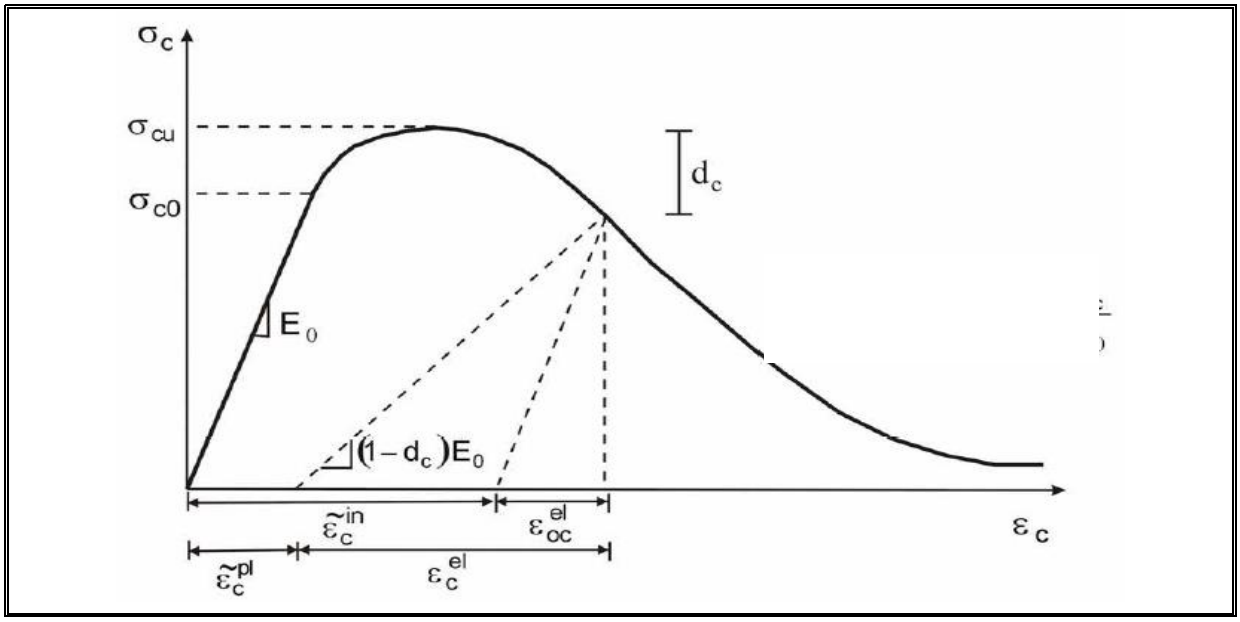

Figure (B-2) Uniaxial compressive behavior of concrete [87].

To define the compression stress-strain relation of concrete in ABAQUS, user needs to enter the stresses (σc), inelastic strains ($\varepsilon_c^{\sim in}$) corresponds to stress values, and damage properties (dc) with inelastic strains in tabular format. Therefore, total strain values should be converted to the inelastic strains using Eq. (B-2):

$$\tilde{\varepsilon}_c^{in} = \epsilon_c - \varepsilon_{oc}^{el} \quad \text{(B-2)}$$

Where, $\epsilon_{oc}^{el} = {}^{\sigma_c}/_{E_o}$, the elastic compression strain corresponding to the undamaged material, and $\varepsilon_c = \text{total compression strain}$

Compression and tension damage parameters describing crushing and cracking behavior were defined as tables within CDPM. The following equations developed by **(Birtel and Mark) [90]** were successfully used in obtaining the compression and damage parameters. Damage parameters take values ranging from 0 (no damage) to 1 (fully damaged), representing the level of damage.

$$dc = 1 - \frac{\sigma c\, E_c^{-1}}{\varepsilon_c^{pl}\left(\frac{1}{bc} - 1\right) + \sigma c\, E_c^{-1}} \quad \text{(B-3)}$$

$$dt = 1 - \frac{\sigma t\, E_c^{-1}}{\varepsilon_{ct}^{pl}\left(\frac{1}{bt} - 1\right) + \sigma t\, E_c^{-1}} \quad \text{(B-4)}$$

$$\varepsilon_c^{pl} = b_c\, \tilde{\varepsilon}_c^{in} \quad \text{(B-5)}$$

$$\varepsilon_t^{pl} = b_t\, \tilde{\varepsilon}_t^{ck} \quad \text{(B-6)}$$

The coefficients b_c and b_t take values between 0 and 1. Birtel and Mark suggested bc=0.7 and bt=0.1.

Further, corrective measures should be taken to ensure that the plastic strain values (ε_c^{pl} and ε_t^{pl}) calculated using (eq. B-5 and eq. B-6) are neither negative nor decreasing with increased stresses **[88]**.

C.3.2 Uniaxial Behavior of Ultra High Performance Concrete.

C.3.2.1 Uniaxial Compression Behavior for Ultra High Performance

Behavior of normal concrete and high compressive strength concrete under loads is different from behavior of UHPC because of its ductility and its high strength against compressive load as well as tensile load for UHPC. Many

studies about mechanical properties of UHPC, were conducted but there are very few studies described the behavior of UHPC .

Zheng et al. [91] found that for UHPC, the strain at peak stress (ϵ_o) ranges from 0.004 to 0.005, while ultimate strain(ϵ_{cu}) ranges from 0.006 to 0.0075.

In the present study, the compression stress-strain relationship for UHPC can be idealized by a multilinear isotropic stress-strain curve Figure (B-3) uses the following equations:

$fc = \epsilon\, Ec$ for $0 \leq \epsilon \leq \epsilon_1$ (B-7)

$fc = 0.7\, f\square c + \frac{0.3 f\square c}{\epsilon_0 - \epsilon_1}(\epsilon - \epsilon_1)$ for $\epsilon_1 \leq \epsilon \leq \epsilon_0$ (B-8)

$fc = f\square c$ for $\epsilon_0 \leq \epsilon \leq \epsilon_{cu}$ (B-9)

Where; ϵ_1=strain corresponding to $0.7\, f\square c$ defined by :

$\epsilon_1 = \frac{0.7 f\square c}{Ec}$ (Hookes law)

Values of ϵ_o and ϵ_{cu} found by **(Hannawayya) [92]** for UHPC are adopted in the present finite element analysis, (ϵ_o=0.0044, ϵ_{cu} =0.0063).

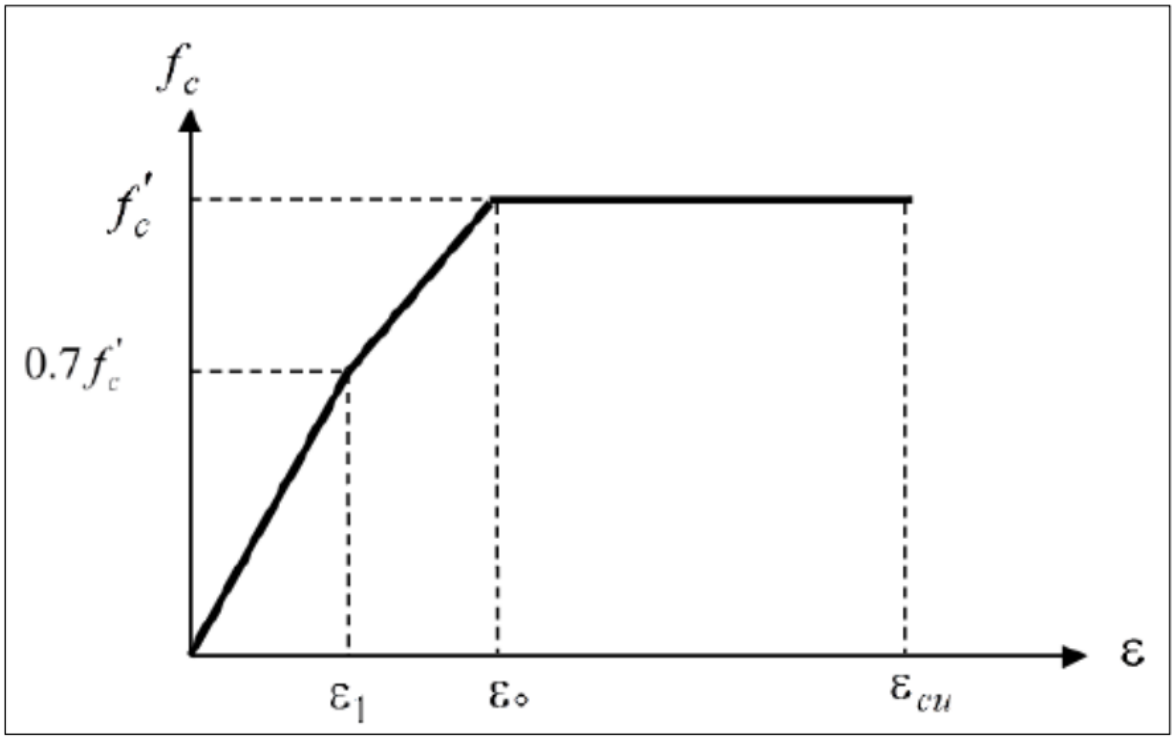

Figure(B-3) Typical Stress-Strain Diagram for UHPC under Uniaxial Compression [92].

B.3.2.2 Uniaxial Tensile Behavior for UHPC

Stress-strain relationship of UHPC with strain rate effects in tension as shown in Figure (B-4), calculated using the tensile stress-crack opening relationship of UHPC, which proposed by **Fujikake et al. [93]** as follows:

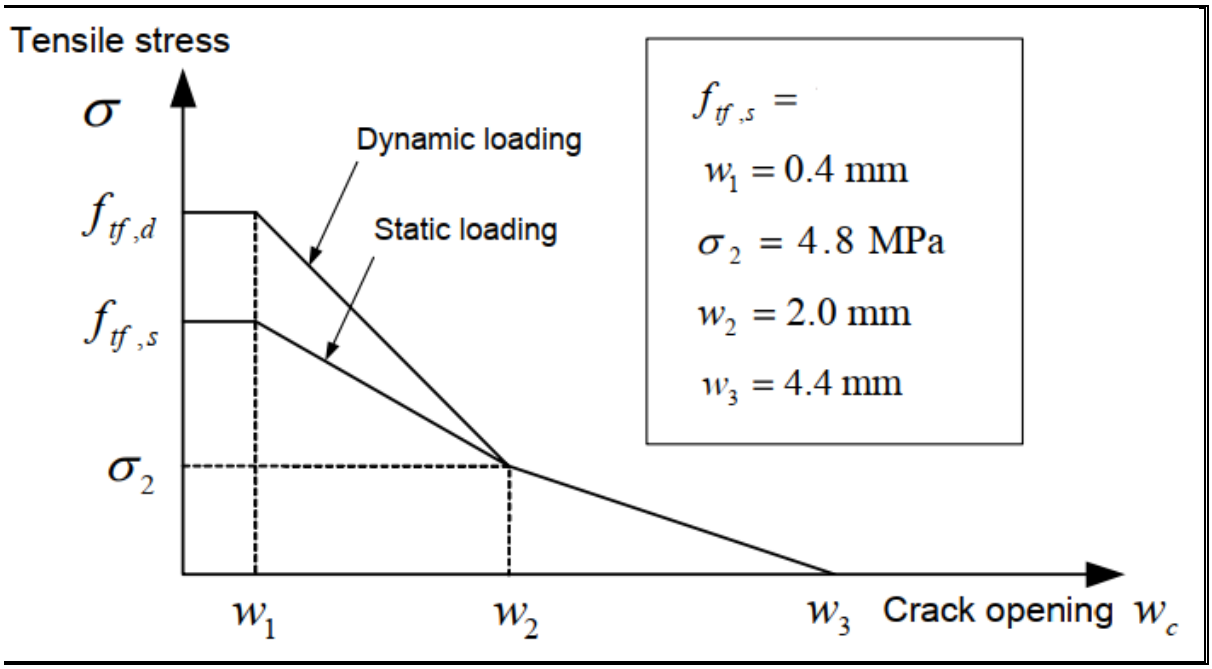

Figure (B-4): Tensile stress-strain relationship for UHPC reproduced from [93].

Wc = crack opening, σ_2 = 4.8 MPa; w_1= 0.4 mm, w_2 = 2.0 mm, w_3 = 4.4 mm, $f_{tf,s}$ = static tensile strength = 8.23 MPa,

B.4 Material Properties for FEM

B.4.1 Concrete Model Properties

The concrete material parameters in the concrete damaged plasticity model that should be used are: the modulus of elasticity E_0, the Poisson's ratio v and the compressive and tensile strengths of concrete In order to simulate concrete with normal compressive strength, the unconfined stress–strain relationship model for concrete as proposed by **(Popovics) [94]** was used. This relationship based on the concrete cylinder strength, as described in equations (B-10) and (B-11).

$$\frac{f_c}{\grave{f_c}} = \frac{n \times \left[\frac{\varepsilon_c}{\varepsilon_{co}}\right]}{(n-1)+\left[\frac{\varepsilon_c}{\varepsilon_{co}}\right]^n} \qquad \text{(B-10)}$$

$$n = (\,0.4 \times 10^{-3} \times \grave{f_c}(psi)) + 1.0 \qquad \text{(B-11)}$$

Where:

fc'= the compressive strength of cylinder at maximum stress.

ε_{co}= strain of concrete at maximum stress, n = a curve-fitting factor.

On the other hand, tensile stress-strain (σ-ε) relationship was assumed linear up to the uniaxial tensile strength and then determined using the exponential function in the equation (B-12) **[95]**.

$$\sigma = f_t \times \left[\frac{\varepsilon_t}{\varepsilon}\right]^{(0.7+1000\varepsilon)} \quad \varepsilon_t = \frac{f_t}{E_o} \qquad \text{(B-12)}$$

B.4.2 Steel Reinforcement Model Properties

The required input parameters for material definition of steel bars, includes density, elastic and plastic behavior. Elastic behavior of steel material is defined by specifying Young's modulus (Es) and Poisson's ratio (v) of which typical values are 200000 MPa and 0.3, respectively. Plastic behavior is defined in a tabular form, included yield stress and corresponding plastic strain. According to **(Hibbit et al.) [88]**.true stress and logarithmic strain should be defined. Input values of stress in each point for an isotropic material are calculated according to Eqs. (B-13) and (B-14). A higher number of input points lead to results that are more accurate.

$$\sigma_{true} = \sigma_{nominal}\,(1 + \varepsilon_{nominal}) \qquad \text{(B-13)}$$

$$\sigma_{in}^{pl} = \ln(1 - \varepsilon_{nominal}) - \left(\frac{\sigma_{true}}{E_s}\right) \qquad \text{(B-14)}$$

C.4.3 Steel Plate Model Properties

The steel plates were modelled using an isotropic linear elastic material model by Eq. (B-15) with solid elements for all models. The assumption for the material of loading and supporting plates is to avoid problems in solution due to the large deformations that will be developed or stress singularity in the plates.

$$f_s = E_s \varepsilon_s \ (\text{MPa}), \quad \varepsilon_s \leq \varepsilon_y \qquad \text{(B-15)}$$

الخلاصة

يعتبر فشل قص التثقيب هو الأخطر والمسيطر في تصميم الالواح المسطحة ، لذلك أجريت هذه الدراسة لتقوية البلاطة المسطحة ضد فشل قص الثاقب باستخدام الخرسانة الهجينة والخرسانة المسلحة (خرسانة فائقة الأداء). اشتمل الجزء التجريبي من البحث الحالي على خمسة عشر عينة. بلاطات مسطحة مربعة بأبعاد (90 * 90 سم) وسماكة (8 سم) وجميع العينات تحتوي على حديد تسليح الانثناء.

عينتان من الخرسانة العادية ، إحداهما هي النموذج المرجعي لحالة الدراسة الأولى ، والأخرى من الخرسانة العادية أيضًا ، ولكنها تحتوي على حديد تسليح القص الثاقب ، وهو النموذج المرجعي لحالة الدراسة الثانية. حالة الدراسة الأولى ، تتكون من ثلاث مجموعات مصبوبة من الخرسانة الهجينة (الخرسانة العادية و UHPC) لنصف سماكة البلاطة في جهة الانضغاط (اتصال العمود بالبلاطة). تتكون كل مجموعة من ثلاثة نماذج، المجموعة الأولى لها شكل تقوية مربع في وسط اللوح على طول الضلع (1d + c) حيث (d) العمق الفعال (c) طول ضلع مقطع العمود، و (2d + c) للثاني (3d + c) للثالث. المجموعة الثانية هي نفس عينات المجموعة الأولى، لكن منطقة التقوية (UHPC) مائلة بزاوية 45. في المجموعة الثالثة، استخدمنا الشكل الدائري للتقوية مع مساحة مكافئة لنماذج الأولى و المجموعات الثانية. تحسنت مقاومة النموذج للقص بنسبة كبيرة لنماذج الخرسانة الهجينة مقارنة بالنموذج المرجعي للخرسانة العادية ، ووصلت إلى الضعف.

بالإضافة إلى التحسن في مقاومة البلاطة لفشل قص التثقيب مع زيادة مساحة التقوية (UHPC) ، فقد ساعدت أيضًا الخرسانة فائقة الأداء في زيادة الخواص الهندسية الأخرى مثل امتصاص الطاقة والليونة والصلابة ، وهذه الخصائص لها تم تحسينه لأن هذه الخرسانة تحتوي على ألياف فولاذية.

أما بالنسبة لحالة الدراسة الثانية ، فهي تتكون من أربع عينات من الخرسانة الهجينة بالإضافة إلى العينة المرجعية التي تحتوي على تقوية قص التثقيب. ركزت على استبدال تقوية قص التثقيب بـ (UHPC) بنصف أو كل سمك اللوح ، ثم قمنا بتدوير منطقة التسليح بزاوية 45 لإعطاء نتائج رائعة بنسبة 70٪ للعينة المرجعية.

في الجزء الثاني من هذه الدراسة ، عنصر محدود ثلاثي الأبعاد (FE) تم إجراء نموذج باستخدام نموذج اللدونة التالفة للخرسانة وخصائص المواد التي تم الحصول عليها من الاختبارات المعملية لمحاكاة الألواح المسطحة من الخرسانة المسلحة مع أو بدون تقوية ضمن حزمة برامج العناصر المحدودة التجارية ABAQUS / standard 2017. و قد أظهرت النتائج العددية أن تنبؤات المحدود اتفق نموذج العنصر بشكل جيد مع البيانات التجريبية من حيث حمل التكسير والحمل النهائي والانحراف النهائي بمتوسط فروق حوالي (5٪) و (٪ 1.5) و (7٪) على التوالي. أجريت دراسة بارامترية للعديد من المتغيرات التي لم يتم أخذها في الاعتبار في البرنامج التجريبي باستخدام نموذج FE المصادق عليه مثل ؛ تأثير قوة ضغط الخرسانة وتأثير أبعاد العمود.

جمهورية العراق
وزارة التعليم العالي والبحث العلمي
جامعة بابل
كلية الهندسة
قسم الهندسة المدنية

تحسين سلوك القص الثاقب للألواح المسطحة باستخدام خرسانة فائقة الأداء

رسالة مقدمة إلى كليَّةِ الهندسة ـ جامعةِ بابل

كجزء مِنْ متطلبات نيل درجة الماجستير في علوم الهندسة المدنية (هندسة الإنشاءات)

من قبل

حسين يوسف طالب عباس

بكالوريوس علوم في الهندسة المدنية 2012

أشراف

الأستاذ المساعد الدكتور: نبيل حسن علي

2023م **1444هـ**